TRANSPORTATION RESEARCH RECORD

579

Earthquake-Induced Dynamic Response of Bridges and Bridge Measurements

9 reports prepared for the 54th Annual Meeting of the Transportation Research Board

TRB

TRANSPORTATION RESEARCH BOARD

NATIONAL RESEARCH COUNCIL

Washington, D. C., 1976

Transportation Research Record 579
Price $4.80
Edited for TRB by Marjorie Moore

subject areas
03 rail transport
22 highway design
51 highway safety
52 road user characteristics

Transportation Research Board publications are available by ordering directly from the board. They may also be obtained on a regular basis through organizational or individual supporting membership in the board; members or library subscribers are eligible for substantial discounts. For further information, write to the Transportation Research Board, National Academy of Sciences, 2101 Constitution Avenue, N.W., Washington, D.C. 20418.

The project that is the subject of this report was approved by the Governing Board of the National Research Council, whose members are drawn from the councils of the National Academy of Sciences, the National Academy of Engineering, and the Institute of Medicine. The members of the committee responsible for the report were chosen for their special competence and with regard for appropriate balance.

This report has been reviewed by a group other than the authors according to procedures approved by a Report Review Committee consisting of members of the National Academy of Sciences, the National Academy of Engineering, and the Institute of Medicine.

The views expressed in individual papers and attributed to the authors of those papers are those of the authors and do not necessarily reflect the view of the committee, the Transportation Research Board, the National Academy of Sciences, or the sponsors of the project.

LIBRARY OF CONGRESS CATALOGING IN PUBLICATION DATA

National Research Council. Transportation Research Board.
Earthquake-induced dynamic response of bridges and bridge measurements.

(Transportation research record; 579)

1. Bridges–Earthquake effects–Addresses, essays, lectures. 2. Bridges–Vibration–Addresses, essays, lectures. 3. Bridges–Testing–Addresses, essays, lectures. I. Title. II. Series.
TE7.H5 no. 579 [TG265] 380.5'08s 624.2'52 76-28765
ISBN 0-309-02493-5

CONTENTS

STRONG-MOTION INSTRUMENTATION PROGRAM FOR STATE HIGHWAY BRIDGES

R. B. Matthiesen, U.S. Geological Survey

The State Bridge Seismic Network, supported by the Federal Highway Administration, was established in spring 1974 to instrument highway bridges in seismically active regions. This network is being integrated into the existing National Strong-Motion Instrumentation Network operated by the U.S. Geological Survey. Six bridges in California, Alaska, and Nevada have been instrumented. The most recently installed instrumentation uses a central recording system that permits greater flexibility in locating transducers. For bridge structures with numerous expansion joints, adjacent sections are instrumented so that relative motion across the joints can be interpreted. The response during the 1971 San Fernando earthquake of a seven-story, reinforced concrete building supported by a moment-resistant frame is used to illustrate a simplified interpretation of results from such systems. Instrumentation of representative types of structures will lead to improved modeling and analysis of the response of bridge structures to earthquakes.

•IN SPRING 1974, the Federal Highway Administration established a program to encourage the highway departments of states in seismically active regions to instrument representative types of highway bridges. This program was motivated by the failure of several freeway interchange and overpass bridges during the 1971 San Fernando earthquake (1, 2). Prior to that event, bridge failures during earthquakes in the United States had not caused serious alarm, although the impact of earthquakes on transportation systems had been pointed out as a potentially serious problem (3), and several cases of failure of bridge abutments or displacement of bridges from their piers during earthquakes had been reported (4, 5, 6, 7).

The State Bridge Seismic Network supported by FHWA is to be incorporated into the existing National Strong-Motion Instrumentation Network operated by the U.S. Geological Survey (USGS) for the National Science Foundation and several other cooperating agencies at the federal, state, and local levels. A brief review of the existing network, of concepts for instrumentation of bridges, of the nature of the results to be expected, and of the interpretation of such results is appropriate.

ORGANIZATION OF THE NETWORK

In 1932, the U.S. Coast and Geodetic Survey inaugurated a program of strong-motion seismology intended to furnish data considered essential to the design of earthquake-resistant structures (8). The responsibility for establishing an instrumentation network to achieve this objective was assigned to the Seismological Field Survey (SFS). After several administrative changes that first placed the SFS under the Environmental Science Services Administration (ESSA) and then the National Oceanic and Atmospheric Administration (NOAA), in 1973 NSF was assigned the responsibility for the SFS program. NSF subsequently requested that the USGS operate the program and coordinate it with the strong-motion instrumentation programs of other agencies and organizations. The USGS established the Seismic Engineering Branch to perform this function.

The strong-motion instrumentation program was initiated with the installation of nine low-sensitivity, short-period seismographs (accelerographs) at locations selected by

local engineers. Less than 8 months later, instruments installed at Los Angeles, Vernon, and Long Beach recorded ground motions from the 1933 Long Beach earthquake. These first useful records of damaging earthquake motions indicated amplitudes as large as 0.25 *g* and provided the impetus for additional instrumentation. The network rapidly expanded to 50 instruments, located primarily in the San Francisco Bay area and the Los Angeles basin but including other seismically active areas of the western United States.

During the succeeding 30 years, there were a gradual increase in the number of instruments and several improvements in the instrumentation. The principal instrument used in the network was the strong-motion accelerograph designed and developed by the C&GS in cooperation with the National Bureau of Standards. A few displacement meters were developed and included in the network. The original accelerograph was relatively large and required extensive and frequent maintenance. Consequently, by 1962 the network had only expanded to 70 accelerographs.

In 1958, a low-cost instrument, the seismoscope, was developed to supplement the accelerographs in evaluating ground motion. The seismoscope record can be interpreted to yield a single point on the relative velocity response spectrum of the ground motion. Because the cost of accelerographs has decreased, the seismoscope is no longer considered an appropriate instrument for further expansion of the network.

In 1963 the first commercially designed accelerograph featuring numerous design improvements was marketed. These instruments overcame many of the inadequacies of the earlier accelerographs and consequently accelerated the expansion of the strong-motion instrument network. By 1974 the network (Figure 1) had increased to approximately 1,200 accelerographs.

From its inception, the program has received the cooperation of numerous outside organizations and individuals. The original advisory board to the SFS subsequently evolved into the Earthquake Engineering Research Institute, a professional organization of engineers, seismologists, and regulatory officials. In the early years, housing and facilities for the instruments were provided by public and private organizations. In recent years, a majority of the accelerographs incorporated into the network have been purchased by outside organizations. Approximately half of the 1,200 accelerographs at the present time are in high-rise buildings as a result of the numerous building codes that require instrumentation at several levels in such buildings.

The recent rapid expansion of the network has brought about the initiation of concerted effort to develop a rational plan for the national network as a coordinated program among cooperating agencies and organizations at the federal, state, and local levels. A balance is to be achieved between the networks designed to determine the nature of the strong ground motions in different regions of the country and those designed to determine the response of representative types of structures. The emphasis is on research that can be applied to improving the process of design of earthquake-resistant structures and facilities.

SELECTION OF STRUCTURES AND INSTRUMENTATION

Because of the importance of understanding structural response to earthquakes at the damage threshold and above and because such information will have an immediate impact on design criteria for structures throughout the country, the structures to be instrumented should be located in areas where the rate of potentially damaging seismic activity is high. On this basis, the highest priority is to instrument structures in California, Alaska, and Nevada, areas about five times more active than the northern Rockies, about 10 times more active than either the Puget Sound region or the lower Mississippi valley, and about 15 times more active than the East Coast (9). On the other hand, a modest investment in instrumentation in all seismically active regions is a prudent hedge given the uncertainty in the historic record of damaging earthquakes.

The structures selected should represent the current predominant construction types within each state, but special or new types of construction should also be considered. The structures should be relatively simple in design so that the records obtained may

be readily interpreted and the knowledge gained may provide significant insight into the response of bridge structures in general. Preferably, the structures selected should be those for which the dynamic characteristics of the structure, the foundation system, and the local soils are known. In any event, the instrumentation scheme must be based on known or estimated mode shapes for the particular type of structure being instrumented.

The FHWA program has been defined such that proposed and current bridge construction in zone 3 (as defined in the Uniform Building Code) may be considered as candidate structures. The criteria on which the limits of zone 3 were defined are being reviewed with a view to revising the seismic risk map. In the meantime, the existing map is being used as a guideline, and more recent geologic or seismic data are also considered.

Six bridges located in California, Alaska, and Nevada have been instrumented. In four cases, the instrumentation is of the type used in ground installations and for the instrumentation of buildings. Although this instrumentation is most appropriate for ground installations and may be used effectively in buildings, the dynamic characteristics of bridge structures and the relative inaccessibility of the desired measurement points make this instrumentation undesirable for use on bridges. The most recently installed instrumentation on bridge structures uses a central recording station tied to appropriately located remote accelerometers. This system has the following advantages:

1. The periodic maintenance is confined to the central recording station, which may be located for convenient access;
2. Single- or multiple-axis accelerometers may be located at specific and perhaps relatively inaccessible locations;
3. Appropriate acceleration traces may be placed on the same record for interpretation of the phase relations between traces; and
4. The same system may be used to record "down-hole" accelerations if this is desired because of the site conditions.

One remote transducer-central recording system has proved suitable for bridge instrumentation, and others are being evaluated.

Early accelerographs recorded on paper, but the newer instruments record on film. Film recording provides a record that is more permanent than paper and is adaptable to automatic digitization, which could be important in processing the records from a large bridge structure. The analog tape recording accelerograph systems that have been developed were found to have a smaller dynamic range than the film recording systems. Two direct digital recording systems have been commercially developed specifically for measuring strong-motion accelerations. The suitability of these systems is being evaluated, and they may be found to be the most appropriate systems when numerous channels of data are to be obtained from a structure in a seismically active area.

INTERPRETATION OF ACCELEROGRAPH RECORDS

The primary purpose of installing strong-motion instrumentation in structures is to provide a means to verify and improve the techniques for analytically modeling the dynamic characteristics of the structures. In particular, it provides the only means for evaluating the appropriate levels of modal damping to be used for modeling this parameter at the levels of response experienced during a strong earthquake (10).

With the limited number of installations, only one record of small-amplitude response of a bridge structure to an earthquake has been obtained to date. Instruments on the interchange of I-5 and Calif-14 near San Fernando, California, recorded the motion at ground level and at the top of one column of this structure during the 1973 Point Mugu earthquake. These records are shown in Figure 2. This structure was damaged during the 1971 San Fernando earthquake and had not been completed at the time of the Point Mugu earthquake. Imbsen and Gates (11) have attempted to correlate the measured

Figure 1. National Strong-Motion Instrumentation Network, 1974.

Figure 2. Accelerograms from interchange of Interstate and Calif-14 during Point Mugu earthquake.

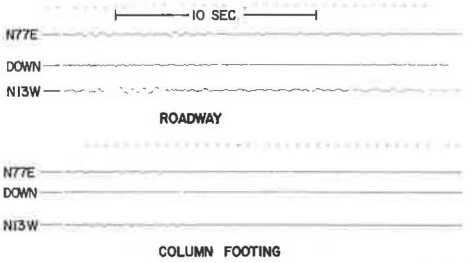

Figure 3. Accelerograms from 8244 Orion Boulevard during San Fernando earthquake.

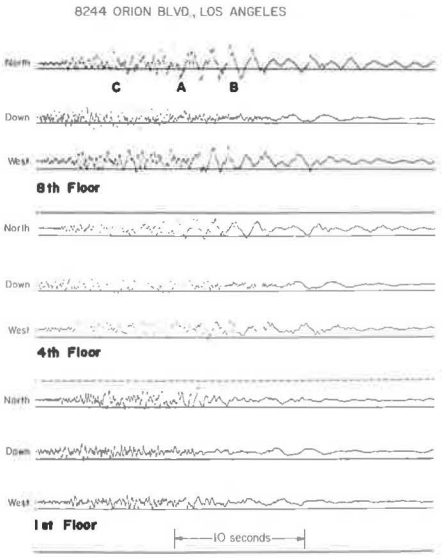

Figure 4. First mode shape for 8244 Orion Boulevard during San Fernando earthquake.

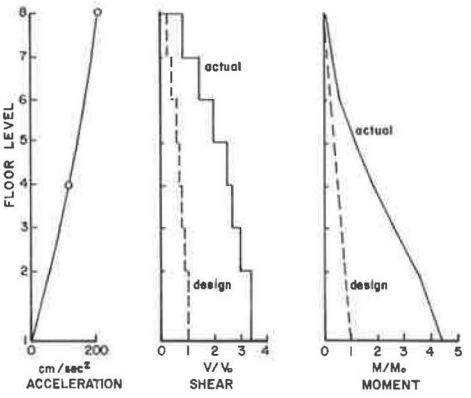

Figure 5. Second mode shape for 8244 Orion Boulevard during San Fernando earthquake.

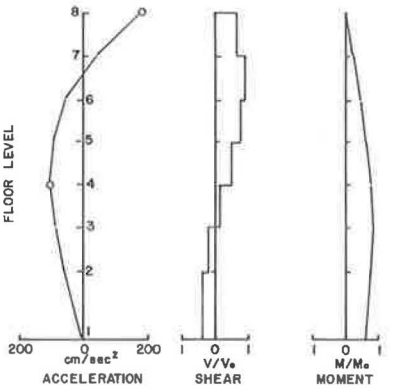

response with the response calculated from a dynamic analysis of the structure by using the measured input. Although the correlation was not so close as desired, the results did suggest methods for improving the modeling of the structure, particularly damping and modeling of the intermediate hinges at expansion joints. Since completion of the structure, the instrumentation is not accessible for maintenance.

As an illustration of the nature of the records to be expected from this instrumentation program and a simple interpretation that can be made if the structure is adequately instrumented, the response during the San Fernando earthquake of a seven-story reinforced-concrete building with a moment-resistant frame in the exterior walls is discussed. Accelerograph records from the roof (eighth level), the fourth floor, and the ground floor are shown in Figure 3. The maximum ground accelerations at this site were 0.27 *g* in the north-south direction, 0.14 *g* in the east-west direction, and 0.17 *g* in the vertical direction. In the later part of the ground motion record, a long period wave with strong vertical and east-west motion and lesser north-south motion is clearly a strong surface wave.

The records from the fourth floor and the roof contain more distinct frequency components than the record from the ground, inasmuch as the building amplifies the motion at frequencies corresponding to its natural frequencies. In the earlier parts of the records of lateral motion from the roof and fourth floor, the response is entirely in the higher modes. The first mode response becomes apparent about 8 sec after the start of the record. In the north-south record from the roof, a change in the first mode period may be noted at the point labeled A about 11 sec from the start of the record. At this point, the response is a combination of the first and second modes. The first mode period lengthens from about 1.0 to about 1.5 sec. It is thought that the damage to the building occurred at this point in time. The maximum response in the first mode occurs somewhat later in time at about point B.

For response in the north-south direction, the maximum accelerations in the first mode of 0.21 *g* at the roof and 0.12 *g* at the fourth floor were used to draw a first mode shape (Figure 4). By multiplying the indicated accelerations at each level by the values of floor weight used in the design, the lateral forces that correspond to first mode response are obtained and story shears and moments may be determined. A comparison of shears and moments to the values used in design is shown in Figure 4 for each floor level and indicates that the structure experienced first mode forces significantly greater than the design values.

The maximum response in the second mode was estimated to have occurred at point C (Figure 3). A procedure similar to that used to obtain first mode response was used to obtain the lateral forces corresponding to the maximum response in the second mode (Figure 5). The results for the second mode should not be added to those for the first mode because the two maximums did not occur at the same point in time, although both were close to their maximums at point A (Figure 3).

This interpretation points up the importance of understanding the dynamic characteristics of the system, in particular the mode shapes, when the locations for the instrumentation on a structure are selected. Because the response can be characterized by the natural modes of vibration, the instrumentation must be located away from the node points of any of the modes that may contribute to the column shears and moments. Although not illustrated by this example, it is important to locate the instrumentation such that lateral and torsional modes can be separated. The modal frequencies are generally more closely spaced in bridge structures than in buildings. This factor can complicate the analysis and implies that more extensive instrumentation is required. For bridge structures with numerous expansion joints, adjacent sections should be instrumented so that the relative motions across the expansion joints can be evaluated. This motion may be associated with the damping of the systems response. For long-span structures, intermediate locations along the deck may have to be instrumented.

CONCLUSION

If structures are to be monitored through use of strong-motion instrumentation, their

dynamic response must be understood when the instrumentation program is planned, although certain standard procedures for instrumentation of each class of bridge may evolve from a coordinated program. The coordination of the various state programs into a Highway Bridge Seismic Network to form a part of the existing National Strong-Motion Instrumentation Network is expected to provide the data necessary to improve seismic design practice for bridge structures.

REFERENCES

1. The San Fernando, California, Earthquake of February 9, 1971. U.S. Geological Survey, Prof. Paper 733, 1971.
2. P. C. Jennings, ed. Engineering Features of the San Fernando Earthquake, February 9, 1971. California Institute of Technology, EERL 71-02, June 1971.
3. Committee on Earthquake Engineering Research. Earthquake Engineering Research. National Academy of Sciences, 1969.
4. Committee on the Effect of the Earthquake on Highway Structures. The Effects of the San Francisco Earthquake of April 18, 1906, on Engineering Constructions. Trans. ASCE, Vol. 59, No. 263, 1907.
5. R. Kachadoorian. Effects of the Earthquake of March 27, 1964, on the Alaska Highway System. U.S. Geological Survey, Prof. Paper 545-C, 1968.
6. C. M. Duke. Foundations and Earth Structures in Earthquakes. Proc. Second World Conference on Earthquake Engineering, Tokyo, July 1960.
7. H. Kawasumi, ed. General Report on the Niigata Earthquake of 1964. Tokyo Electrical Engineering College Press, 1968.
8. D. S. Carder, ed. Earthquake Investigations in the Western United States, 1931-1964. U.S. Department of Commerce, Publ. 41-2, 1964.
9. S. T. Algermissen. Seismic Risk Studies in the United States. Proc. Fourth World Conference on Earthquake Engineering, Santiago, Chile, Jan. 1969.
10. G. C. Hart and R. Vasudevan. Earthquake Design of Buildings: Damping. Journal of Structural Division, ASCE, 1974.
11. R. Imbsen and J. Gates. Recent Innovations in Seismic Design and Analysis Techniques for Bridge Structures. Proc., 42nd Annual Conference of SEAOC, Oct. 1973.

PRACTICAL RETROFIT MEASURES TO IMPROVE THE SEISMIC PERFORMANCE OF EXISTING HIGHWAY BRIDGES

Eberhardt Privitzer and R. R. Robinson, IIT Research Institute, Chicago; and
J. D. Cooper, Federal Highway Administration

A conclusion of the studies of the earthquakes in Alaska in 1964 and San Fernando in 1971 was that to design a bridge to entirely resist the effects of strong-motion seismic loading is both impractical and uneconomical. Interest in retrofitting existing highway bridges to minimize such damage increased dramatically after the San Fernando earthquake, which caused extensive damage to the California freeway system, including bridges under construction and those newly completed. Cost-effective retrofit measures can be practically and economically implemented and have the effect of minimizing damage resulting from strong-motion seismic loading rather than eliminating it entirely. This paper describes various types of retrofit measures and discusses a numerical seismic method of analyzing their effectiveness. A bridge in northern California, a region of high seismic activity, is described and analyzed. The bridge is mathematically modeled as a three-dimensional space frame and is subjected to a hypothetical earthquake in the form of ground surface displacement time histories based on a statistical evaluation of the seismicity of the site. The bridge is first analyzed as built to determine whether retrofitting is necessary and, if so, the failed components. The candidate retrofit measure is then incorporated into the bridge model, and the analysis is performed again. Results from both cases in the form of displacement and force-time history plots are presented and discussed, and the performance of the retrofit measure is evaluated.

•ON MARCH 25, 1964, south-central Alaska, one of the most active seismic regions in the world, suffered an earthquake of unusually large magnitude: between 8.3 and 8.6 on the Richter scale. The engineers who inspected the highway system after the earthquake concluded that to design a bridge to totally resist the effects of strong-motion seismic loading is both impractical and uneconomical (1).

The San Fernando earthquake of February 9, 1971, although of a much lower magnitude (approximately 6.6), caused considerable damage to freeway structures. A report of the damage sustained by these structures during the earthquake (2) recommended that overpasses and bridges in areas not affected by the earthquake be reexamined to determine their seismic resistance and, if necessary, that they be modified to at least prevent collapse in the event of strong seismic loading. As a result of the San Fernando earthquake investigations, the California Department of Transportation established a $5 million retrofit program to increase the seismic resistance of 120 bridges by introducing relative longitudinal motion restrainers at points of discontinuity (i.e., hinges and bearing seats) in the superstructure (Figure 1).

Interest in retrofitting highway bridges to increase their seismic resistance has become fairly widespread since the San Fernando earthquake. Outside of California, no retrofit measures have been implemented on existing bridges. The damages sustained by bridges in both the Alaska and San Fernando earthquakes and conclusions based on postearthquake inspections indicate that, if areas of potentially low seismic resistance on a bridge could be practically and economically modified to restrict earthquake damage, the savings of money and possibly lives after just one severe earthquake would easily outweigh the cost of retrofitting. Obviously, in regions of great seismicity (a

Figure 1. California hinge restrainer type C2.

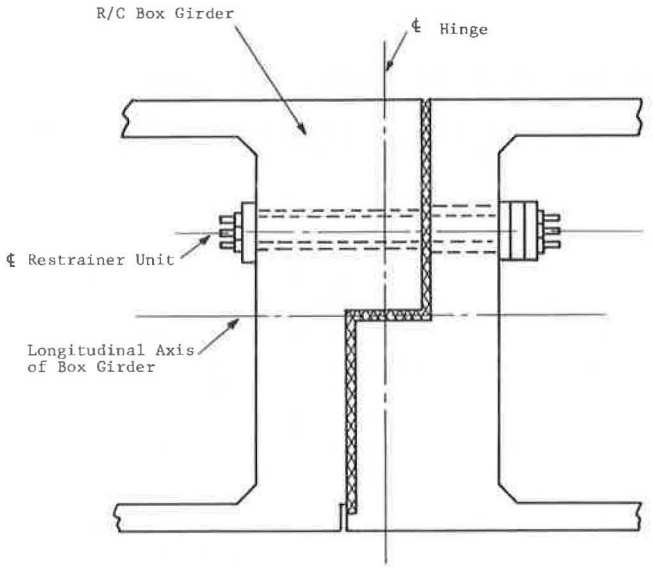

Figure 2. Relative longitudinal motion restrainer and high-strength cable for preventing uplift of superstructure.

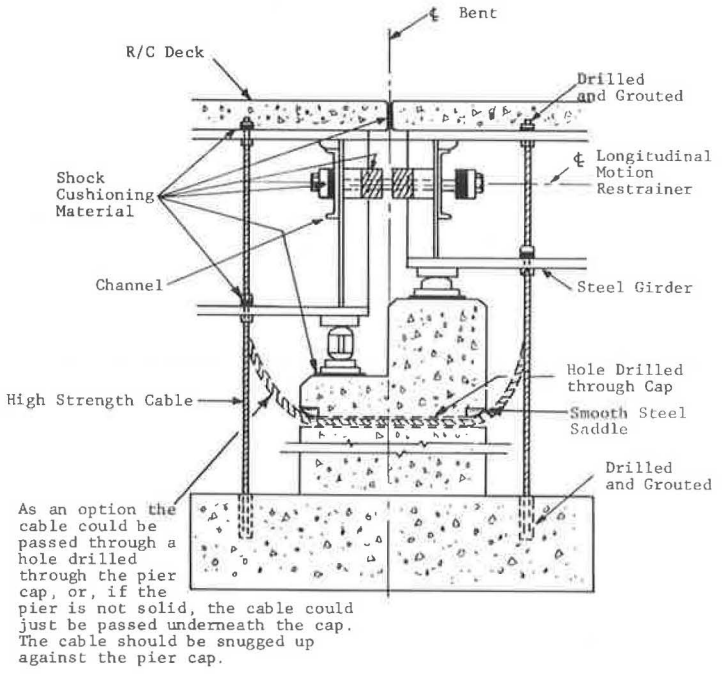

function of the frequency of occurrence and the magnitude of earthquakes) the possible benefits are great.

Before any bridge is retrofitted, decisions must be made on whether the bridge actually needs retrofitting and, if it does, what types of retrofit measures to use. For a retrofit measure to be cost effective, it must be both practical and economically feasible to use, and its purpose is to minimize damage rather than to eliminate it entirely. One method for determining whether a bridge needs retrofitting is a numerical seismic analysis of the candidate bridge subjected to a hypothetical earthquake based on the seismicity of the bridge locality (unless the bridge can be analyzed by thoroughly inspecting the bridge details). If the analysis indicates that some type of critical failure (extensive enough so that the bridge could not remain in even emergency use) will occur, the retrofit measure should be based on the mode and extent of failure. Strengthening a component that is susceptible to a particular mode of seismic damage may actually lead to a different mode of failure or possibly to failure of another component. For example, a bridge may experience large relative longitudinal displacements between spans or at the abutments. Reducing these displacements by some type of longitudinal motion restrainer can increase the seismic loading of an intermediate support, which may fail and, in turn, lead to failure of the superstructure. The retrofit measure selected should be incorporated into the numerical bridge model, and the model should again be subjected to seismic loading to check its effectiveness in minimizing damage.

RETROFIT MEASURES

A retrofit measure is any means of increasing the seismic resistance of an existing bridge. There are many ways to do this; the problem is to find those that are cost effective. The following retrofit measures are being investigated (3):

1. Restricting longitudinal, vertical, and lateral relative displacements of the superstructure at expansion joints, bearing seats, and so on by means of cables, tie bars, shear keys, extra anchor bolts, and metal stoppers (Figure 2);
2. Restricting rigid body motion of the superstructure by connecting it (e.g., with high-strength steel cables as in Figure 2) to a supporting or an adjacent foundation or pier cap, by enlarging bearing areas, or by placing stoppers at edges of bearing areas;
3. Reducing induced vibrations by installing energy absorbing devices such as elastomeric bearing pads at bearing seats or adapting the new Japanese shock absorber type of damper that allows slow movement, such as displacement due to creep, shrinkage, and temperature change, with negligible resistance but that develops a large resistance in the case of a rapid displacement, i.e., high velocity, such as that caused by an earthquake (4) (Figure 3); and
4. Strengthening supporting structures.

As a specific example of item 4, the strength of an existing column can be increased by adding longitudinal and spiral reinforcement to the exterior of the column and then bonding the added reinforcement with a new layer of high-strength concrete by using pressure grouting procedures or gunite. The additional longitudinal reinforcement can also be extended into the cap and the footing, and thus the flexural strength of the column-to-cap and column-to-footing connections is increased (Figure 4).

These are not the only methods of cost-effective retrofitting. Numerical seismic analysis, based on the finite element method, allows us to approximate the differential equations of motion for a structure by a system of linear algebraic equations. The degree of accuracy attainable is limited by factors such as the time and money available; hence, the determining test of the cost effectiveness of some retrofit measures may be their performance during actual seismic loading.

Using the shaking table to test retrofit devices will probably be proposed in the near future. Such testing will require that the bridge, or a portion thereof, be modeled along with the retrofit device. Again, time and money are the factors to be considered. The time involved in the mathematical modeling of a bridge is considerably less than that

Figure 3. Possible adaptation of Japanese shock absorber type of damper.

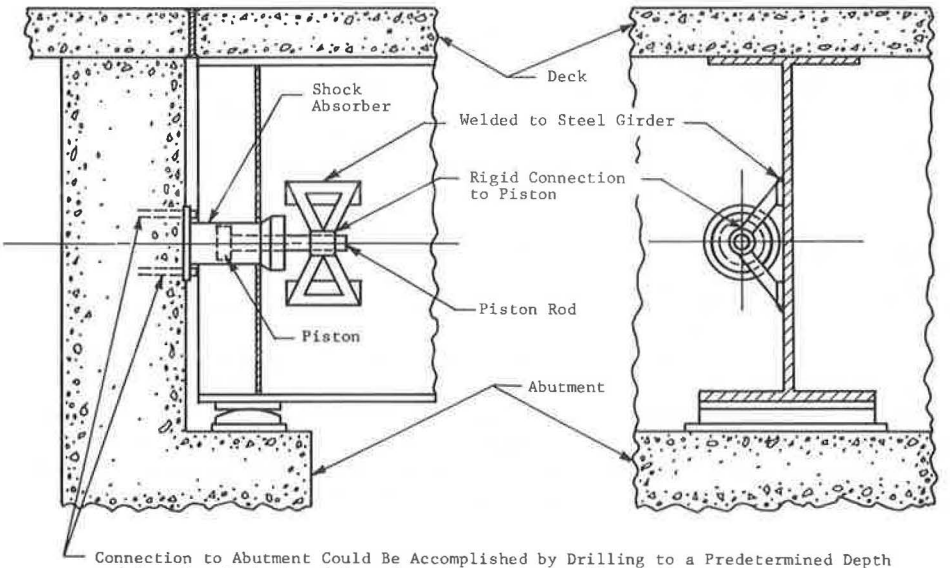

Figure 4. Strengthening of column.

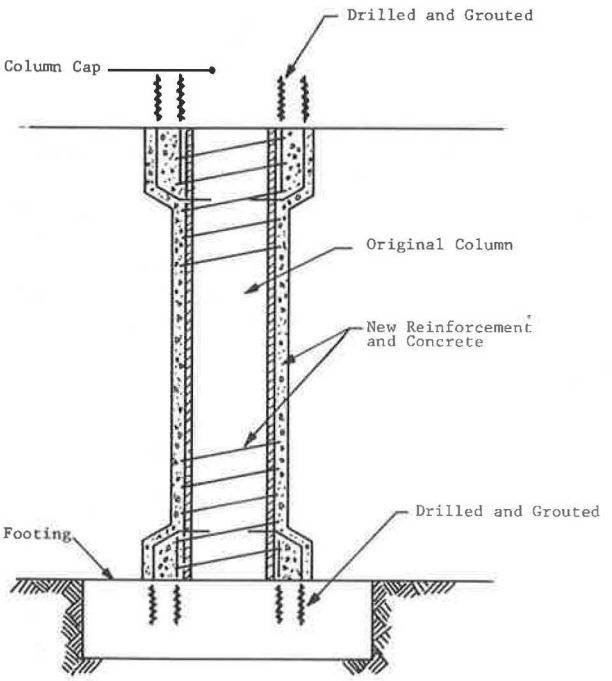

required to make a realistic scale model of the whole bridge or even of just selected portions of interest. Constructing a physical model of only a portion of a bridge eliminates the ability to see how different parts of the bridge interact with each other, which is important in determining the cost effectiveness of a retrofit measure. After the mathematical model of the bridge is completed, relatively little time is required to incorporate various retrofit measures into the model. Aside from the difficulty of modeling a bridge for shaking table testing, there is also the problem of applying realistic seismic loading. The problem is not difficult numerically, but with a shaking table it requires inducing three independent directions of translational motion, which, to the authors' knowledge, cannot be achieved by any existing shaking tables.

A shaking table test could be used to check the results of a numerical analysis. If a mathematically modeled bridge were subjected to the type of motion reproducible by a shaking table, the response should be the same from both tests. Hence, shaking table testing could have an important role in the development of seismic analysis computer programs.

APPLICATION OF TECHNIQUE

The bridge chosen for the analysis, one of seven currently being studied (3), is the Bahia Overcrossing, bridge number 23-161, near Benecia, California (Figure 5). It is a two-span continuously reinforced concrete box girder, built-in at the abutments, with a single-column reinforced concrete bent [3 by 8-ft (0.9 by 2.4-m) cross section] as the intermediate support. The stub abutments are founded on a single row of piles with enough flexibility to allow for normal longitudinal movement. The intermediate support is founded on pile footing. The soil of the bridge site consists primarily of loose to dense dark brown silt with some fine to coarse sand and gravel.

The hypothetical earthquake used in the bridge analysis was generated by a procedure (3) that, based on a statistical evaluation of the seismicity of the bridge site, results in simulated ground surface displacement time histories (Figure 6). Figures 7 through 9 show selected displacement, force, and moment time histories resulting from the seismic analysis of the unretrofitted bridge. When these results were compared with previously calculated ultimate moments, shear, and axial forces, the internal bending moment near the top of the column about the lateral axis of the structure approached and exceeded the ultimate value (the largest magnitude attained was 120 percent of the ultimate) repeatedly for approximately 16 sec corresponding to the period of strongest vertical and horizontal motion. The axial force in the superstructure repeatedly approached the calculated ultimate during this same time interval, but this is not deemed to be a serious threat to the structural integrity of the bridge.

It should be noted that the computed ultimate bending moment was based on the assumption that the column was under pure bending. This results in a lower ultimate than one based on combined axial and bending loading, which is actually the case. To determine the effectiveness of the retrofit measure, however, we will assume that the column failed in flexure. The area most vulnerable to damage is the top portion of the column. An immediate retrofit measure is to strengthen the column by using the method shown in Figure 4. Figure 10 shows the time history plot of the internal bending moment near the top of the retrofitted column. The largest magnitude attained is 88 percent of the computed ultimate bending moment for the retrofitted column. Adding longitudinal reinforcing bars and concrete to the exterior of the column leads to an increase in the maximum bending moment of the column during the hypothetical seismic loading. The ratio of the moment for the retrofitted case to the unretrofitted is 1.19. At the same time, the retrofit leads to a 61 percent increase in the computed ultimate bending moment; the ratio of the retrofitted case to the unretrofitted was 1.61. There was essentially no increase in the internal forces for the unretrofitted portions of the structure, i.e., the superstructure.

Figure 5. Bahia Overcrossing, 5 miles (8 km) northwest of Benecia, California.

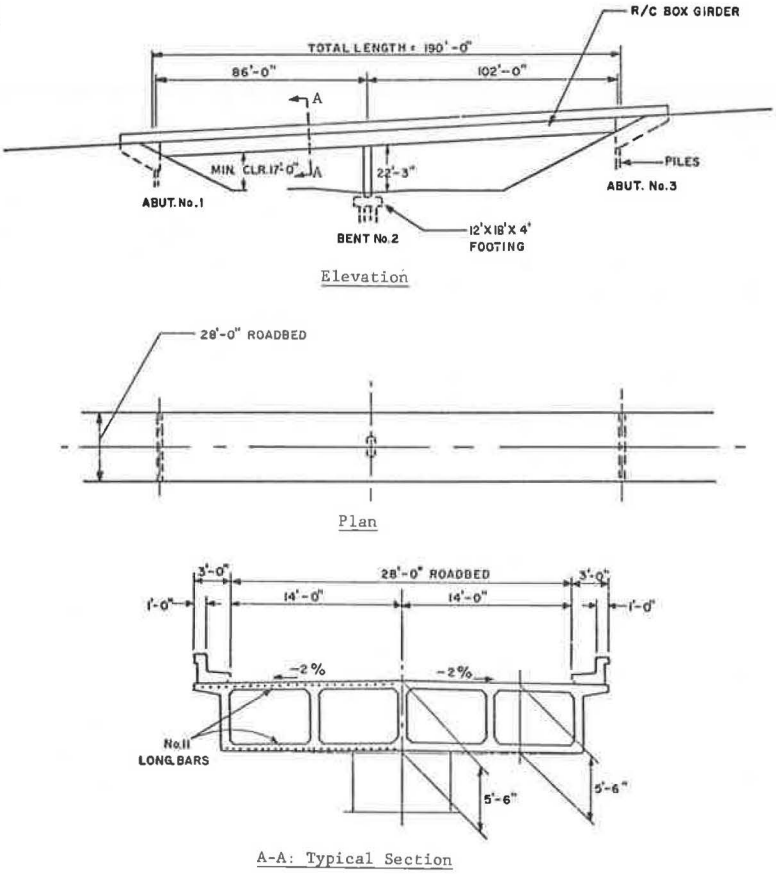

Figure 6. Seismic characteristics of bridge site.

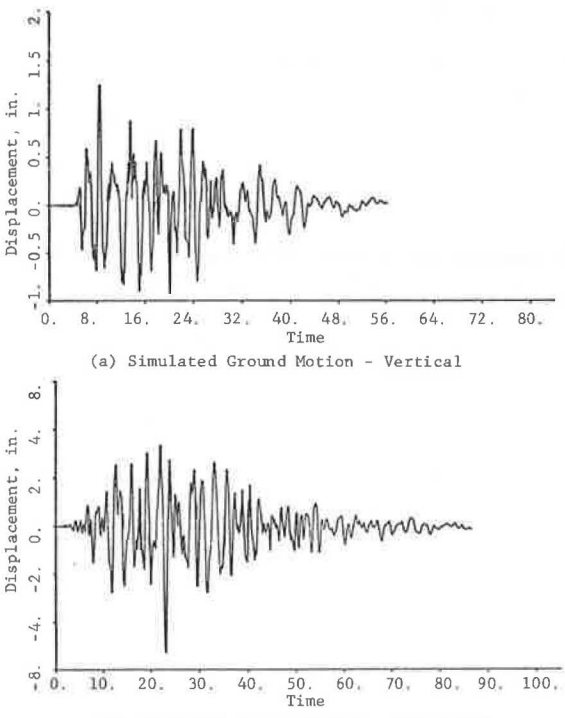

Engineering Seismicity: 5.295
Richter Magnitude: 8.10
Maximum Horizontal Ground Displacement (inches): 5.25
Maximum Vertical Ground Displacement (inches): 1.25

Figure 7. Vertical displacement at middle of span 1 over time.

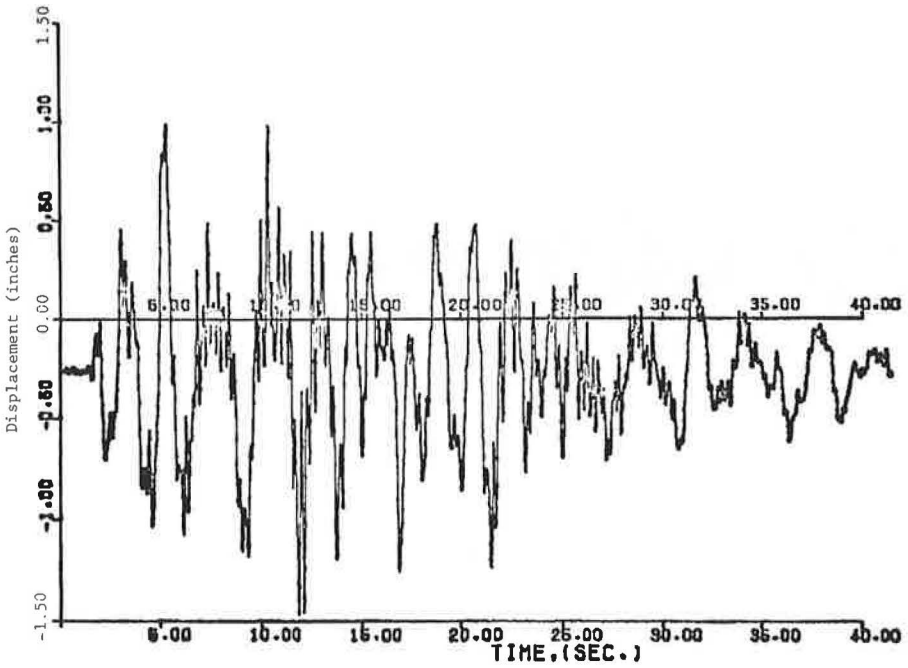

Figure 8. Axial force in superstructure over time.

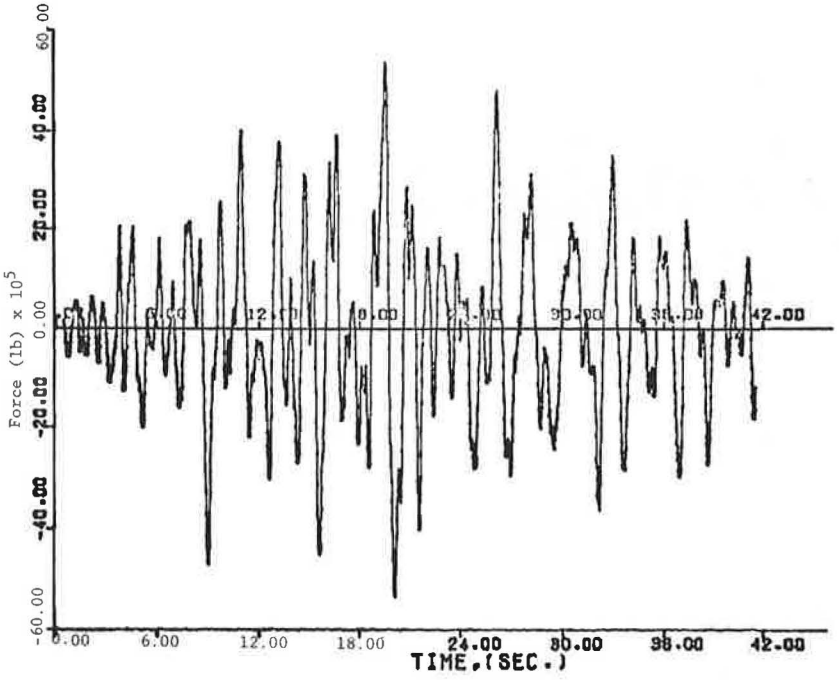

Figure 9. Bending moment at top of column over time.

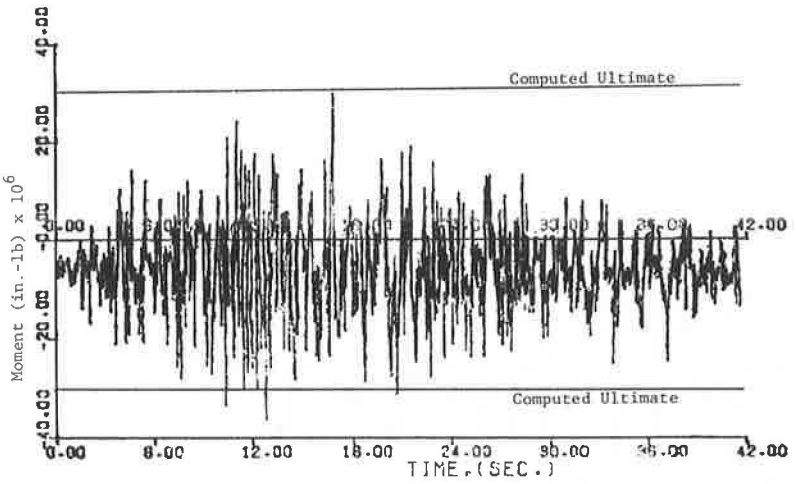

Figure 10. Bending moment at top of retrofitted column over time.

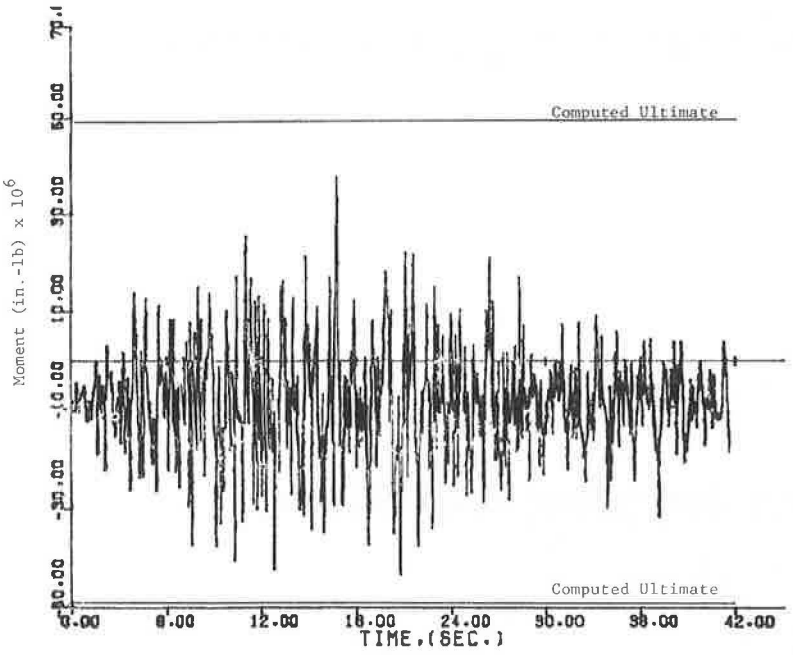

SUMMARY AND CONCLUSIONS

Designing a bridge to totally resist damage caused by strong-motion seismic loading is both impractical and uneconomical. If areas of potentially low seismic resistance on an existing bridge could be practically and economically modified (retrofitted) to restrict earthquake damage, the saving of money (and possibly lives) after just one severe earthquake would easily outweigh the cost of retrofitting.

When a mathematically modeled bridge was subjected to a hypothetical earthquake, an area of possible failure was the top portion of the column, where the bending moment

(about the lateral axis of the structure) attained a value 20 percent greater than the computed ultimate. After the model was altered to simulate the strengthening of the column by using the method shown in Figure 4, the bending moment of the retrofitted column reached a peak value of 88 percent of the computed ultimate for the retrofitted column. This, combined with the observation that the structural integrity of the superstructure was not affected by the retrofit, leads to the conclusion that, for this bridge, strengthening the column by adding longitudinal reinforcing bars and concrete to the exterior of the existing column is an effective retrofit measure. Also, because interference with traffic would be minimal and the cost would be fairly low, we can say that this is a cost-effective retrofit measure for this bridge.

REFERENCES

1. G. G. Sturman. The Alaska Highway System. In The Great Alaska Earthquake of 1964: Engineering, National Academy of Sciences, Washington, D.C., 1973.
2. P. C. Jennings and J. H. Wood. Earthquake Damage to Freeway Structures. Engineering Features of the San Fernando Earthquake of February 9, 1971, Rept. EERL 71-02, June 1971.
3. Techniques for Retrofitting Existing Bridges to Reduce Susceptibility to Earthquake Damage. IIT Research Institute, Project J6320, in progress.
4. S. Inomata. Japanese Practice in Seismic Design of Prestressed Bridges. PCI Journal, July-Aug. 1972.

SEISMIC RESPONSE OF A CURVED HIGHWAY BRIDGE MODEL

D. Williams and W. G. Godden, University of California, Berkeley

This paper reports research on a model relating to the seismic resistance of large multispan curved overcrossings. The feasibility of developing a model that satisfies the necessary similitude requirements of such a complex structure and that is also capable of being tested on the 20 by 20-ft (6.1 by 6.1-m) shaking table is outlined. The small-amplitude dynamic characteristics of the 1:30 scale model of a hypothetical prototype are examined, and for this elastic range the experimental results compared satisfactorily with those obtained analytically. The response of the microconcrete model to a progressively more intense simulated seismic excitation applied horizontally in the asymmetric direction is described. The severe damage at the expansion joints during strong excitation is outlined, and ways of reducing such damage are suggested. The influence of expansion joint design on the seismic behavior points to the need for joint restrainers, of adequate ductility, to tie adjacent girders together.

•HISTORICALLY, highway bridges have proved particularly vulnerable to the action of strong-motion earthquakes (1). Many of these structures consisted of single- or multiple-span simple trusses or girders supported on massive piers and abutments. Damage was primarily due to foundation failure and often resulted in progressive collapse.

Even the more continuous designs of some modern bridge structures may be equally vulnerable to damage in earthquakes. In long, multiple-span, reinforced concrete bridge structures, the design of the expansion joints and the long columns has a profound influence on the structural integrity of the system under dynamic loading, and, because of the nonlinear discontinuous behavior of the deck, the dynamic characteristics are very complex. In short, stiffer bridges, foundation interaction effects become increasingly dominant; therefore, their seismic response is equally complex.

After the San Fernando earthquake on February 9, 1971 (1, 2), in which the just-completed South Connector Overcrossing at the interchange of I-5 and Calif-14 suffered damage and partial collapse (Figure 1), a comprehensive, multiphase research project sponsored by the Federal Highway Administration was initiated at the Earthquake Engineering Research Center, University of California, Berkeley. The aim of the project was to investigate the effectiveness of existing bridge design methodology in providing adequate structural resistance to seismic disturbances. Interim measures to correct certain design deficiencies were quickly undertaken after the earthquake (3); however, such structures are still designed mainly by using a static seismic coefficient method similar to that formerly used (4).

Phases 1 and 2 of the project were a literature survey of seismic effects on highway bridges and an analysis of the seismic response of long, multispan highway bridges. The results of these phases have recently been published (1, 5). Phase 3, an analysis of short, stiff highway bridges, will be published shortly (6). Phase 4, which supplements the analytical investigation of phase 2, is the subject of this paper, and a detailed report on this subject is in preparation (7).

The major objectives of phase 4 were to perform detailed model experiments on a shaking table to identify and examine the parameters affecting the seismic response of large, curved multispan overcrossings so that experimental dynamic response data can be generated with which to verify the validity of response predictions.

Other objectives of phase 4 were to investigate those concepts that were difficult to model analytically and to construct a model from prefabricated components with sufficient versatility to allow a variety of tests to be undertaken with the same basic model.

One limitation of this model is that the base excitation represents rigid ground motion over the entire table; hence, there is no means of simulating the spatial effects of ground motion.

FEASIBILITY STUDY

Initially the feasibility of undertaking model studies of the complete South Connector Overcrossing on the shaking table at Berkeley was examined. This structure (Figure 2) is typical of modern large curved highway bridges and, because of its partial collapse, has been the subject of considerable interest following the San Fernando earthquake. Essentially, it was four curved reinforced concrete or prestressed concrete box girders with a total span of 1,349 ft (411 m), separated by expansion joints, and supported on a single line of massive columns varying in height from 15 to 140 ft (4.6 to 43 m). Table 1 gives the first seven natural frequencies of the prototype for two expansion joint conditions: zero friction in the axial direction and fully locked joint.

The 20 by 20-ft (6.1 by 6.1-m) shaking table made from reinforced and posttensioned concrete weighs 100 kips (45 Mg) and is driven by hydraulic actuators in the vertical direction and one in the horizontal direction (8, 9). The acceleration response spectra for harmonic motion of the unloaded table are shown in Figure 3. The typical operating frequency range is 0 to 10 Hz. For relatively light test structures of less than 10 kips (4540 kg), these response values are reduced very little.

Because of the large geometric and time scale factors that would be required to model the complex dynamic behavior of this particular overcrossing, modeling the complete structure on the shaking table was not considered feasible. However, an analytical study of the natural frequencies and mode shapes of the prototype (5) suggested that the west half of the bridge, which was supported on short columns, contributed very little to the dynamic response of the complete bridge. Accordingly, a smaller hypothetical prototype that incorporated the important features of the east half was modeled. Hence, this structure, which terminated in an abutment at each end, included the expansion joints, the deck curvature, and the long columns. It was designed in such a way that the lower mode shapes and frequencies were similar to those of the prototype bridge. Moreover, because scaling effects in the dynamic response of small concrete models are unknown, the model was considered primarily as a small structure, and its behavior was correlated with analytical studies. For this reason, the system was idealized further by making it symmetrical and by making the columns of equal length (Figure 4). Ideally the model should be subjected to a realistic seismic excitation; and, because of limitations in the performance of the shaking table, a frequency ratio of about 1 should be adopted. Unfortunately in this nonlinear study, scale effects made this impracticable.

Another major problem in modeling a system of this kind is satisfying the requirements of bringing all inertial forces, including gravitational forces, into the same force scale. Given the complexity of the structure and the nonlinear response characteristics due to sliding, impacting, cracking, and yielding, a true-scale weight-distorted model made in prototype material was considered the best compromise solution.

The model adopted had a geometric scale of $L_r = 1/30$. To maintain a force ratio of $F_r = L_r^2$ required that a substantial amount of lead weight be added. The resulting time ratio was $T_r = \sqrt{L_r} = 1/5.5$; the acceleration ratio between model and prototype was then $a_r = 1$. This model closely resembled the central portion of the prototype bridge (piers 2 through 6). Analytical studies confirmed that this model adequately reproduced the lower natural frequencies and mode shapes of a scaled version of the prototype.

Table 1 gives frequencies computed by the linear dynamic analysis program BSAP (5) for the following systems: the prototype of zero friction in the axial direction and infinite friction, the prototype for these two values scaled to a frequency ratio of 5.5, the model as designed, and the model with revised boundary and expansion joint conditions. The differences between the last two sets of values are discussed later.

Figure 1. South Connector Overcrossing after San Fernando earthquake.

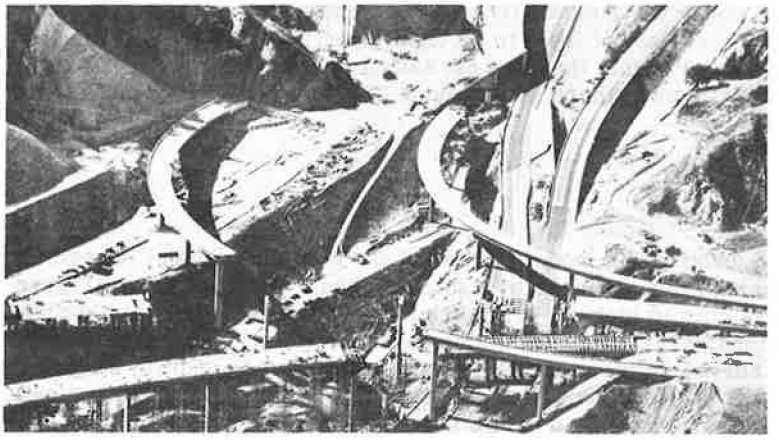

Figure 2. Structural system of South Connector Overcrossing.

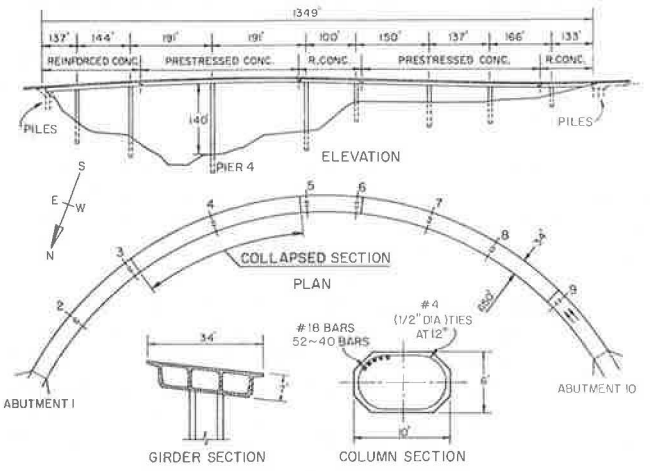

Table 1. Computed natural frequencies (in hertz) at joint friction of zero and infinity.

	Prototype		Scaled Prototype		Model			
					As Designed			
					0			
Mode	0	∞	0	∞	Roller[a]	Pinning[b]	∞	As Built
1	0.20	0.72	1.1	4.0	2.0	2.0	3.04	5.0
2	0.36	0.99	2.0	5.5	2.48	3.0	6.95	5.7
3	0.50	1.45	2.8	8.0	2.49	3.2	7.0	7.7
4	0.89	1.54	4.9	8.5	3.0	7.0	8.9	8.5
5	1.26	1.80	6.9	9.9	3.26	7.02	9.3	8.6
6	1.44	2.15						11.1
7	1.45	2.25						14.3

[a]Roller at abutments. [b]Pinned at abutments.

The earthquake excitation applied to the model was scaled to a frequency ratio f_r = 5.5. This required that the high-frequency component be filtered out, but the shaking table response spectra indicated that sufficient capability was available to ensure that all significant vibration modes of the structure could be adequately excited.

MODEL DESIGN AND CONSTRUCTION

In view of the time and expense of fabricating such a complex model in concrete and the desirability of gaining as much experimental data as possible from the same basic model, the model was assembled from replaceable components: deck, expansion joint, and column components. In this way damage could be isolated, and the damaged components could be either repaired or replaced. A view of the completed model on the shaking table is shown in Figure 5.

Superstructure

Except in the vicinity of the expansion joint where impact and large shear forces make damage unavoidable, it was desirable that the superstructure behave elastically for the large number of tests planned. To achieve this the section was overdesigned by a factor of approximately 2; the aim was to maintain steel stresses below 20 ksi (138 MPa). Although the prototype would normally be a multicell box girder section, a rectangular solid section with similarly scaled bending and torsional stiffnesses was adopted to avoid the difficulties associated with constructing a box girder on such a small scale. The dynamic response should not be sensitive to this difference.

The reinforcement and formwork are shown in Figure 6. The concrete used was a high-strength (8,000 psi or 55 MPa), shrinkage-resistant microconcrete to eliminate shrinkage cracking, which would adversely affect the damping characteristics of the model. The 10 by 3 by 2-in.-wide (254 by 76 by 51-mm) lead weights were attached by means of two bolts running through the deck to increase the weight of the superstructure to the required scale value. In this way the added weight contributed very little to deck stiffness, and extraneous damping was minimized.

Columns

The prototype column reinforcement is shown in Figure 2. If correctly modeled the test column should contain between 40 and 52 deformed bars of $\frac{1}{16}$-in. (1.5-mm) diameter, which should have the same stress-strain characteristics as the No. 18 (57-mm) prototype rebars. In an effort to accomplish this, suitable wires were deformed by both indentation and protrusion and then were subjected to a range of annealing conditions, but the resulting stress-strain properties were not completely satisfactory. To simplify matters, a column section of equivalent strength was designed by using four No. 2 (6-mm) rebars with a yield strength of 50 ksi (345 MPa). The steel was butt welded to the column end plates, and extra shear keys were provided to prevent premature failure by shear in these regions.

The columns were made by using a 4,500-psi (31-MPa) normal portland cement microconcrete. It has essentially the same stress-strain characteristics as plain prototype concrete except for the more gradual falling branch, which more closely resembles confined prototype concrete and probably reflects the greater tensile strength associated with microconcrete.

Inelastic cyclic bending tests of the column elements (Figure 7) confirm the validity of using this procedure to simulate the nonlinearity of well-designed prototype reinforced concrete columns. Reasonably stable behavior with acceptable stiffness deterioration is evident at a displacement ductility factor of 3, which could have been increased by more closely spaced stirrups. As designed, the lower 9 in. (229 mm) of the model columns had 16 gauge mild steel stirrups at $\frac{1}{2}$-in. (12.7-mm) centers.

Figure 3. Shaking table performance limits.

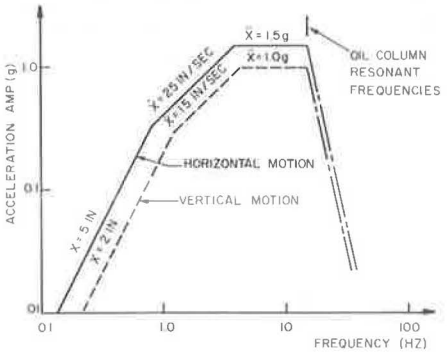

Figure 4. Schematic of test model.

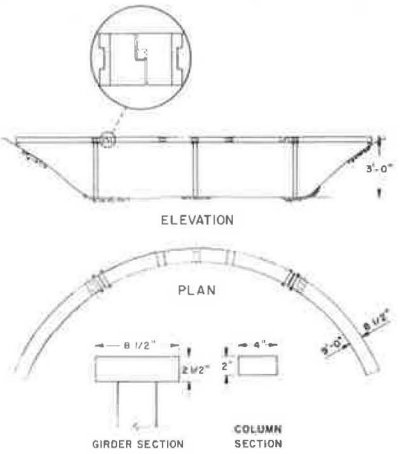

Figure 5. Completed model ready for testing.

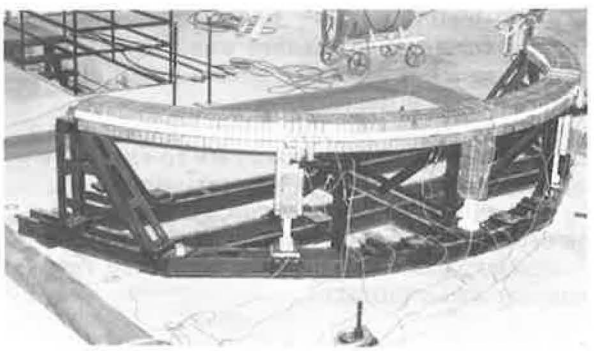

Figure 6. Model before casting.

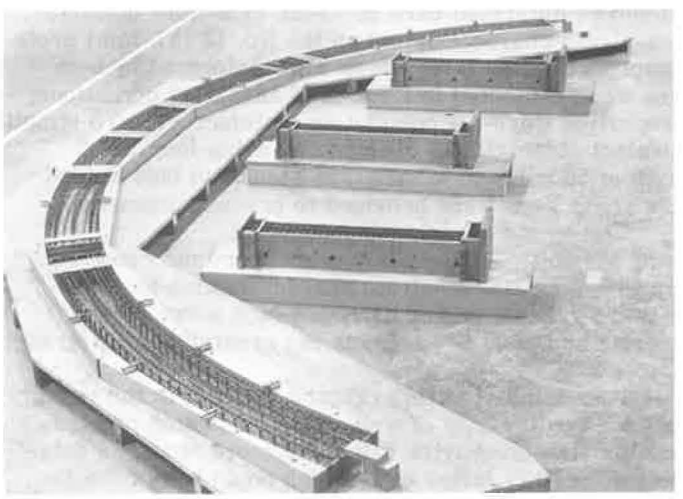

When the bridge system was assembled, the deck girders were clamped to the column heads, the close-fitting machined connection detail simulating a rigid joint.

Joint Restrainers

For the first test series the girders were tied together at the expansion joints by means of $5\frac{1}{2}$-in.-long by $\frac{3}{32}$-in.-diameter (140 by 2.4-mm) mild steel joint restrainers mounted on each side and parallel to the bridge axis. These restrainers had respective yield and ultimate strengths of approximately 420 and 475 lb (1870 and 2115 N) and yield and ultimate strain limits of 0.2 and 20 percent. This represents large ductile restraint.

DISCUSSION OF TEST RESULTS

Small-Amplitude Tests

Before the completed model was subjected to simulated seismic excitation, the dynamic characteristics of the model were studied under small-amplitude vibration. Mode shapes, frequencies, and damping ratios were ascertained from accelerometer measurements during free vibration.

The first mode (Figure 8), which is essentially longitudinal motion of the central girder-pier subsystem combined with antisymmetric motion in the horizontal plane at 5 Hz, was easily excited by hand. However, the second mode, which is essentially symmetric rigid body motion of the superstructure in the horizontal plane at 6.7 Hz, was difficult to excite manually and invariably reverted to the first mode, even in those cases where the symmetry of the mode was enforced by snapping tensioned cables attached to three points.

Based on free vibration decay tests of these two modes, a viscous damping of approximately 3 percent critical was obtained. Given the complexity of the system with the expansion joints and the large amount of added weight, this value was acceptable.

Knocking the head of the central column sharply by hand in the transverse direction excited mode 7, a symmetrical bending mode of the central girder in the horizontal plane at a frequency of 15 Hz (Figure 9). It was, in fact, excited more readily than mode 2.

Another symmetrical mode (mode 5), predominantly bending of the deck in the vertical plane (Figure 9) with a frequency of 11 Hz and a damping ratio of 2 percent critical, was excited by knocking the deck in the vertical direction. No effort was made to obtain the antisymmetric vertical bending modes inasmuch as these would not be excited with rigid base excitation.

Forced harmonic motion techniques in which the shaking table was used to provide a base motion were also applied to determine the small displacement dynamic response characteristics of the model. For the very small amplitude required, adequate control of the table is difficult to maintain in such a test, and this method is not considered very suitable for small models. Ideally, to determine mode shapes and frequencies for such a complex structure requires use of a multiple-channel shaker system in which several shakers can be placed on the structure and adjusted to produce predominant response in any natural mode.

When the model was assembled, the stiffness characteristics of the free-standing weighted columns after they had been securely attached to the base structure were checked. Results from free vibration tests in both principal directions on all three columns indicated that the measured stiffness was consistently 25 percent of that calculated by assuming full fixity at the base. This was confirmed by static load-deflection tests on the columns. Inasmuch as the calculated value of EI was substantiated by results from load-deflection tests on identical beam specimens, it was concluded that, in spite of the stiffness of the base system, base flexibility had a large effect and consequently would have to be taken into account for a more appropriate analysis. However, for the special purpose program, a reduced value of EI, which is more convenient and

Figure 7. Inelastic cyclic bending behavior of column element.

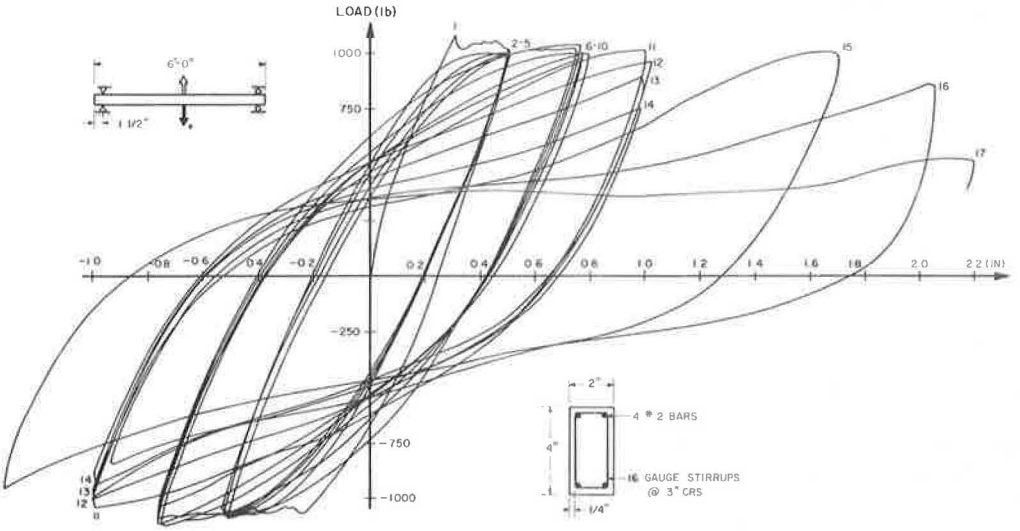

Figure 8. Fundamental mode shape of test structure.

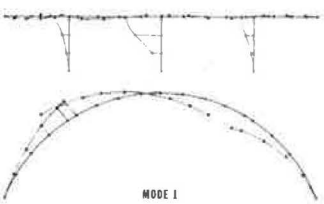

Figure 9. Characteristic shapes of modes 2 through 7.

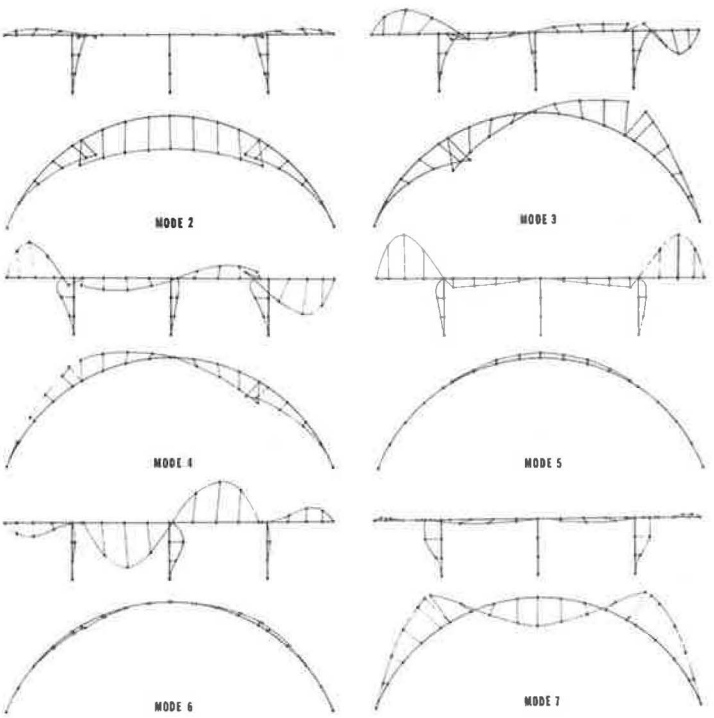

has essentially the same effect in the significant modes, was used.

Linear Dynamic Analyses

This information was used for the lumped parameter system and finite element idealization of the model shown in Figure 10; then, linear dynamic analyses were undertaken by using the computer program BSAP to determine the theoretical dynamic characteristics of the test structure.

When the experimental values were correlated with those calculated from the linear analysis, the importance of the spring stiffness provided by the elastomeric bearing pad at the expansion joint became evident. Initially only two joint conditions were provided for: zero friction in the axial direction and finite friction. During preliminary small-amplitude testing it was observed that, although motion took place at the expansion joints, sliding did not occur inasmuch as shear strain deformations in the elastomeric bearing pad at the hinge allowed relative rotation and translation to take place. The longitudinal shear and torsional stiffnesses of the pad were determined, and appropriate springs were incorporated into the mathematical model to allow for this behavior.

With this revision, model analyses were performed, and the frequencies (Table 1) and mode shapes (Figures 8 and 9) agreed closely with the experimental results.

Seismic Tests

The model was subsequently subjected to progressively more intense simulated seismic excitation applied horizontally in the asymmetric X-direction. The command excitation was artificially generated motion, the same as that used for postearthquake studies of the Olive View Hospital (10). It consists of a 2-sec parabolic buildup to 8 sec of strong motion, followed by exponential decay during the next 5 sec. Maximum spectral acceleration values occur for frequencies of 2.5 Hz. This motion was scaled in time to give 3 sec of excitation, and the actual table motion shown in Figure 11 is effectively filtered at 14 Hz by the hydraulic system. The real time-scaled accelerogram includes high-frequency components up to about 25 Hz, but based on response characteristics this difference should be insignificant.

During each test, data in the form of digitized linear variable differential transformer (LVDT) output were collected at 100 samples per second per channel on the data acquisition system (9). The LVDTs were mounted on a very stiff instrumentation framework so that the X- and Y-components of the relative global displacements near the points corresponding to nodes 9, 14, and 23 of the mathematical idealization (Figure 10) could be measured. The relative movement on each side of both expansion joints was similarly measured.

The sequence of tests showing peak base accelerations is given in Table 2. Typical response maxima for the X- and Y-components at the top of column 1 (node 9) and the X-component at the top of column 2 (node 14) are also included.

The response was essentially oscillatory motion in the first mode (Figure 8). Even in the final test where peak table accelerations reached 0.87 g this is still true, as shown by the response histories in Figure 11, although the response frequency was reduced to approximately 3.5 Hz.

In this test series the expansion joint suffered severe damage in the form of impact spalling of adjacent surfaces, major cracking of the hinge seat, and failure of the shear key (Figure 12). The joint restrainers had displacement ductility factor requirements of approximately 20.

The only damage to the columns was minor flexural cracking at the bases. Major damage was confined to the expansion joint zone, and although the joint restrainers were subjected to heavy ductility demands no catastrophic collapse occurred.

Figure 10. Lumped parameter analytical model.

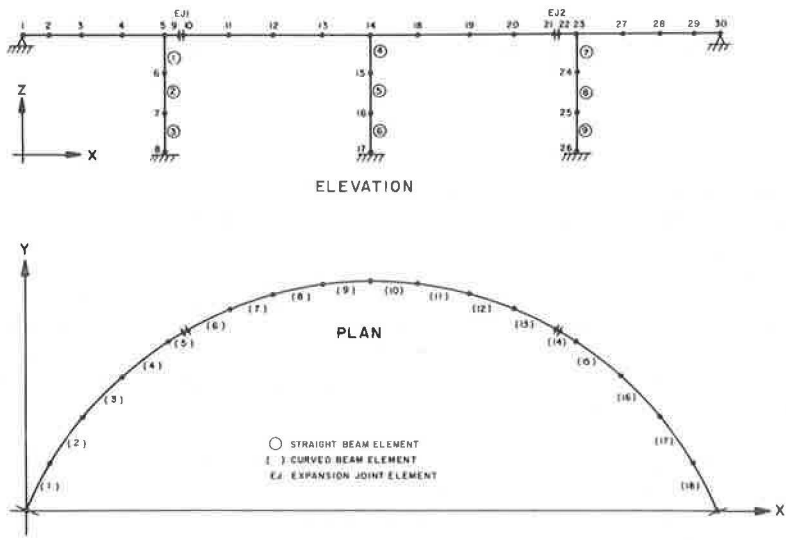

Figure 11. Response histories for final test.

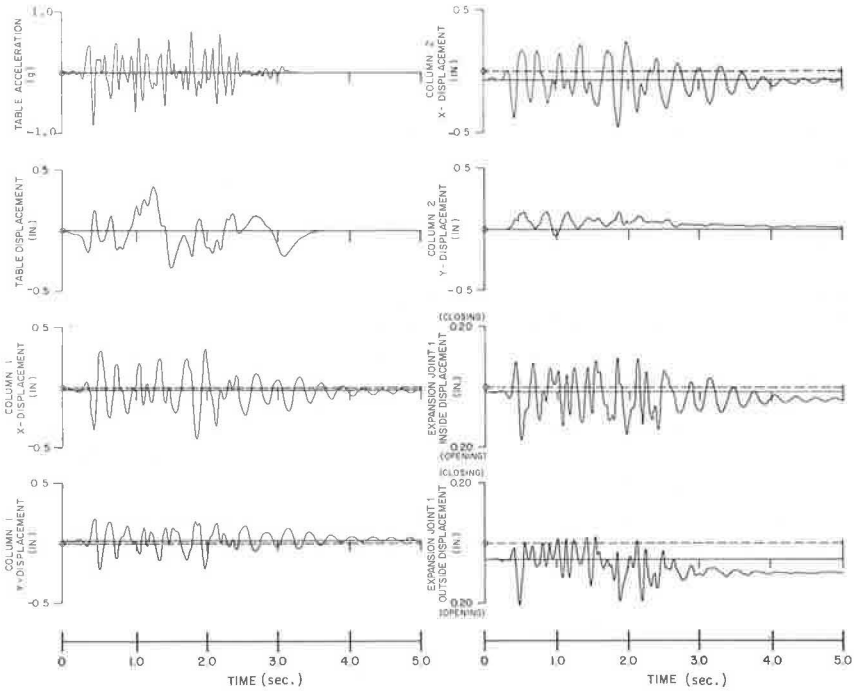

Table 2. Response maxima.

Test Number	Peak Table Acceleration (g)	Displacement (in.)		
		Column 1		
		X-Component	Y-Component	Column 2, X-Component
1	-0.06	0.03	0.02	0.03
2	-0.13	0.11	0.08	0.11
3	-0.23	0.17	0.12	0.18
4	-0.38	0.23	0.16	0.23
5	-0.60	0.37	0.20	0.32
6	-0.75	0.40	0.19	0.29
7	-0.87	0.42	0.21	0.31

Note: 1 in. = 25.4 mm.

Figure 12. Damaged expansion joint.

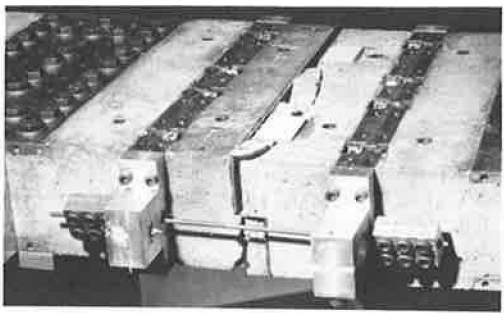

CONCLUSIONS

The results of the first series of tests indicated that, if adjacent girders are effectively tied together at the expansion joint with due regard to ductility demand, a bridge of this type should be capable of withstanding large seismic disturbances without major inelastic drift and without total collapse. However, inasmuch as the major damage in the bridge consistently occurred at the expansion joints because of impact and the high values of vertical and horizontal shears and torsion in this vicinity, special attention must be paid to the detailed design of the deck in this location. Because dynamic analyses of three-dimensional nonlinear systems are extremely difficult, further response data of both a qualitative and quantitative nature are essential to a better understanding of the dynamics of such complex structures and to the development and verification of theoretical analyses.

Continuing experimental work planned for this model includes the following series of tests.

1. The repaired model will be subjected to the simulated seismic excitation applied horizontally in the symmetric direction, both alone and also with simultaneous vertical excitation.
2. A parameter study of expansion joint design will be undertaken. Models incorporating hinge restrainers of various strength and expansion joints with collapsible sacrificial buffers will be tested.
3. The model will be retested in a four-column design, with the central girder supported on two columns.

ACKNOWLEDGMENTS

The work reported was sponsored by the Federal Highway Administration, U.S. Department of Transportation. The authors are grateful for the support and to James Cooper, FHWA, for his interest and cooperation.

The opinions expressed in this paper are those of the authors and do not necessarily reflect the official views of the Department of Transportation.

REFERENCES

1. T. Iwasaki, J. Penzien, and R. Clough. Literature Survey—Seismic Effects on Highway Bridges. Earthquake Engineering Research Center, Univ. of California, Berkeley, EERC 71-11, Nov., 1972.
2. P. C. Jennings. Engineering Features of the San Fernando Earthquake, February 9, 1971. Earthquake Engineering Research Laboratory, California Institute of Technology, EERL 71-20, June 1971.
3. Report on Evaluation and Modification of Earthquake Resistant Design Criteria. California Division of Highways, March 16, 1971.
4. Bridge Planning and Design Manual: Volume 1—Design Specifications. California Division of Highways, Nov. 1972, Sect. 2-25.
5. W. S. Tseng and J. Penzien. Analytical Investigations of the Seismic Response of Long, Multiple-Span Highway Bridges. Earthquake Engineering Research Center, Univ. of California, Berkeley, EERC 73-12, June 1973.

6. M. C. Chen and J. Penzien. Analytical Investigation of the Seismic Response of Short, Simple or Multiple-Span Highway Bridges. Earthquake Engineering Research Center, Univ. of California, Berkeley, in preparation.
7. D. Williams and W. G. Godden. Experimental Model Studies on the Seismic Response of High Curved Overcrossings. Earthquake Engineering Research Center, Univ. of California, Berkeley, in preparation.
8. D. Rea and J. Penzien. Dynamic Response of a 20 ft × 20 ft Shaking Table. Proc., Fifth World Conference on Earthquake Engineering, Rome, June 1973.
9. D. Rea and J. Penzien. Structural Research Using an Earthquake Simulator. Proc., Structural Engineers Association of California, Monterey, Oct. 1972.
10. A. K. Chopra, V. V. Bertero, and S. Mahin. Response of the Olive View Medical Center Main Building During the San Fernando Earthquake. Proc., Fifth World Conference on Earthquake Engineering, Rome, June 1973.

SEISMIC DESIGN CRITERIA FOR BRIDGES

Robert C. Cassano, Division of Structures, California Department of Transportation

After the earthquake at San Fernando on February 9, 1971, significant changes were made in structural details of bridges designed by the Division of Structures, California Department of Transportation. New seismic design criteria were developed that consider both fault proximity and local soil conditions. Response coefficient curves, which are a key element of these new criteria, were developed by determining average elastic response spectra for rock motion and then modifying these spectra to reflect the influence of soil conditions. Considerable engineering judgment was used in assessing ductility and acceptable risk so that the elastic curves could be scaled down to a desirable level for design. Response coefficient curves can be used to find suitable equivalent static force coefficients or as design spectra for use in a dynamic analysis of a response spectrum. The simplified design method is adequate for small structures, but a dynamic analysis is required to accurately predict the response of long, curved structures with intermediate hinges and widely varying column lengths.

PEOPLE have always been in awe of great earthquakes. The fear and confusion that they feel after witnessing sudden death and massive destruction have evoked profound contemplations. For example, after the great Lisbon earthquake of 1755, which killed more than 60,000 people, about half of them in the collapse of churches, John Wesley wrote a sermon on The Cause and Cure of Earthquakes, in which he blamed the Lisbon earthquake on the original transgressions of Adam and Eve. The Moslems might have thought it just retribution for the cruelties of the Portuguese Inquisition had not the Mosque of Al-Mansur in Rabat also lain in ruins (1).

The 1971 San Fernando earthquake was small compared to the one in Lisbon. Fortunately, the casualties were a thousand times smaller: 63 deaths instead of 60,000. Likewise, our contemplations were less profound. Rather than questioning why earthquakes occur, we concentrated on changes we should make in our design practice to improve the performance of future structures.

Before February 9, 1971, none of the approximately 11,000 bridges in the California highway system had failed or been extensively damaged by earthquakes. Even though many bridge structures in the region of extreme ground shaking at San Fernando survived with negligible to moderate damage, this event triggered a turning point in bridge design.

When the damage at San Fernando was investigated and the evidence examined, we reached two major conclusions:

1. Deficiencies in details, especially at connections, played a major role in all of the spectacular failures; and
2. California earthquake design criteria, although more conservative and rational than current AASHTO specifications, needed a major revision.

IMPROVED DETAILS

The first conclusion led to immediate action to revise details that performed poorly. Two of the most important changes were the modification of column details and the addition of restraining devices at expansion hinges and bearings.

The column tie reinforcement for new bridges is predominantly of the spiral type.

Figure 1. Spiral reinforcing for rectangular column.

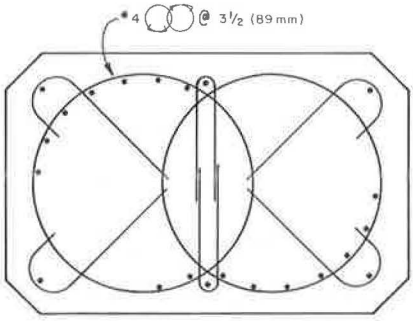

The spirals interlock to confine rectangular column concrete as shown in Figure 1. The superior performance of spiral columns over tied columns was abundantly evident in the review of both bridge and building damage. For columns 30 ft (9.1 m) high or less, lap splices are no longer permitted. For higher columns, 60 diameter lap splices are permitted for No. 11 and smaller bars except within 10 ft (3 m) of moment-carrying connections. Butt-welded and mechanical butt splices that conform to state specifications are permitted anywhere in main column reinforcement.

Narrow hinge seats fared badly under the violent shaking of the San Fernando earthquake. Figure 2 shows a typical hinge restrainer now used on new box girder structures. We also avoid the use of bearings that do not provide a positive tie down, such as the simple rocker bars that were once commonly used on simple span steel girder structures.

NEW DESIGN CRITERIA

Development of new criteria was necessarily preceded by a crash effort to become better educated in earthquake engineering. As an interim measure, we doubled the previously used static earthquake design factors for bridges with spread footings and increased by 2½ times the factors for bridges founded on piles. This change brought our ceiling design force levels to about 0.20 and 0.25 *g*.

The criteria that we implemented in February 1974 are innovative in that they consider site peculiarities such as fault proximity and soil depths more accurately than older codes. They also consider the dynamic characteristics of the structure being designed, because they are essentially a design spectrum technique. Response coefficient curves (Figure 3) were developed by starting with average rock response spectra, then modifying them to reflect soil conditions, and scaling them down to force levels that we can afford to accommodate. To select the proper curve the designer must know the maximum anticipated rock motion and the approximate depth of alluvium.

To understand these criteria we will look first at the code format and then at the rationale used in developing its key element, the response coefficient curves. Finally, we will look briefly at application of the criteria in bridge design.

CODE FORMAT

$$EQ = C \cdot F \cdot W \tag{1}$$

where

EQ = equivalent static horizontal force applied at the center of gravity of the bridge,
F = framing factor = 1.0 for bridges where single columns or piers resist the horizontal forces and 0.8 for bridges where continuous frames resist horizontal forces applied along the frame, and
W = total dead load weight of the bridge.

$$C = \frac{A \cdot R \cdot S}{Z} \tag{2}$$

Figure 2. Typical hinge restrainer unit for a box girder bridge.

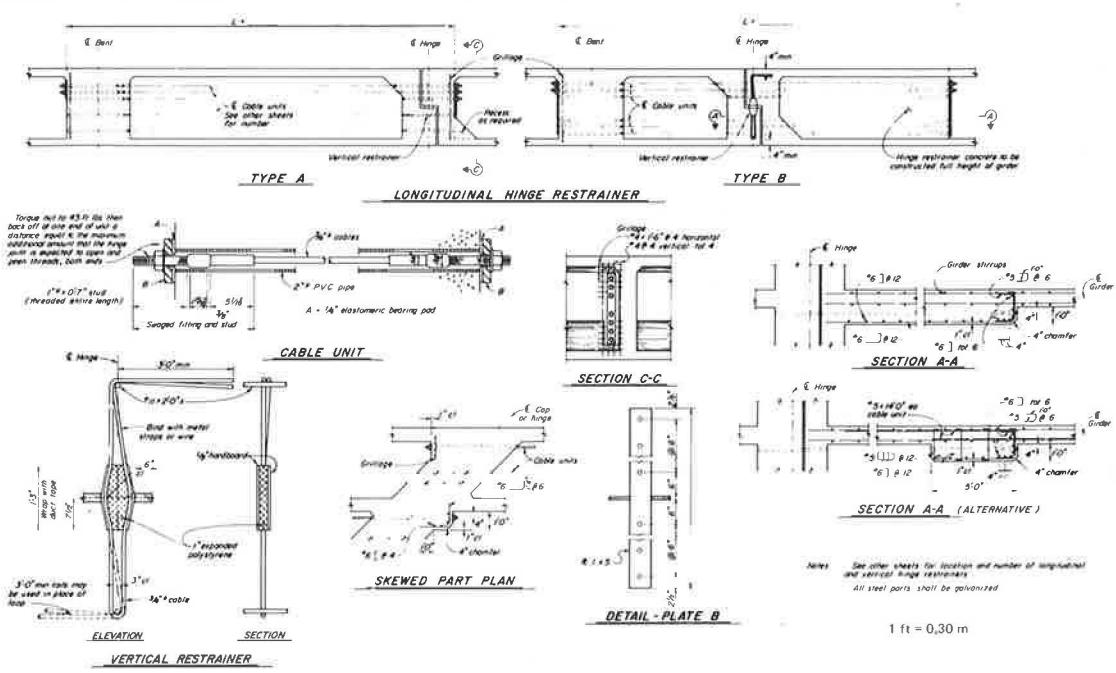

Figure 3. Response coefficient curves for (a) 0 to 10-ft-deep (0 to 3-m) alluvium, (b) 11 to 80-ft-deep (3.4 to 24-m) alluvium, (c) 81 to 150-ft-deep (25 to 46-m) alluvium, and (d) more than 150-ft-deep (46-m) alluvium.

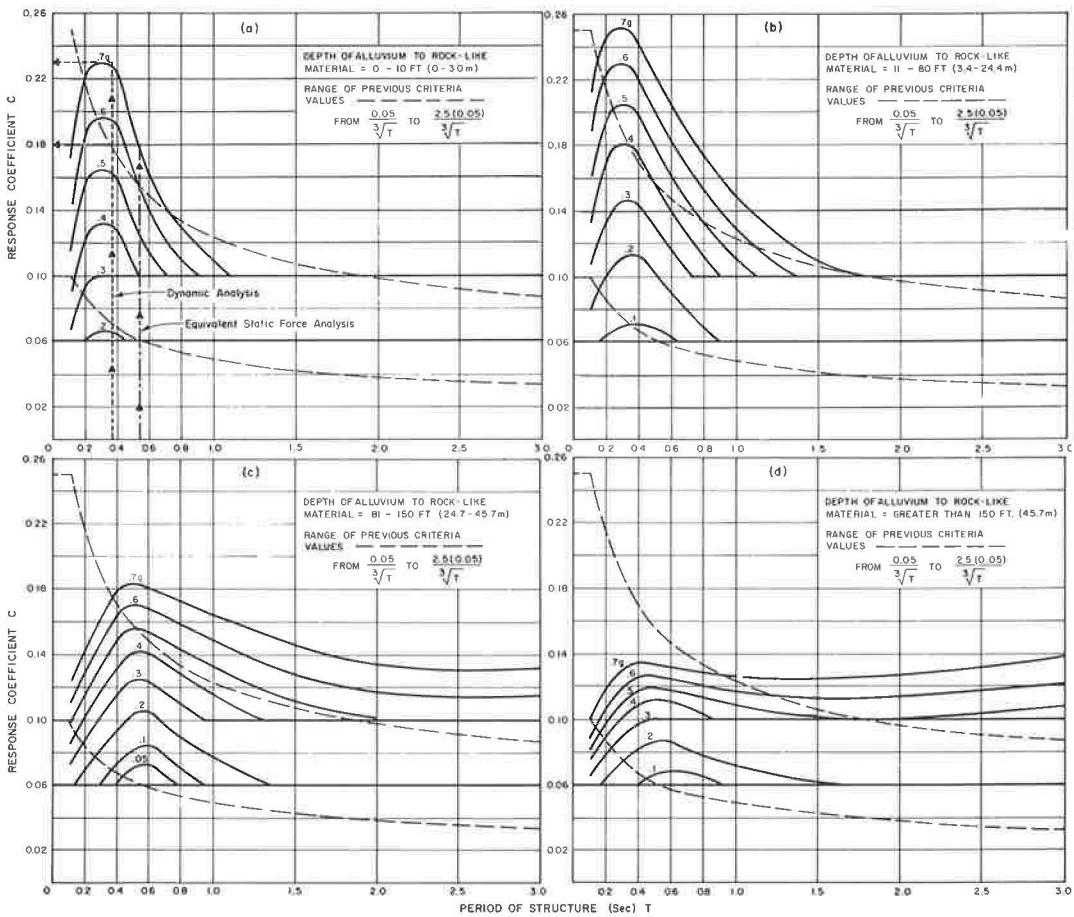

Figure 4. Maximum bedrock accelerations expected from earthquakes in California.

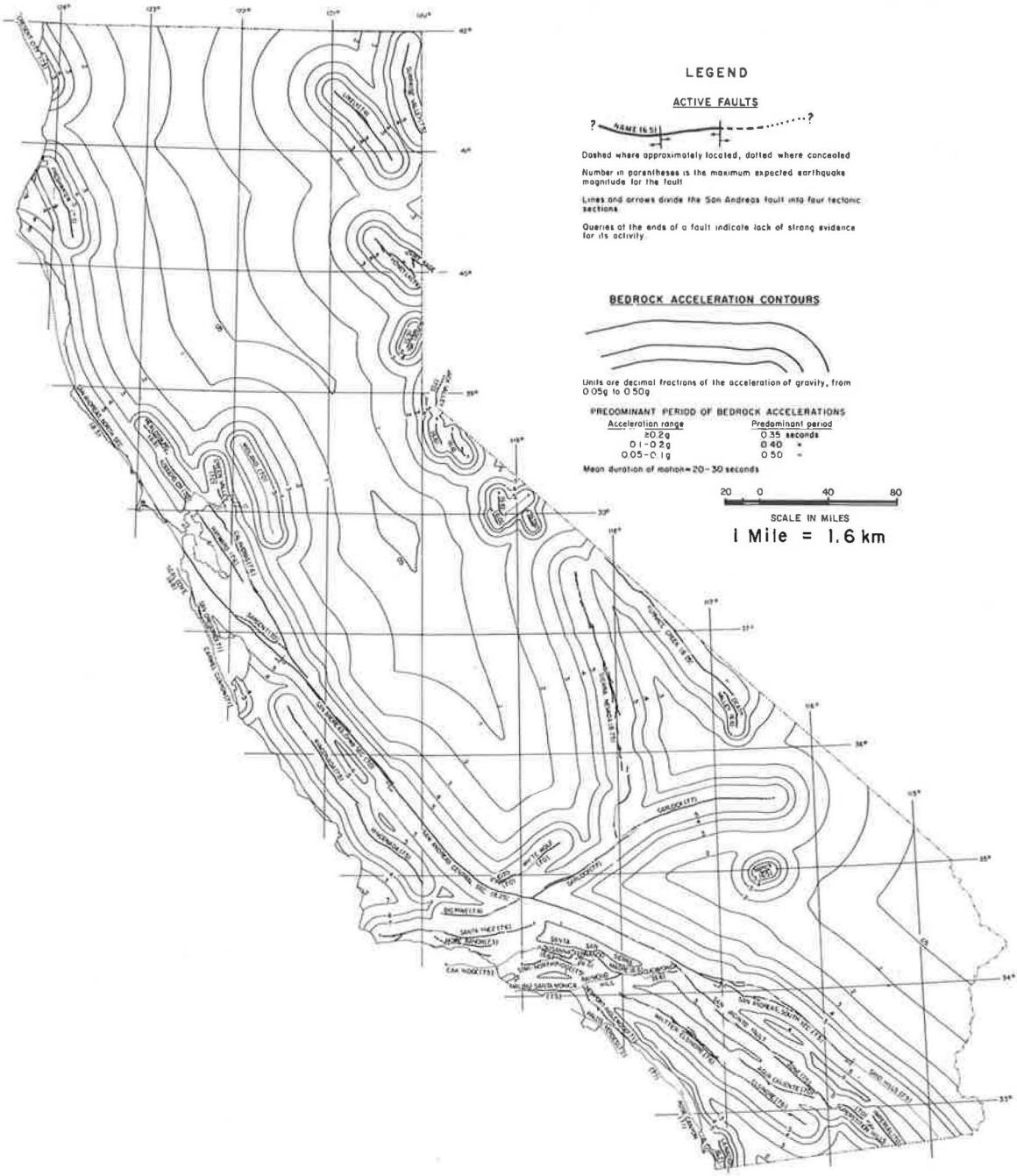

where

C = combined response coefficient (values of coefficients for various depths of alluvium to rock-like material are given in Figure 3),
A = maximum expected acceleration at bedrock at the site in terms of g,
R = normalized rock response,
S = soil amplification spectral ratio, and
Z = reduction for ductility and risk assessment.

ROCK ACCELERATION AND RESPONSE SPECTRA

The rock acceleration level A to be used at a particular site is taken from a map of California that delineates anticipated rock acceleration levels with a series of contour lines (Figure 4). This map was developed by the California Division of Mines and Geology (2). (The map is tentative and is intended as a tool for official use only. It is not intended for direct engineering use without consideration of foundation conditions and type of structure.) The technique used in its development involved plotting known active faults and assigning maximum credible earthquake magnitudes to them based on probable maximum length of rupture. These magnitudes were then related to acceleration levels, and the acceleration values were attenuated with distance from the fault.

The peak rock acceleration cannot be used by itself to get a design force. The dynamic characteristics of a structure greatly affect its response to a given ground motion. A structure with natural frequencies that are in resonance or "tuned in" with a ground motion will respond much more severely than one that has a natural frequency that is out of phase with the ground motion. Typically, a response spectrum is used to delineate this action.

Figure 5 shows normalized response spectra that we developed for 5 percent damped accelerations at rock outcrop locations. These curves, which define R in equation 2, were developed by using five actual recorded rock outcrop accelerograms. Multiplying the ordinates shown in the figure by the peak rock acceleration expected at a particular site will produce an average smoothed elastic rock acceleration response spectrum for that site.

INFLUENCE OF SOIL CONDITIONS

It is generally recognized that the type and depth of soil over bedrock will modify the rock motion dramatically. In some soils, the accelerations can be intensified by a factor of several hundred percent. Various methods for determining the influence of the soil have been proposed and are now being considered by various code-making bodies.

To develop the S-factor, we analyzed several hundred alluvial soil columns by using different earthquakes and varying the depth and density of the soil through use of a computer program called SHAKE that was recently developed at the University of California, Berkeley (3). This program analyzes a one-dimensional soil column for wave motions propagating from rock level to the top of the column and computes motions at the top of the soil column.

To separate the effect of soil from that of other factors such as unusual peaks and valleys in a particular response spectrum, we examined spectral ratios, i.e., the surface acceleration spectra divided by the rock acceleration spectra. The soil amplification curves thus computed were very smooth and regular and appeared to adequately represent soil effects only. The amplification curves varied only slightly with different earthquake motions. S-values from the soil amplification curves such as the one shown in Figure 6 are used as multipliers to find surface spectra from rock spectra.

We found that depth of the soil to rock-like material was the major variable affecting soil response. Figure 7 shows this phenomenon. For two sites where equal rock acceleration levels are anticipated, a structure with a natural period of 0.4 sec would experience a greater response when located on 50 to 80-ft-deep (15 to 24-m) alluvial deposits than when located on deposits of 150 to 250-ft-deep (46 to 76-m) alluvium. Con-

versely, a structure with a 2-sec period would experience a greater response when founded on the deeper soils.

We also found that the maximum rock acceleration has a significant influence on the amplification spectra. As the maximum rock acceleration increases, the amplification decreases and the predominant period of the soil column, indicated by the peak value on the amplification curve, lengthens.

To make use of these amplification curves requires that the site of the structure be investigated to determine the depth of alluvium. In California, this is no problem because we have been making borings at every bridge site for years to facilitate foundation design. We are now expanding this investigation to include an evaluation of soil response as well as an assessment of risks from liquefaction and landslides. For most sites, an experienced soils engineer or engineering geologist, using soil descriptions and standard penetration values, can select the proper amplification curve. For unusual sites, we have developed field procedures to measure shear wave velocities from which specific amplification values can be calculated.

REDUCTION FOR DUCTILITY AND RISK

Because our curves are based on elastic analysis, we were faced with the problem of scaling them down for use in design. Past experience has shown that, because of inelastic response, increased damping, ductility, and other factors, structures can resist considerably higher acceleration levels than are indicated by an elastic analysis. The state of the art has not progressed to a point where all these parameters can be adequately considered in the analysis. Therefore, considerable engineering judgment must be applied in reducing the elastic force levels to design levels. Forces determined elastically are commonly divided by ductility factors ranging from 2 to 6. We selected a general ductility factor of 4 for all bridges.

The theoretical elastic response values were adjusted further based on our assessment of reasonable risk. Our goal is to avoid total collapse under a severe earthquake. From a cost-effectiveness point of view, it is not a good investment to proportion bridges to avoid damage.

Short, low-period bridges such as the common two-span overcrossings are quite stable and less vulnerable to collapse than high structures. Even if columns are severely damaged, the stability provided at the abutments prevents the bridge from overturning. With increased column ties and greater use of spirals, collapse due to column disintegration is not likely to occur. These lower bridges can be readily shored up and restored to traffic use or removed under controlled conditions. Because the probability of collapse and loss of life is minimal for this type of structure, these bridges can be designed for lower force values than high, single-column bent, long-period bridges, which are more vulnerable to collapse.

An additional reduction factor for risk of 2.0 was assigned to the short stiff bridges with periods of 0.6 sec and less. This factor was then decreased linearly to 1.0 for bridges with a period of 3 sec. The ductility and risk factors were combined to produce a reduction curve, Z (Figure 8). The resulting total reduction values ranged from 8 at a 0.6-sec period to 4 at a 3-sec period. This curve was used to reduce the elastic response spectra to the final design coefficient curves for C.

In addition, a frame factor F was applied to the final design coefficient. The framing factor for single-column bents and piers is 1.0 and for continuous frames is 0.8. This factor is simply a numerical coefficient reflecting the increased stability and energy-absorbing characteristics of continuous frames compared with single-column bents.

MINIMUM FORCE LEVELS

No doubt faults exist in California that have not yet been identified and thus are not reflected on the seismic map. The fundamental assumption of the criteria, i.e., that ground motion can be predicted by attenuating rock acceleration with distance and by

correcting it to a surface motion by modeling the overlying soil, is controversial. Some engineers think this procedure is a gross oversimplification. These critics point out that factors such as variations in source mechanism, the influence of terrain, and the chance combination of surface and body waves make it impossible to predict surface accelerations with reasonable accuracy by using our simplified procedure. We readily admit that this method is an idealization that does not account for all possible variables. However, we and many other professionals think it is the only practical method currently available for quantifying major variables. Because of the many uncertainties involved, as part of our design criteria we have established threshold values to be used regardless of an apparently favorable combination of factors. A minimum C-value of 0.10 is used where we expect a peak rock acceleration of 0.3 g or greater. For areas where peak rock acceleration is less than 0.3 g, a minimum C-value of 0.06 is used.

APPLICATION OF THE CODE

A designer currently has two approaches that he may use to apply these criteria. He may use the C-value to determine an equivalent static force, or he may perform a dynamic analysis. Using the equivalent static force method, the designer must obtain the period of the first mode of vibration in the direction under consideration. In addition, he must distribute the earthquake force to the substructure elements. This approach can give reasonable results for simple bridges that respond in one predominant mode of vibration. Dynamic analysis techniques are being used for geometrically complex structures that respond in many significant modes of vibration. The curves developed as part of these criteria can be used for the response spectrum technique that accounts for the effects of several modes. This approach results in a more accurate prediction of the response of structures subjected to earthquake loadings.

The equivalent static force method does, however, require an accurate determination of the fundamental period of vibration. As an illustration, compare the fundamental transverse period obtained for a two-span bridge by using three methods:

1. The formula for a single degree-of-freedom, lumped mass system (Figure 9),
2. A dynamic analysis using a multiple degree-of-freedom, lumped mass idealization (Figure 10), and
3. Field testing the actual structure.

The results are given in Table 1 along with the resulting force coefficients and column shears.

The formula method ignores the bending and torsional stiffness of the superstructure. This introduces an error in the determination of the period, which results in an incorrect C-value. In addition, it results in an inaccurate distribution of forces to the substructure elements.

SUMMARY

At the present time in California we are designing most simple structures by using the equivalent static force method. We are using dynamic analyses for all major structures. We think our new criteria used in a static analysis are a great improvement over older codes because they account for the major variables that influence earthquake force levels. However, because of the inaccuracies inherent in any static approach, the trend is toward using the response coefficient curves to define a design earthquake for a response spectrum analysis for most bridges with a fundamental period of less than 3.0 sec. For major structures with longer periods or those that have unusual configurations or foundation conditions, we will use a more rigorous individual dynamic analysis.

Figure 5. Normalized rock acceleration spectrum.

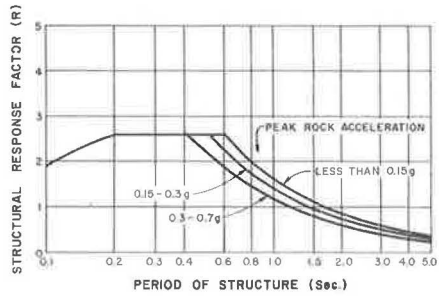

Figure 6. Soil amplification curves for 80 to 150-ft-deep (24 to 46-m) alluvium.

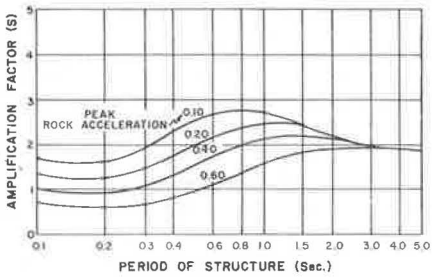

Figure 7. Soil amplification for different depths.

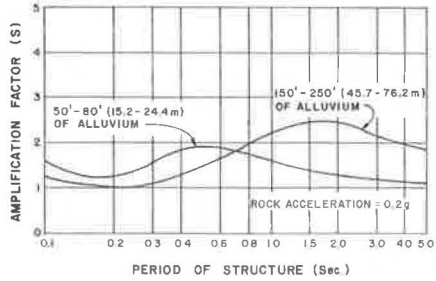

Figure 8. Reduction curve for ductility and risk assessment.

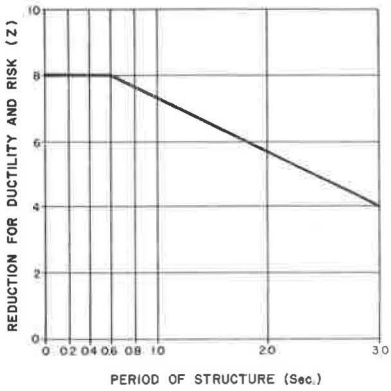

Figure 9. Simplified method for period determination.

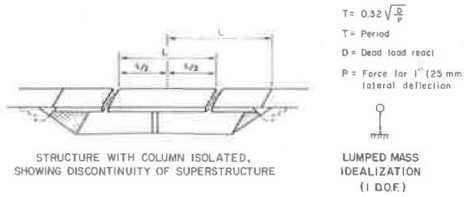

Figure 10. Dynamic analysis for period determination.

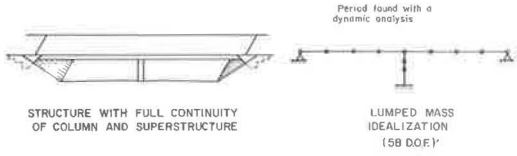

Table 1. Comparison of results from different analyses.

Method of Analysis	Period (sec)	Force Coefficient[a]	Column Shear (kips)
Simplified	0.54	0.18	212
Dynamic	0.37	0.23	270
Field test	0.33		

Note: 1 kip = 4.45 kN.

[a]From Figure 3.

ACKNOWLEDGMENTS

Many engineers and several engineering geologists in the Division of Structures, California Department of Transportation, have contributed greatly to improvements in earthquake engineering of bridges. The following employees have been particularly effective in these developments: James H. Gates developed normalized rock spectrum and soil amplification curves. Roy A. Imbsen developed guidelines for applying these criteria so that reasonable accuracy can be maintained with simplified methods, and he is responsible for sophisticated dynamic analysis of major structures. Adlai F. Goldschmidt developed techniques for measuring shear wave velocities in soils and expanded the geological report to include an assessment of potential soil problems from seismic forces. Oris H. Degenkolb developed hinge restrainer details. John B. Poppe improved column reinforcing details. I. Nagai coordinated the overall development of these criteria.

REFERENCES

1. W. Durant and A. Durant. The Story of Civilization, Volume 9, The Age of Voltaire. Simon and Schuster, 1965.
2. R. W. Greensfelder. A Map of Maximum Expected Bedrock Accelerations From Earthquakes in California. California Division of Mines and Geology, Jan. 9, 1973.
3. P. B. Schnabel, J. Lysmer, and H. B. Seed. SHAKE, A Computer Program for Earthquake Response Analysis of Horizontally Layered Sites. Earthquake Engineering Research Center, Univ. of California, Berkeley, EERC 72-12, 1972.

APPLICATIONS OF A BRIDGE MEASUREMENT SYSTEM

G. G. Goble, Fred Moses, and Anthony Pavia, Case Western Reserve University

Recent efforts to record bridge strain histories due to highway truck traffic have been prompted by modifications in fatigue code, introduction of high-strength steel alloys and more fatigue-sensitive welded bridge details, and increases in truck weights and volumes. This study was designed to improve measuring and processing systems and to expand both the amount and the type of information recorded in bridge studies. Truck headway and type, lane location, and corresponding strain record and maximum stress range were recorded and processed on 10 slab-girder bridges for almost 20,000 truck passages. This paper describes the measurements and processing system developed and discusses applications of the measurement data to fatigue design including impact, girder load distribution, fatigue life stress cycles, predicted and measured stresses, and the potential for weighing trucks in motion on bridges.

•DURING the last 20 years, as measurement equipment has been improved and interest in the fatigue of bridges has increased, many studies have been reported of field measurements of highway bridges (1, 2). These studies recorded strain due to random truck passages at various bridge girder locations. Such data have been used to plot histograms of peak stress ranges expected over the lifetime of a bridge. From such field data and laboratory information on fatigue behavior of bridge elements, estimates have been made of fatigue life.

In the last few years there has been even further impetus for recording strain histories. Bridge measurement studies have been conducted in Illinois, Connecticut, Virginia, Maryland, Michigan, Pennsylvania, Indiana, Alabama, Tennessee, Missouri, other states, and Canada (3 through 11). These studies have been sparked by modifications in fatigue codes, introduction of high-strength steel alloys and more fatigue-sensitive bridge details, rapid growth in truck weights and volumes, and several instances of reported bridge fatigue cracks.

This study was designed to improve the state of the art in measurement systems by expanding both the quantity and the type of information recorded in a bridge study. A shortcoming of most of the reported field studies has been the difficulty of accumulating large numbers of bridge strain records. In early work the data were recorded on an oscillograph, and converting this record to a usable digital form either was slow and tedious or required very expensive record analysis equipment (3, 4). Some recently developed measurement systems use magnetic tape, but expensive data processing systems in some cases have made it necessary to turn off the tape recorder between truck crossings. Hence, the systems cannot be used on arteries that have large volumes of truck traffic. The FHWA system on the other hand used a magnetic tape recorder followed by instantaneous field processing of strain ranges (12). (The FHWA system for acquiring bridge loading data was originally developed to encourage a national effort to collect bridge strain data. The original system has become obsolete and is no longer operable.) One result is that the records have not been saved for any further processing and information.

CASE BRIDGE MEASUREMENT SYSTEM

Based on reported measurement systems and the present need for additional bridge

strain data, the following requirements and aims were proposed for the Case bridge measurement system developed in this project.

Truck Type Information

Annual loadometer survey data give weight information for different truck types. Hence, to correlate truck weight with strain records requires that, for each recorded truck passage, the type of truck be identified. Only a few bridges are located so that nearby weighing stations can be used in conjunction with bridge strain studies. Measurement reports from other states have frequently mentioned that many heavy trucks seem to exit a highway before reaching the weighing stations. Thus, to obtain a good representation of truck vehicles, the measurement system should include a technique for recording truck type, which is automatically processed with the strain data.

Truck Headway and Lane Location

It has been suggested that a significant proportion of damaging loadings are caused by closely spaced trucks simultaneously loading a span. This is recognized in the AASHTO specification for bridge loading that applies to fatigue design (13). It requires all lanes to be simultaneously loaded and, therefore, gives a high load distribution factor for calculating individual girder moments. One aim of this project was to obtain data to develop a model for truck headways and lane location and the frequency of multiple truck crossings on a bridge. In addition, because vehicle velocity may influence headways, this information should also be obtained.

Permanent Records of Processed Data

The easiest way to handle strain records is to process them immediately and convert the records to strain histograms. This is the technique used in the FHWA field measurement system. An objection to this approach is that the records are then no longer available for further processing. One goal of this project was to retain these records for further processing on problems such as bridge dynamics, damping, and load distribution to the stringers. In addition, the nonsinusoidal shape of the actual strain record including its many dynamic oscillations is ignored in current laboratory fatigue testing. These records should be saved because at some future date the exact strain shape record may be found to be significant for fatigue life. For these reasons all recorded data were retained in either digital or analog form.

Fully Automated Data Processing

Because an understanding of bridge loadings is a statistical problem, a large number of truck crossings must be recorded. If any part of the data processing requires that the data be examined manually, the volume that can be processed is severely limited. Therefore, the conclusion was reached that although some manual data acquisition may be acceptable it must be avoided if at all possible in the data processing phase.

Use of Available Instrumentation

Inasmuch as the project had only a 2-year term, it did not involve development and testing of instrumentation. Wherever possible proven equipment was used. A project had been active at Case for several years in which dynamic measurements were made under pile hammers during driving. Both money and time could be saved by using the equipment available from that project wherever possible.

Based on previous field experience it was felt that the project aims could be met in the following manner.

1. Separate the data acquisition on the magnetic tape recorder from the data processing, and do all of the processing in the laboratory and computing center.
2. Use field personnel to manually record information on truck arrival time, headway, and lane information on the tape through generated pulses. Although this required up to a three-man crew it is considerably easier to develop such a system than to try to automate the acquisition of these data. Even a completely automated system would probably need a minimum of two crew members.
3. Store the processed information in digital form on tape. All software programs were written for an available minicomputer.

Work on the project began in August 1971. To avoid inclement weather, we began field testing of the system in September and made strain recordings on a single four-channel tape recorder. In October, the total initial system was tested during 24 hours of continuous recording. The data processing system was developed on an incremental basis. The process of analog-digital conversion proceeded until the available high-speed computer storage was filled. Then the analog tape recorder was stopped until the digital data were processed and printed. The process could thus be continued in small steps. This system was simple enough to be quickly implemented, and the field data were tested. The software for the final processing system, which enabled us to process continuously without having to stop the tape recorder intermittently, was then developed. This system will be described briefly.

By the end of the fair weather season in 1972, six additional bridges had been instrumented and five had been tested. These data were processed during the winter. Further field instrumentation and data acquisition continued in spring 1973, and the data were processed immediately. All field work was completed on the 10 bridges tested in July 1973, and processing was completed in August.

FIELD EQUIPMENT

A schematic of the system is shown in Figure 1. In addition to the strain gauges, two boxes containing a number of buttons that the operators pressed to record truck type and traffic lane are included. In this manner, pulses are generated that interrupt the strain signal for a short period of time. The button boxes are powered and the entire system is managed by a power unit that transmits the signals to the appropriate tape recorder channels. The elements in Figure 1 will be described in detail.

The strain gauges used were standard dual-pattern resistance gauges. They were attached by using contact cement and standard procedures. The Wheatstone bridge was completed at the active gauges by a terminal box containing two inactive gauges. Experience with bridge measurements showed that electronic noise is a serious problem because of the small strain levels encountered. Therefore, the bridge was completed as near as possible to the active gauges, and then shielded cable was used from the gauges to the signal conditioners. By using dual-configuration gauges and hence two active arms in the bridge, the output was doubled.

Separate signal conditioners and amplifiers were used. Both were obtained as government surplus property and thus were not specially selected. The signal conditioners were from Trans-Data, Inc., model BC1031. The differential amplifiers were model 2210 manufactured by Dana. An excitation of 2.5 V was used. An important factor that led to selection of these instruments was that they have very low noise characteristics. Long-time stability is not particularly important because the event measured is so short. In fact, experience showed that, for the continuous bridges tested in Ohio, a considerable apparent zero drift occurred because of temperature effects in the statically indeterminate structure. However, this slow change causes no difficulty inasmuch as stress change due to short-time loads was being measured.

The button boxes and photoelectric cells were constructed by the project (14). Two

button boxes were used to record traffic characteristics: one for truck type and one for traffic lane location. Each of these boxes was equipped with 10 buttons. When a button was pressed an electronic pulse of a particular amplitude characteristic of that button was generated. Thus, as many as 10 truck types could be recorded. Likewise, traffic lane location was recorded.

Each of the button boxes was linked to a photoelectric cell. One of these devices was set up at the entrance to the bridge. A light beam was set up on the opposite side of the road focused on the photocell. The passage of a vehicle interrupted the light beam and generated an electronic signal. However, only truck arrivals were noted. The system operated as follows.

When an approaching truck was observed by the button box operator, he pressed the button denoting the type of truck. This was not done until no other vehicles were between the truck and the light beam. Pressing the button set the circuit to be triggered when the light beam was interrupted. This generated the pulse and also lighted a signal indicator on the button box to show that the pulse was triggered. If a button was not pressed, interruption of the light beam was ignored. Thus, not only was the truck type given by the amplitude of the signal, but also by its position the precise arrival time was recorded.

The second button box-photocell system was set up some distance down the traffic stream and performed in the same fashion. The first box was used to record truck type, and the second box recorded lane position. With accurate arrival time data, truck speed and distance headway could be determined.

The button boxes were constructed so that, optionally, they could be used without the photocells. In this mode of operation, the pulse was generated immediately when the button was pressed. Using the button boxes in this fashion was convenient when several trucks arrived at the bridge so closely that the photocells did not have sufficient time to reset themselves. Also, this procedure was used when the volume of automobile traffic was so high that it interfered with the light beam as trucks approached the bridge.

A typical event record is shown in Figure 2. When the pulse was triggered, a square wave pulse went to the recorder. The signal from the strain gauge was interrupted, and a pulse characteristic of the button pressed was generated. After a 20-millisec time lapse, a zero signal, also of 20 millisec, was generated. The pulse amplitude was given by the difference between the two. This avoided problems caused by zero drift of the strain gauge circuit. The strain signal was interrupted for a total of 40 millisec. During this time interval, a truck traveling 60 mph (97 km/h) moved a distance of 3.52 ft (1.13 m).

The power unit was constructed by the project. It provided the power for the button boxes and allowed the strain record to be interrupted and the truck type signals and lane position signals to be placed on the appropriate channels.

The tape recorders used were Hewlett-Packard model 3960, instrumentation magnetic tape recorder. This is a portable unit that can record four channels of FM data at one of three speeds: $^{15}/_{16}$, $3^{3}/_{4}$, and 15 in./sec (2.4, 9.5, and 38 cm/s). This instrument performed well but did not have a sufficient number of channels to record the desired number of gauges simultaneously. However, because one of these instruments was available from another project, funds were saved by acquiring only a second one. Because the data were relatively slow, a recording speed of $^{15}/_{16}$ in./sec (2.4 cm/s) was used. Thus, more than 6 hours of continuous recording could be done on an 1,800-ft (550-m) tape reel.

One characteristic of the button box pulse data recorded on the tape unit should be noted. The pulse that was received by the recorder had a very fast rise time and a sharp cutoff. The bandwidth of the recorder was not wide enough to record these square wave pulses. Data in Figure 2 show that the recorded signal overshoots to some degree. However, this signal can still be satisfactorily processed.

DATA PROCESSING

As indicated earlier, one advantage of the data acquisition activity was the ability to

Figure 1. Field equipment system.

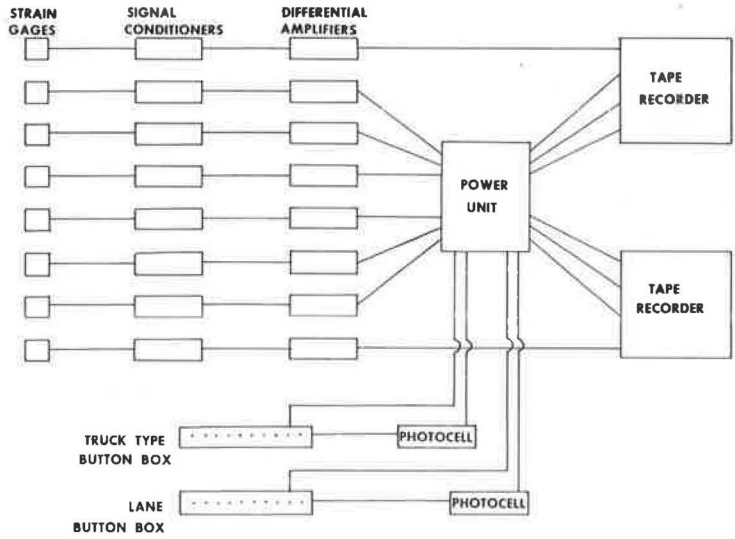

Figure 2. Typical event.

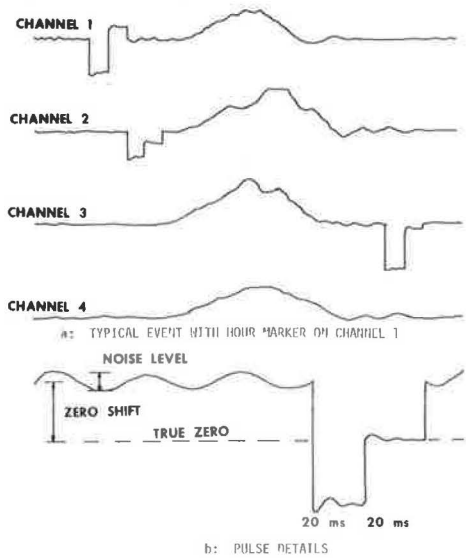

Figure 3. Processing equipment system.

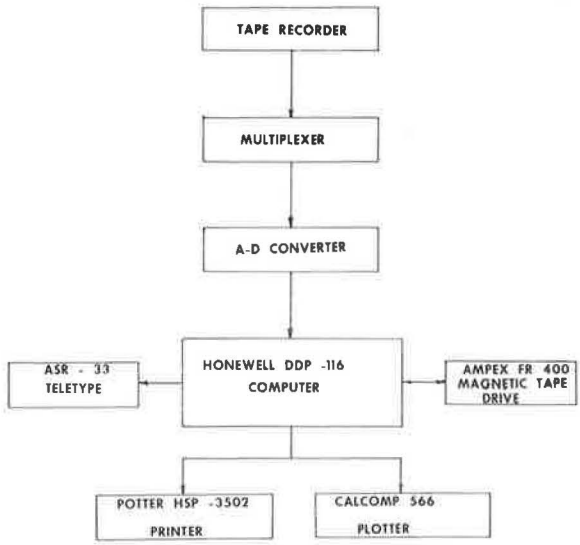

fully automate the data processing. The functions of the system were to convert the analog record into digital form, to sense the arrival of a truck at the bridge (an event), to determine useful data from the button box records, to store the strain records or specific parameters from them, and to transfer the entire event record to magnetic tape. The software for this system was actually developed in an incremental fashion. Only the final system is discussed here.

The processing system is shown in Figure 3. The tape recorder is one of the two tape recorders used to record field measurements. The multiplexer was designed and constructed by the project and can accommodate the four channels of the tape recorder. It condenses four channels of analog data into one channel with a sequence of 2-3-4-1-2-3 and so on. Sampling frequencies of 200, 400, 600, 800, 1,200, and 2,400 samples/sec/channel are available.

The analog-digital (A-D) converter is a Texas Instruments series 834 converter. It receives the single channel of analog data from the multiplexer and converts each sample to digital form.

The computer is a Honeywell DDP-116 computer. It is a solid-state, internally stored program, general-purpose digital computer and is organized as a parallel 16-bit binary machine. The memory cycle time is conservatively rated at 1.7 μsec, and it has a memory capacity of 16,384 words. The instruction repertoire includes 63 commands. Software includes a DDP-116 assembler, debug system, input-output system, diagnostic programs and subroutine library, and FORTRAN IV compiler. The remaining hardware items in the system are commonly available and have obvious functions.

PROCESSING SOFTWARE SYSTEM

A complete and detailed description of the processing software is beyond the scope of this report (14). The processing scheme enables real-time processing of data. This means that while data are being fed into the computer they are being operated on, and the results are simultaneously outputed. Essentially, the entire process depends on the ability of the computer to accomplish all the required operations in the time gap between consecutive inputs of data.

How much time is available between bits of data depends on the sampling frequency of the multiplexer. Two factors that influence the selection of the sampling rate are the tape recorder speed and the form of the data, particularly in regard to the shape of the pulses generated by the various button boxes. As stated previously, data are recorded in the field at a tape speed of $^{15}/_{16}$ in./sec (2.4 cm/s), and the duration of a button box pulse is 20 millisec followed by a zero pulse that is also 20 millisec long (Figure 2). To ensure that processing time was substantially less than recording time, we used the next higher tape speed of $3^{3}/_{4}$ in./sec (9.5 cm/s). Because the processing speed is four times faster than the recording speed, the length of a pulse is reduced by a factor of four. The question to be answered now is how many samples are required in a period of 5 millisec so that such a pulse will be identifiable. Because a sample may be chosen along the rising or the descending portions of a pulse or in the region of the peak where there can be much variation in magnitude, at least three samples were necessary for proper identification. Three samples per 5 millisec is equivalent to a sampling frequency of 600 samples/sec/channel. However, because the A-D converter and, hence, the computer, receive data as though they came from one channel, the overall sampling rate is 2,400 samples/sec. At this frequency the time between successive samples if 416 μsec. It is during this time that all required operations must be performed.

It is useful to discuss the general function of the program to give its general capabilities. As indicated above the program must recognize the arrival of a truck. This problem is quite simple because of the truck type-arrival pulse. From this pulse it must identify the truck type and determine its precise arrival time. It must then store the digital record of the strain trace for each of the gauges and identify the lane pulse and hence the lane location and the time of passage of the truck past this point. The program also determines stress range and stores the entire record on digital magnetic

tape. The system must also keep a running value for the zeros of all strain gauges. This can be accomplished by maintaining a running average gauge output during times when there is no truck on the bridge. Finally a proper record length must be stored for cases when multiple trucks are present on the bridge at the same time.

The data accumulated during an event are read out to digital magnetic tape. This can include the entire strain record as well as the traffic data. Several bridges were processed in this manner. However, experience showed that a very large volume of digital tape was required to store the results, much more than in its analog form. Therefore, only processed results of current interest were stored, and strain records were not included. The latter data can be most efficiently and inexpensively stored in analog form.

FIELD MEASUREMENTS

The 10 bridges tested in this study were selected to be representative of bridges used by the Ohio Department of Transportation. Since the continuous noncomposite girder is the dominate type in Ohio it, of course, dominated the bridge types tested. Table 1 gives the bridges selected and their characteristics. (All the bridges were steel.) Almost 20,000 truck passages were recorded.

A 24-hour continuous test was conducted on bridge 1 as a preliminary study in October 1971. From the hourly truck traffic volume, the optimum time for testing was determined to be from 8:00 a.m. to 8:00 p.m. As a result five bridges were tested for periods of about 24 hours each spread over 2 days. It was later observed that for the volumes of truck traffic available a total of 12 hours of data would be sufficient for each of the remaining five bridges to give an accurate picture of stress history. This was accomplished by testing between the hours of 10:00 a.m. and 4:00 p.m.

DISCUSSION OF RESULTS

Stress range histograms, truck type distributions, and samples of stress records have been reported elsewhere (14). Only the important results of this study are presented below.

Stress Measurements

Significant stresses in the steel girders (more than 4 ksi or 28 MPa) were found only in the center of end and middle spans of continuous girders and usually on the girders supporting the main traffic lane. The stress ranges adjacent to the piers near the coverplate ends are usually less than 3 ksi (21 MPa). However, these stresses are relatively more significant because they occur in regions where the fatigue sensitivity is greater because of coverplate attachment. High stresses (more than 4 ksi or 28 MPa) were also often found on diaphragms. Such stresses have been reported in other studies and are due to the deformation pattern in the girder-slab structural system. It is not conclusive, however, from the measurements whether diaphragms should be increased or decreased in size or number.

It appears from the stress measurements that the stresses due to random truck traffic are significantly below the fatigue design allowable stresses. Because fatigue-causing loading was the main purpose of the field study it was observed that the margin of safety against fatigue in all the bridges studied is quite large. This conclusion, of course, presumes that the truck weights and volumes now being carried will remain constant over the life of the bridge. In fact, field studies such as this one, which may be used to justify the safety of raising legal allowable loads, may in time lead to premature fatigue damage.

Although allowable design stress margins appear adequate when compared with measured values, the field results did show higher stresses than were observed in several other states (3 through 11). This is probably an indication of the industrial nature of

the state of Ohio and the type of materials transported over the roads such as steel and machine products.

Truck Headway Data

This field project was perhaps the first in the United States to record precise headways and frequencies of multiple truck crossings in conjunction with bridge strain measurements. These headway data can be used independently as empirical information for a model of truck spacings and hence truck loadings. It indicates that for fatigue design the assumption that all lanes are simultaneously loaded is overly conservative. The most commonly proposed spacing model is based on the Poisson distribution and is often used in relation to automobile spacings. It gives probability of the time between successive trucks along a roadway as

$$F(t) = 1 - e^{-ut} \simeq ut$$

for small headways where

$F(t)$ = probability that the time between successive trucks is less than t and
u = truck volume in vehicles per unit time.

Dividing headway into discrete time intervals gives

$$F(t_2) - F(t_1) = u(t_2 - t_1)$$

The headways given in Table 2 are divided into 0.2-sec intervals; for the Poisson model to be accurate the values should be constant (at $u \times 0.2$ percent) in the small (<3 sec) headway range. The number of occurrences predicted for the short time intervals by the Poisson model is also given in the table. In most cases the values in Table 2 given by the Poisson model are higher than the measured value, indicating that the model is a conservative prediction as far as truck loading superpositions are concerned. The model is not accurate in the small headway values because it implicitly assumes that as a truck gets close to a preceding truck it moves to the passing lane as if the first truck is not even present. This assumption ignores driver behavior and reaction times and thus is not accurate in short headways.

For headways greater than 1 sec the agreement between model and observation is quite reasonable. For example, for bridge 3, $u = 70$ trucks per hour, and Table 2 shows 1.5 percent of observed headways less than 1 sec. The Poisson equation predicts $(70/3,600) \times 1$ or 1.9 percent should have headways less than 1 sec. Similar good agreement can be seen in the other bridges except for bridge 10, which only had 1 lane in each direction and thus clearly inhibited trucks from getting close and attempting to pass. It is clear then from both the Poisson model and the results in Table 2 that for commonly encountered truck volumes the frequency of more than one truck on the bridge at a time is small. This suggests that current bridge loadings need to be revised as far as fatigue is concerned.

Impact

The magnitude of impact due to bridge and truck dynamics can only be measured by comparing stresses of identical vehicles in a crawl and at a normal speed. This was not done in this study. However, studying the stress records may give some indication of the impact by looking at the magnitude of dynamic oscillations. In general, the im-

Table 1. Description of bridges.

Bridge	Location	Type[a]	Lanes	Girder No.	Girder Spacing	Span Length	Route Type	Truck Passages
1	Cuy271-721	BC	3	8	7'4"	41'-66'-41'	Urban Interstate	3,771
2	Cuy71-384	BC	2	5	9'6"	37'3"-46'-37'3"	Suburban Interstate	1,995
3	Cuy71-100	BC	2	6	7'11"	44'-63'-44'	Suburban Interstate	1,507
4	Lak90-526	BC	2	8	7'4½"	64'-80'-64'	Suburban Interstate	1,268
5	Ric71-1068	GC	2	6	7'11"	68'-114'-114'-68'	Rural Interstate	1,267
6	Atb90-1450	BC	2	6	7'11"	48'7¼"-81'-48'7¼"	Rural Interstate	1,624
7	Por80S-130	BC	2	6	7'11"	48'-60'-60'-48'	Suburban Interstate	1,703
8	Cuy90-2181	BSi	4	Varies		75'	Urban Interstate	2,958
9	Sum21-778	BC	2	5	7'6"	36'-45'-36'	Non-Interstate, divided	1,053
10	Por14-1131	BC	2	5	7'4"	48'-60'-48'	Undivided	1,733

Note: 1 ft = 0.3 m; 1 in. = 2.5 cm.

[a]B = rolled beam, G = welded plate girder, C = continuous, and Si = simple span.

Table 2. Truck headway occurrences.

	Bridge										
										10[a]	
Headway (sec)	1	2	3	4	5	6	7	8	9	A	B
0.00 to 0.20	4	10	5	0	2	1	0	19	2	0	0
0.21 to 0.40	16	3	4	0	1	3	0	14	3	0	0
0.41 to 0.60	23	15	5	1	2	4	9	15	5	0	0
0.61 to 0.80	33	9	3	4	5	9	7	42	3	0	1
0.81 to 1.00	30	14	5	3	2	3	7	41	4	0	0
1.01 to 1.20	28	20	14	5	3	7	12	54	9	0	0
1.21 to 1.40	49	17	8	6	14	4	23	56	8	1	0
1.41 to 1.60	45	19	7	4	9	11	36	46	5	1	1
1.61 to 1.80	49	30	10	3	10	13	20	63	15	3	6
1.81 to 2.00	51	21	8	6	14	9	11	65	7	6	3
2.01 to 2.20	38	11	3	6	14	14	7	50	21	7	5
2.21 to 2.40	44	12	8	2	11	10	16	48	5	5	5
2.41 to 2.60	51	10	12	2	18	8	17		8	10	6
2.61 to 2.80	34	10	10	4	15	8	10		5	14	2
2.81 to 3.00				4	16	11				18	3
3.01 to 3.20				6	15	7					
3.21 to 3.40	3,276	1,794	1,405	6			1,528	2,445	970	902	734
3.41 to 3.60				2	1,116	1,502					
>3.60				1,204							
Total	3,771	1,995	1,507	1,268	1,267	1,624	1,703	2,958	1,053	967	766
Predicted occurrences	36	10.5	6	4	7.4	6.3	13	42	5.3		
Hourly truck volume	170	95	70	60	105	70	140	250	90		150
Percentage in passing lane	53	5.1	3.7	2.1	3.4	3.6	5.1	59	3.0		

[a]Dual-direction bridge.

Table 3. Measured girder distribution factors.

Bridge[a]	Girder Spacings	α	Bridge[a]	Girder Spacings	α
1	7'4"	15	7	7'11"	12.5
2	9'6"	14.6	9	7'6"	13.6
3	7'11"	15	10	7'4"	16.3
4	7'4½"	13.5	Average		14.7
5	7'11"	17.8	Code value		5.5
6	7'11"	14.5			

Note: 1 ft = 0.3 m; 1 in. = 2.5 cm.

[a]Bridge 8 had variable girder spacings.

pact oscillation is less than 15 percent of the peak stress range and is thus somewhat less than the AASHTO code value (13). However, for fatigue damage both the impact oscillation, which increases the maximum stress, and the residual vibration after truck passage, which reduces the minimum stress, must be considered. This is because fatigue life of highway bridges is now thought to be controlled strictly by stress range magnitude, which is the difference between maximum and minimum stress (15).

Girder Distribution Factors

By locating gauges on parallel girders in a span in this study it was possible to estimate the distribution of total truck bending moment to the individual girders. The girder distribution factor is

$$M_g = M_{WL} \frac{S}{\alpha}$$

where

M_g = moment range on critical girder,
M_{WL} = moment range on total bridge cross section due to wheel load,
S = girder spacing, and
α = measured constant.

A summary of values from bridges tested is given in Table 3. The average percentage of total wheel load moment distributed to the most critical girder is S/14.7 compared with the AASHTO code value of S/5.5. Measured girder distribution values are slightly below the generally reported S/12.5 to S/13.5 because we used stress range rather than maximum stress to determine the distribution. Based on these field measurement studies, for fatigue loading of multilane slab-girder bridges, one-half the usual distribution factor to the girder should be used—that is, a value of S/11, where S is the spacing in feet (meters) between girders. Although this value may be modified by further analysis it is clear that the assumption that parallel lanes be fully loaded is conservative as far as repetitive fatigue load is concerned.

Truck Weighing

Some bridge measurements made in conjunction with a weighing station showed the feasibility of using the bridge itself as a load scale for directly weighing trucks as they cross the bridge. This would enable a large number of vehicles to be weighed economically and to avoid the known problem of trucks exiting and bypassing open weighing stations. Information should automatically be obtained on gross truck weight, axle length, and perhaps axle load distribution. An example of such correlation of gross weights with stress range measurement is shown in Figure 4. The strain shown is the sum of stress ranges on the six parallel girders, and the vehicles in the figure are tractor trailers with wheel bases of 30 to 31 ft (9.1 to 9.4 m). In most cases where section modulus is difficult to estimate, calibration by weighing known trucks is necessary.

Measured and Predicted Stresses

Table 4 gives predicted versus measured average stress range and standard deviation of stress range at four girder locations on the same bridge (bridge 2, 14). The predicted values were obtained by combining a truck weight histogram with a bending

Figure 4. Stress range (from six gauges) versus truck weight.

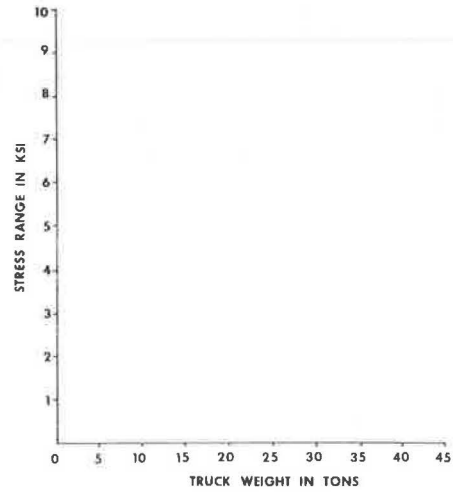

Table 4. Predicted and measured stress ranges.

Location	Average Stress (psi)		Standard Deviation (psi)	
	Predicted	Measured	Predicted	Measured
Middle of end span	1,439	1,385	711	626
End of cover plate in end span	1,119	908	558	336
End of cover plate in center span	941	954	462	613
Middle of center span	1,356	1,438	624	550

Note: 1 psi = 6.9 kPa.

Table 5. Predicted and measured average stress ranges of multiple crossings.

Location	Stress Range (psi)	
	Predicted	Measured
Middle of end span	1,704	1,683
End of cover plate in end span	1,337	1,153
End of cover plate in center span	1,021	1,142
Middle of center span	1,738	1,766

Note: 1 psi = 6.9 kPa.

moment influence line at each girder location. The truck weight histogram was compiled from the combined Ohio loadometer survey inasmuch as a weighing station was not available at the bridge site. The truck type distribution, however, used to combine various vehicle types was recorded at the site as explained above. Despite the fact that there are obvious weight differences expected between the trucks from the loadometer survey and the trucks at the site, the agreement between measured and predicted stress ranges was generally quite good. Table 5 gives stress comparisons for the influence of short headways on truck loading superposition. The predicted or calculated values were based on the Poisson model for headway spacings rather than the observed headway spacing in Table 2. The results given in Tables 4 and 5 are typical of the 10 bridges studied and indicate the possibility of accurately estimating truck loading effects on girder sections.

Fatigue Design

A major conclusion of the field measurements reported to date is that there is a clear

need to separate fatigue loading from yielding or ultimate design load. Fatigue represents an averaging process in which hundreds of thousands and perhaps millions of cycles of load are needed for failure to occur. Thus, it is illogical to use an extremely rare design truck loading that is expected to occur only a few times during the life of the structure. Truck properties are volume, girder load distributions, impact factors, and the assumption of trucks in more than one lane should be based on average conditions. Safety can then be specified in a uniform, consistent manner from site to site with both load and resistance safety factors (16, 17).

ACKNOWLEDGMENTS

This paper was prepared in cooperation with the Ohio Department of Transportation and the Federal Highway Administration, U.S. Department of Transportation.

The contents of this report reflect the views of the authors, who are responsible for the facts and the accuracy of the data presented. The contents do not necessarily reflect the official views or policy of the state or the Federal Highway Administration. This report does not constitute a standard, specification, or regulation.

REFERENCES

1. R. F. Varney and C. F. Galambos. Field Dynamic Loading Studies of Highway Bridges in the United States, 1948-1965. Highway Research Record 76, 1965.
2. C. Heins and C. F. Galambos. Highway Bridge Fatigue Tests in the United States, 1948-1970. Public Roads, Vol. 36, No. 12, Feb. 1972.
3. C. R. Cudney. The Effects of Loading on Bridge Life. Highway Research Record 253, 1968.
4. C. P. Heins and A. D. Sartwell. Tabulation of 24 Hour Dynamic Strain Data on Four Simple Span Girder-Slab Bridge Structures. Civil Engineering Department, Univ. of Maryland, Rept. 29, June 1969.
5. C. F. Galambos and W. L. Armstrong. Loading History of Highway Bridges. Highway Research Record 295, 1969, pp. 85-98.
6. P. P. Christiano, L. E. Goodman, and C. N. Sun. Bridge Stress-Range History. Highway Research Record 382, 1972.
7. T. R. Douglas. Fatigue Life of Bridges Under Repeated Highway Loadings. Highway Research Record 382, 1972.
8. W. T. McKeel, Jr., C. E. Maddox, Jr., H. L. Kinnier, and C. F. Galambos. Loading History Study of Two Highway Bridges in Virginia. Highway Research Record 382, 1972.
9. F. Cicci and P. Csagoly. Assessment of the Fatigue Life of a Steel Girder Bridge in Service. Transportation Research Record 507, 1974.
10. D. W. Goodpasture and E. G. Burdette. Comparison of Bridge Stress History Results With Design-Related Analyses. Highway Research Record 428, 1973.
11. D. G. Bowers. Loading History of Span 10 on Yellow Mill Pond Viaduct. Highway Research Record 428, 1973.
12. C. F. Galambos and W. L. Armstrong. Acquisition of Loading History Data on Highway Bridges. Public Roads, Vol. 35, No. 8, June 1969.
13. Standard Specifications for Highway Bridges. American Association of State Highway Officials, 1969.
14. G. G. Goble, F. Moses, and A. Pavia. Field Measurements and Laboratory Testing of Bridge Components. Case Western Reserve Univ., final rept., Jan. 1974.
15. J. W. Fisher, K. H. Frank, M. A. Hirt, and B. M. McNamee. Effect of Weldment on the Fatigue strength of Steel Beams. NCHRP Rept. 102, 1970.
16. F. Moses and R. C. Garson. New Procedure for Fatigue Design of Highway Bridges. Transportation Research Record 507, 1974.
17. F. Moses, G. G. Goble, and A. Pavia. Truck Loading Model for Bridge Fatigue. Presented at ASCE Specialty Conference on Metal Bridges, St. Louis, Nov. 1974.

FIELD TESTING OF AGUASABON RIVER BRIDGE IN ONTARIO

J. Peter C. King and Paul F. Csagoly,
Ontario Ministry of Transportation and Communications; and
John W. Fisher, Lehigh University

This paper describes the field testing of the Aguasabon River bridge in Ontario, a three-span, continuous, steel girder bridge with parabolic haunches of composite concrete slab construction. As part of the 1973 bridge testing program, the structure was tested both statically and dynamically with two load-testing vehicles. Because this structure had a history of failures of the haunch weld detail and because it was one of several similarly designed structures, it was decided to determine the actual bridge behavior under load as well as its structural adequacy. Outlined are the grid type and other analytical procedures followed to predict stresses and deflections, which are then compared with those values recorded during the static loading. An estimate of the fatigue life of the weld details is made by using the dynamic strain data obtained. General aspects of the behavior of the structure are discussed, and conclusions are drawn on the structural adequacy of the test bridge and the methods used in the analysis and testing.

•THE Ministry of Transportation and Communications, Ontario, has a continuing load-testing program in which about 10 structures are analyzed and load tested each year. This program is designed primarily to determine safe load-carrying capacity of some of the suspect structures of the more than 13,000 highway bridges in the province. To expand the knowledge on the behavior of highway structures under load, these bridges are subjected to rigorous testing. Extensive instrumentation is used and suitable test conditions are provided so that comparison can be made between current design-analytical techniques and actual field results.

The Aguasabon River bridge in northern Ontario was in the 1973 bridge testing program primarily because it had severe weld cracks at three locations on one girder. Because it is one of several similarly designed bridges, it was felt extensive testing of it would give a better understanding of the structural behavior of all these bridges.

STRUCTURAL DESCRIPTION

The Aguasabon River bridge is located on the north shore of Lake Superior on Highway 17 (Trans-Canada Highway), 130 miles (210 km) east of Thunder Bay, Ontario. The three-span, continuous structure, built in 1948, is of composite beam-slab construction designed by the Ontario Department of Highways for an H20 truck load.

The 200-ft (61-m) structure (Figure 1) consists of four 33-in. (84-cm) WF girders, haunched at both piers and abutments. These haunches were fabricated by cutting the bottom flange at the web fillet and welding a parabolic insert, which resulted in a 51.25-in. (1.30-m) section at the piers and abutments (Figure 2).

In 1963, severe cracks, one of them extending 44 in. (1.12 m) into the web along a diagonal line, were found at the vertical weld detail in three of the six haunch inserts of the north interior girder. These cracks were repaired by welding cover plates or insert plates in a fashion similar to that shown in Figure 3. Prior to the 1973 tests, dye-penetrant and magnetic-particle weld inspection techniques were used on the repairs and the 21 remaining vertical welds, with the result that four other weld cracks were discovered. Figures 4, 5, and 6 show two of these weld cracks. The cracked vertical

Figure 1. Aguasabon River bridge.

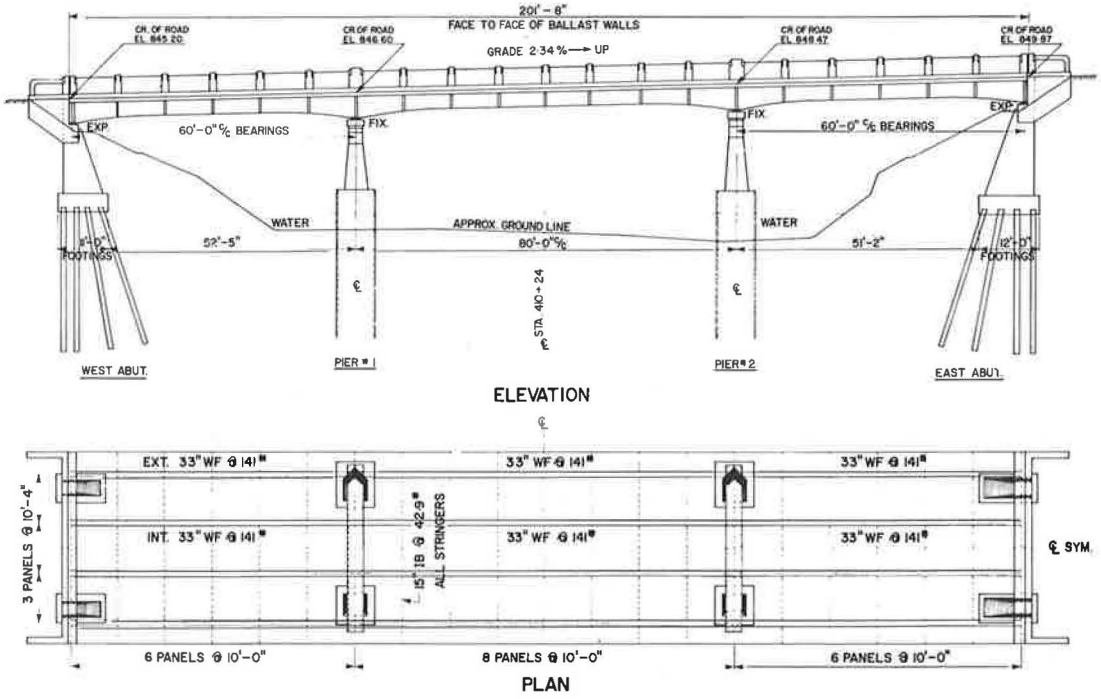

Figure 2. Shear connector and haunch details.

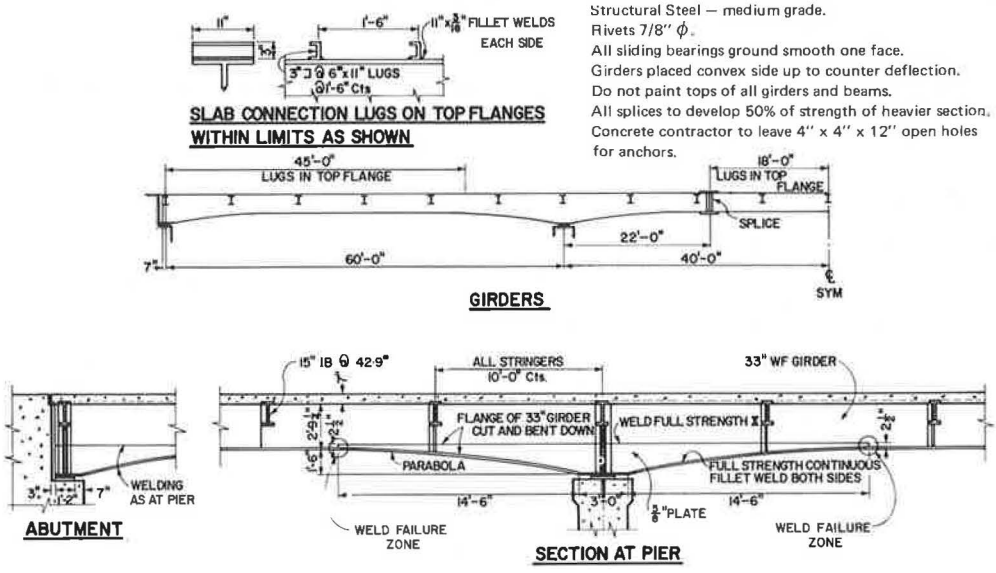

Structural Steel — medium grade.
Rivets 7/8" ϕ.
All sliding bearings ground smooth one face.
Girders placed convex side up to counter deflection.
Do not paint tops of all girders and beams.
All splices to develop 50% of strength of heavier section.
Concrete contractor to leave 4" x 4" x 12" open holes for anchors.

weld area was cut out in a circular shape, and an insert was welded in its place. Where the crack had penetrated the bottom flange, it was gouged out and filled with weld material, at a slow rate of deposit, by using low-hydrogen-coated electrodes. All repaired surfaces were subsequently ground flush to eliminate any stress risers.

The girders are field spliced at two points in the interior span 22 ft (6.7 m) from each pier, theoretically at the points of dead load contraflexure. Field personnel noted that the riveted splice consisted of $\frac{5}{8}$-in. (16-mm) flange plates on the interior and $\frac{1}{2}$-in. (12.7-mm) plates on the exterior girders. All had two $\frac{3}{8}$-in. (10-mm) web plates for the shear splice. Details of the field connection are shown in Figure 3.

The deck system consists of nominal 7-in.-thick (178-mm) two-way reinforced slab panels, continuous over adjacent girders, and 15-in. (381-mm) I-shape floor beams. The floor beam-to-girder connection serves as a vertical stiffener in addition to a shear transfer from floor beam to girder. Channel types of shear connectors were used in the regions of positive dead load moment to ensure composite action.

The piers are of the two-column bent type with concrete-filled sheet pile caissons. The abutments are similar in design but are supported by timber piles. There are no abutment walls, and consequently the fill behind the east abutment has slipped and has undermined the support beam and created a rough approach to the structure. The substructure is generally in good condition except that on the east abutment some of the reinforcing steel is exposed because of excessive spalling of the concrete.

A network of scaffolding was erected beneath the structure to enable free access to all weld and splice areas and to provide a working platform for inspection and instrumentation.

ANALYTICAL TECHNIQUES

The Ministry's Structural Research Section has at its disposal two load-testing vehicles, each capable of carrying a maximum payload of 153,000 lb (69 400 kg) with a gross vehicle weight (GVW) of 197,000 lb (89 350 kg) on five axles. This payload in turn can be placed on the semitrailer in such a manner as to produce any desired tandem axle weight of up to 110,000 lb (49 900 kg). The base length is 52 in. (1.32 m).

The analytical tools outlined above were used to determine the maximum test loads and critical vehicle positions based on a permissible maximum bending stress in the structural steel of 30 ksi (207 MPa).

Superstructure

A multiple-girder grid analysis computer program was developed by the Structural Research Section to determine bending moment, shear, reaction, or displacement of a multigirder bridge under a series of moving or static loads. The use of both transverse and longitudinal strips instead of finite elements as in other more general computer programs reduces the number of unknowns at each node to one, vertical displacement (1). This drastically reduces the amount of computation necessary to obtain the parameters mentioned above. The live load stresses resulting from the application of this program were combined with the computed dead load stresses to arrive at several load positions for maximum stresses at midspan, at the eastern pier, and at the end span for each of the four girders.

Web cutouts, taken from the weld failure zones (Figure 2), were analyzed to determine their chemical composition. Moreover, an examination of the fracture surfaces revealed that they were indeed fatigue cracks originating at extremely large initial weld imperfections and inclusions. Results of the chemical analysis of the base material (A7 steel) were as follows:

Chemical	Percent	Chemical	Percent
Carbon	0.24	Phosphorous	0.01
Manganese	0.74	Sulfur	0.03
Silicon	0.09		

Substructure

A working stress analysis was performed on both piers and abutments by using the vehicle configurations described above. Abutment stresses were within acceptable limits, but the stress in the pier tension reinforcement was extremely high when two fully loaded vehicles were located directly over the pier.

Proposed Test Loads and Test Procedure

As in all forms of structural analysis, many assumptions must be made to establish the load-carrying capacity of a bridge without expending an undue amount of time and effort. Thus this analysis should be supplemented by a careful testing procedure to prevent a catastrophic failure. Two fully loaded vehicles each with a GVW of 197,000 lb (89 360 kg) were approved through the Ministry's standard evaluation procedures as the maximum test loads. These loads were to be applied in four increments while stresses were monitored at the critical areas. The pretest analysis of the structure was used to determine both the maximum test loads and those areas in which stresses may be critical during testing.

Later in this paper, comparisons are made between the test results and the predicted stresses and moments (Table 1). The test load positions for the desired load increments are given in Table 2. These positions are shown in Figure 7.

INSTRUMENTATION

Figure 8 shows the location of the instrumentation used to measure all strains and deflections.

Deflection Measurement

Two theodolites of 1-sec resolution were used to determine deflection by triangulation. In the 50 to 100-ft (15 to 30-m) range in which they were used, an accuracy of ±0.006 in. (±0.15 mm) could be obtained. Because the structure is continuous over the piers and the pier reinforcement was expected to be highly stressed, pier settlement or deflection was also monitored. Without this information, the test results could never be correlated with analytical strains because of the severe effect any movement would have on the distribution of moments. Deflection targets were mounted on the east pier and abutment, at midspan, and at six locations in the end span on all four girders.

Strain Measurement

Thirty-four SR-4 electrical resistance strain gauges were mounted in pairs on the steel girders so that sectional bending moment values could be obtained. One gauge was mounted on the top of the bottom flange and the other on the bottom of the top flange. These were wired in a half active Wheatstone bridge configuration, with bridge completion in the instrumentation van. All but three were used to measure static strain.

These three, as well as an additional three gauges, were monitored through a set of dc high-gain operational amplifiers driving a multichannel light-beam oscillograph.

Figure 3. First north interior field splice and repair to weld failure (1963).

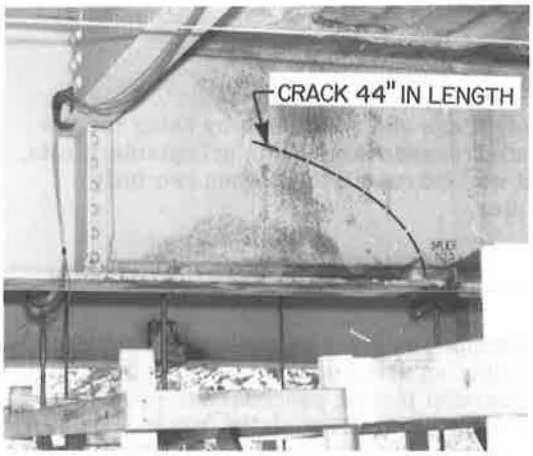

Figure 4. Dye-penetrant crack detection in fourth north exterior weld detail.

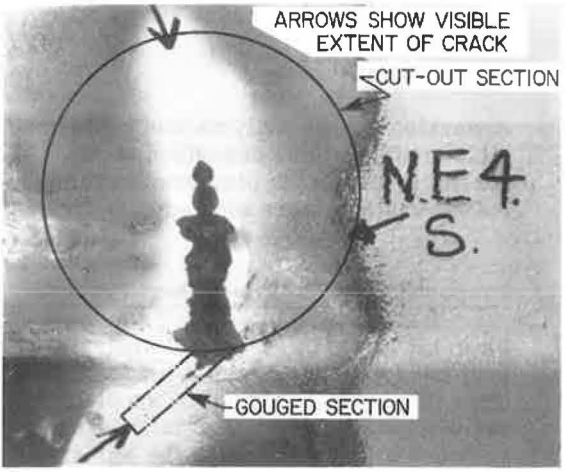

Figure 5. Cutout section of fourth north exterior weld detail.

Figure 6. Cutout section of second north exterior weld detail.

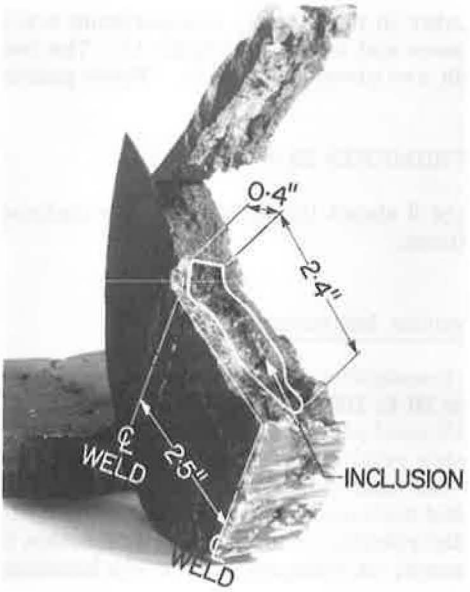

Table 1. Expected maximum live load stresses.

Location	Expected Stresses (ksi)		
	Live	Dead	Total
24-ft maximum end span	-20.1	-9.0	-29.1
44-ft second haunch weld detail	-15.8	+2.5	-13.3
60-ft east pier	+17.4	+14.1	+31.5
80-ft splice zone	-13.9	-2.0	-15.9
100-ft center span	-20.6	-10.5	-31.1

Note: 1 ft = 0.3 m; 1 ksi = 6.9 MPa.
"- = tensile stress; + = compressive stress.

Figure 7. Test positions identified in Table 2.

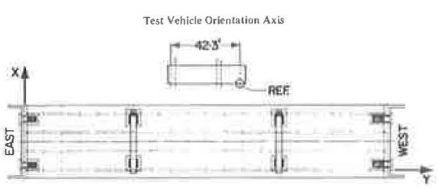

Several hours of continuous dynamic strain data were recorded by means of an FM tape recorder paralleling the light-beam oscillograph. The dynamic gauges were used in the static as well as in the dynamic tests so as not to lose any bending test data. An additional 12 gauges were used to monitor stress at several critical locations (Figure 8). Another strain gauge was mounted on a small block of steel, placed beneath the structure, to serve as an indication of instrument or temperature-induced drift.

TEST PROCEDURE

Dynamic Tests

To determine the fatigue life of the structure requires that its response to a typical heavy vehicle and the statistical distribution of the vehicle population be known. Recordings were made of dynamic strains as the test vehicle, loaded to a gross weight of 91,000 lb (41 280 kg), crossed the bridge at speeds varying from 30 to 50 mph (48 to 80 km/h). This information was used to select the most active gauges for the purpose of recording as well as an actual calibration of the dynamic strain system. Test data were recorded for $32\frac{1}{2}$ hours throughout the testing period.

Static Tests

The first series of tests was carried out with 36 load blocks (2,125 lb or 964 kg per block) on board each test vehicle or a GVW of 122,000 lb (55 340 kg). The strains recorded were generally well below those anticipated. The maximum was 341 μin./in. or 10.3 ksi (71.0 MPa). Because a number of vehicle positions were similar for different tests, several were combined into a single test and others were omitted, mainly because of a lack of time.

Strains measured in the first north interior (NI1) splice plate up until test 5B were roughly twice those found in the corresponding plate on the north exterior (NE) girder [maximum tensile and compressive strain ±77 μin./in. or ±2.7 ksi (18.62 MPa)]. It was observed during the positioning of the secondary vehicle (i.e., test 5B) that the strain gauge affixed to the NI1 splice plate indicated strains of 752 μin./in. or 26 ksi (179.3 MPa). Also, a loud, explosion-like sound was heard by those beneath the structure, and it was assumed to have come from the region of the central span. When the load was removed, a permanent set of 634 μin./in. or 22 ksi (151.7 MPa) was indicated by the strain-measuring instruments if the elastic modulus applied. The remaining gauges indicated that elastic strains existed in the rest of the structure.

To clarify the questionable results from this splice plate, an additional strain gauge was attached near the first and was monitored throughout the second day of testing. When the load was increased to 147,000 lb (66 680 kg) on each vehicle (48 test series) a similar situation was encountered. The explosive sound was heard, louder than before, and plate stresses this time reached 38 ksi (262.0 MPa) or 1,095 μin./in. with a permanent offset of 940 μin./in. The second strain gauge confirmed the readings obtained from the original one. A number of repeated loadings were made with plate movements measured by precision dial gauges, and a similar elastic strain was recorded with increasing permanent set each time. This confirmed suspicions that the splice plate had undergone considerable yielding. The remainder of the tests were completed at this load value, but test series 60 and 72 were abandoned because there was fear that serious structural damage would result. Figure 9 shows a typical loading condition of test series 48.

Table 2. Test vehicle positions.

Maximum Moment		Test	Vehicle Location					
			Primary A			Secondary B		
Location	Sign	Number	X	Y	Direction	X	Y	Direction
End span, 24 ft								
Exterior	+	1	0.67	58.33	West	15.67	58.33	West
Interior	+	2	5.67	56.33	West	15.67	58.33	West
Pier, 60 ft								
Exterior	+	3	0.67	118.33	West	0.67	64.33	West
Interior	+	4	6.67	31.67	East	4.67	75.67	East
Center span, 78 ft								
Exterior	+	5	0.67	61.67	East	15.67	71.67	East
Interior	+	6	4.67	61.67	East	15.67	61.67	East
Exterior	-	7	0.67	5.67	East	15.67	3.67	East
Interior	-	8	0.67	5.67	East	15.67	5.67	East
Center span, 100 ft								
Exterior	+	9	0.67	136.33	West	15.67	128.33	West
Interior	+	10	4.67	138.33	West	15.67	136.33	West
First interior floor beam	+	11	4.67	50.00	West	15.67	50.00	West

Note: 1 ft = 0.3 m.

Figure 8. Instrumentation.

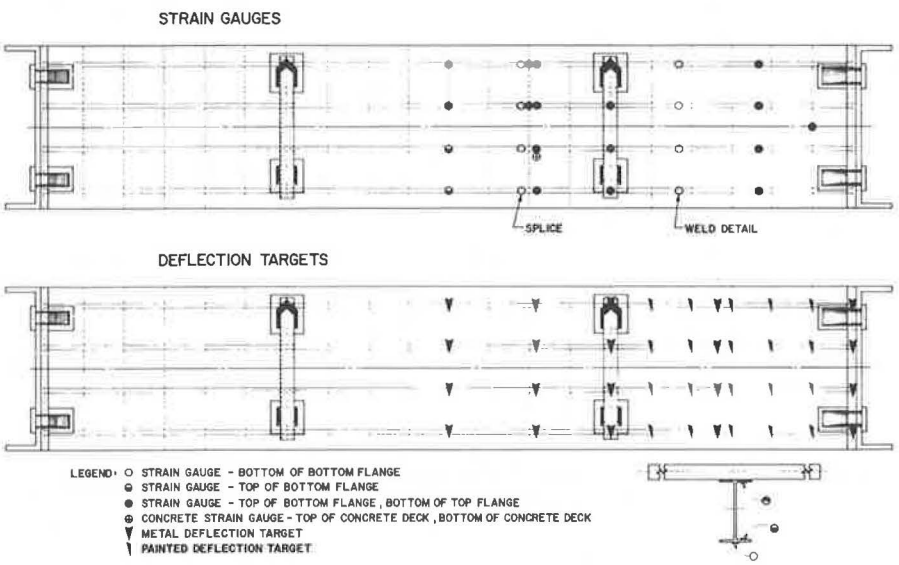

Figure 9. Test 1B-48 maximum moment at east end span.

DATA ANALYSIS

Deflections

The use of triangulation techniques to reduce all deflection data resulted in the deflected shape of the structure under load. Measured deflections were compared to revised deflection results from the multigirder computer program by using loading conditions identical to those used in the field. The maximum recorded deflection was 0.756 in. (19.2 mm) at the center span with a 244,000-lb (110 680-kg) live load on the structure in comparison with the revised calculated deflection of 0.732 in. (18.6 mm). Pier and abutment displacements were negligible. Deflection distribution factors similar to the AASHTO load distribution factors, in terms of girder spacing (2), are given in Table 3.

Static Strains

Sectional values of bending moment were obtained from strain data recorded at two locations (A and B in Figure 10a) for each pair of strain gauges. Two major assumptions were made in this analysis:

1. The distribution of strains throughout the slab and the steel girder is linear, and
2. The steel girder and the slab deflect equal amounts at all test points (i.e., equal curvatures, thus parallel strain distributions in the slab and beam).

Expressions can be derived as outlined in the appendix[1] relating measured strains and the internal forces acting within the partially composite section (3), and sectional bending moments were easily calculated. These in turn were compared with revised multigirder program runs with the actual loading conditions. Distribution factors were derived in a manner similar to that used for deflection. The effect of slip between the girder and slab on the distribution of strain throughout the composite section is currently under investigation by the Structural Research Section. This study may aid in clarifying the behavior of composite structures such as the Aguasabon River bridge.

Dynamic Strains

Figure 11 shows three typical strain records made when the test vehicle was traveling at 45 mph (72 km/h) in the eastbound lane. These and other traces were examined, and a representative histogram of stress range (S_r) was determined (Figure 12). The service life of the welded details of the Aguasabon River bridge was estimated from the measured stress range histogram and the estimated fabricated flaw conditions that existed in the structure.

The stress range histogram was used to estimate the root mean square stress range S_{rRMS} for various minimum stress range conditions. When all stress range levels greater than 0.85 ksi (5.9 MPa) were considered, this resulted in S_{rRMS} = 1.92 ksi (13.2 MPa) at an annual rate of 1,340,000 cycles. This also provided a lower life estimate than when smaller stress range levels were considered.

Service life was estimated from the crack growth relationship developed for welded steel details (8, 9). The semiempirical differential equation of crack growth was taken as

[1] The original manuscript included an appendix on determining strain relationships. That appendix is available in Xerox form at cost of reproduction and handling from the Transportation Research Board. When ordering, refer to XS-66, Transportation Research Record 579.

Table 3. Deflection distribution factors.

Test	24 Ft		78 Ft		100 Ft	
	Deflection Distributor Factor[a]	Deflection[b]	Deflection Distributor Factor	Deflection	Deflection Distributor Factor	Deflection
1A-36	0.491	0.055				
1A-48	0.846	0.026				
1B-48	0.339	0.124				
2A-36	0.331	0.046				
5A-36			0.412	0.085	0.407	0.118
5B-36			0.333	0.129	0.317	0.199
5A-48			0.365	0.074	0.404	0.109
6A-48			0.417	0.084	0.373	0.118
6B-48			0.366	0.172	0.341	0.226
7A-48			NA	NA	0.379	0.029
9A-36			0.367	0.060	0.400	0.095
9B-36			0.336	0.125	0.335	0.194

Note: 1 ft = 0.3 m.

[a]Percentage girder with greatest deflection is of sum of all four deflections.
[b]Sum of all four deflections at a single cross section.

Figure 10. Composite T-beam with incomplete interaction (slip): (a) cross section, (b) forces, and (c) strain distribution.

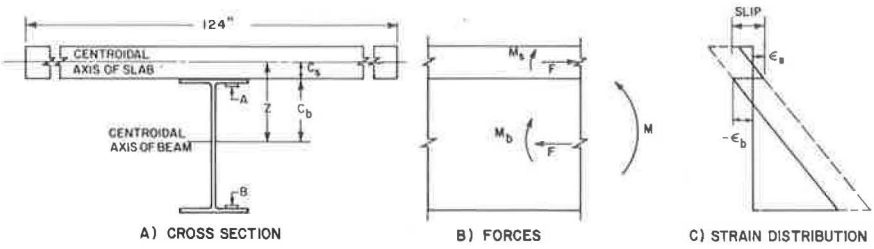

Figure 11. Typical dynamic response.

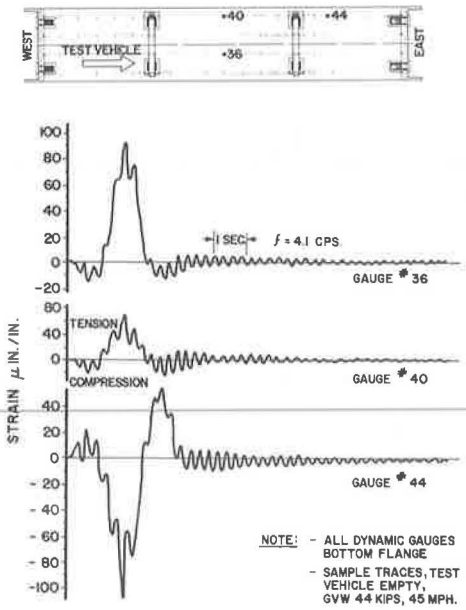

$$da/dN = 2 \times 10^{-10} \Delta K^3 \quad (1)$$

The stress intensity factor was estimated for two stages of crack growth. The first corresponded to the internal weld discontinuity (inclusion) that was fabricated into the vertical groove welds. The fabricated discontinuity was assumed to provide an initial crack condition. The embedded discontinuity was assumed to act as an embedded elliptical crack perpendicular to the bending stress field. For this stage of crack growth, K was estimated as

$$K = \frac{\sigma}{\phi_o} \sqrt{\pi a} \sqrt{\text{Sec} \frac{\pi a}{t}} \quad (2)$$

where

σ = bending stress,
a = half the minor diameter of the elliptical crack,
t = thickness of the weld (0.8 in. or 20 mm), and
ϕ_o = elliptical integral that depends on the minor-to-major axis ratio of the crack.

After the fatigue crack had penetrated the web weld thickness, the remaining life was estimated by assuming that the web crack propagated through the flange as a penny-shaped crack. This model has been demonstrated to be applicable to crack growth in welded beams that experience crack growth from internal flaws in the web-flange welded connection (8). It has also been used to estimate the interval of life for stiffeners welded to the web alone after the fatigue crack had penetrated the web thickness (9). The K-value was taken as

$$K = \frac{2}{\pi} \sigma \sqrt{\pi a} \sqrt{\text{Sec} \frac{\pi a}{2r}} \quad (3)$$

for this stage of growth, where r is the distance from the origin to the bottom of the flange surface.

The life intervals for the two stages of growth were estimated from equations 1, 2, and 3, which resulted in

$$N = \frac{10^{10}}{2} \int_{a_i}^{a_f} \frac{da}{\Delta K^3} \quad (4)$$

During the first stage of growth, the life interval N_1 was estimated by assuming that growth occurred in the direction of the minor axis 2a with a relatively constant major axis 2b, until the weld surface was penetrated (Figure 13). The second stage of growth, in which a penny-shaped crack was assumed, was used until the crack had penetrated the bottom flange thickness.

S_{rRMS} was used to describe the random variable stress field inasmuch as recent studies have shown that it is a satisfactory method for relating constant and variable cycle loading (10, 11). Hence, when ΔK was defined in terms of equations 2 or 3, S_{rRMS} was used for σ.

The results of the analysis (Table 4) revealed that S_{rRMS} = 1.92 ksi (13.2 MPa), and an annual rate of 1,340,000 stress cycles provided the least life prediction. For the inclusion shown in Figure 4, it was estimated that approximately 3½ years would be required before the crack penetrated the bottom flange surface during the first stage of

crack growth. An additional 20 years would be required before the crack penetrated the bottom flange surface during the second stage of crack growth.

The same inclusion was also examined for other locations in the web weld. If the inclusion were centered in the web, as many as 20 years could be required to penetrate the web surface. Smaller inclusions would obviously require a greater time interval (Table 4).

The results of the analysis are in good agreement with field experience with these welded details. The first cracked details were detected in 1963 after about 15 years of service and in all probability had a more severe initial discontinuity than the detail analyzed. An increase in the discontinuity size would decrease the life expectancy. Of the four cracks detected in 1973 after 25 years of service, only one had completely penetrated the bottom flange surface. Given an estimated life expectancy of between 23 and 40 years, these various stages of crack growth are comparable. Details that have no visible damage may have internal cracks that have not yet penetrated the web surface.

Because the weld inclusions far exceeded the level of internal discontinuities that are permitted at groove weld transverse to the bending stress field, the allowable design stress range is not applicable to these details. The design value is based on and assumes normal fabrication conditions, which were not present (4). Hence, comparisons with past or present design conditions provide no insight into the performance of these joints.

DISCUSSION OF TEST RESULTS

Discussions of continuous steel girder bridges have been written by the designer of the Aguasabon River bridge (6, 7). He states that the splice plates are designed for 50 percent of the capacity of the steel girder (WF section). By current specifications, this value appears to be very low; a minimum of 75 percent is now required (2).

Because in test 5B-48 the recorded stress was in excess of that required for yield, it is safe to assume that at least some of the residual strain recorded was due to plastic deformation in the splice material. This theory is further confirmed by tests made with precision dial gauges, which showed that the splice plates slide to a varying extent under a moving load and then hang up on rivets. It was when this movement was prevented that the high stresses were recorded in the splice plate.

The multigirder program requires inertia, torsional stiffness of the exterior girders, and diaphragm stiffness values as input to mathematically describe the structure. As might be expected, any variation in these parameters makes a significant change in computed deflections and moments. The first trial using inertias suggested by AASHTO provided poor agreement with the experimental deflected shape. However, by increasing the inertias in the negative dead load bending moment region, the computed deflections approached the experimental cross-sectional average. The final inertias used corresponded to a fully composite deck throughout the length of the bridge, with 80 percent of the slab width effective. Further variation of the floor beam stiffnesses and the torsional stiffness of the exterior girder would provide better transverse agreement. Correlation between experimental and theoretical moments was not consistent. Good agreement was obtained at midspan, and poor to fair agreement was obtained elsewhere. Figures 14 and 15 show the agreement obtained for test 5A-36 for both deflection and moment respectively.

As many as 20 bridges in the province of Ontario were constructed in the late 1940s by using a design similar to that of the Aguasabon River bridge. Based on the tests, a thorough inspection and analysis of each structure were undertaken. Of these structures, seven were found to have substandard splices and nine were found to have weld details that were prone to fatigue cracking. Subsequently, all of the splices were structurally reinforced and all of the suspect weld zones were repaired.

Figure 12. Stress range histogram (smoothed).

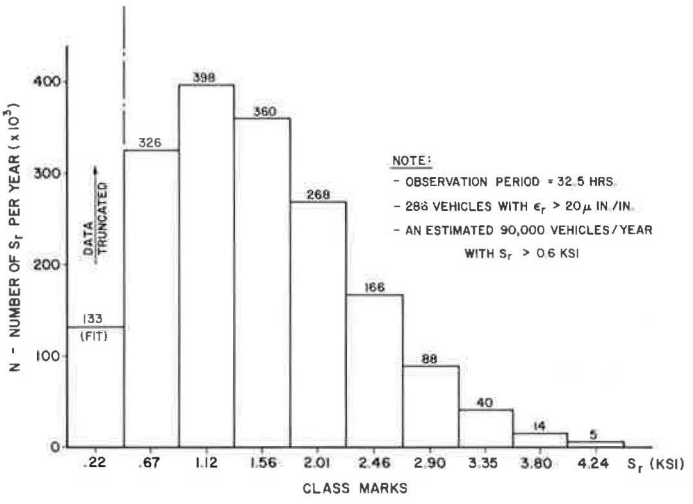

Figure 13. Assumed stages of crack growth.

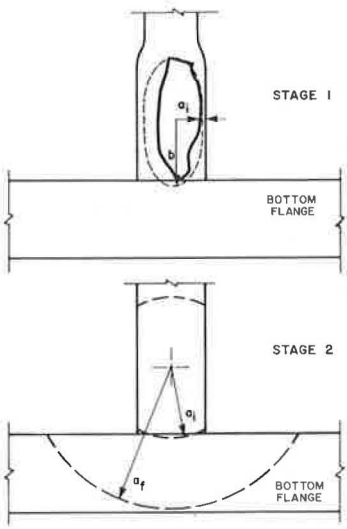

Table 4. Summary of estimated life.

Cracking Stage	Initial Crack Size (in.)	Initial Crack Radius (in.)	Stress Cycles (S_{rRMS} = 1.92 ksi)	Years to Achieve
Crack growth through web	0.25		25,360,000	18.9
	0.30		8,175,000	6.1
	0.32		4,500,000	3.4
Crack growth through flange		1.40	31,700,000	23.6
		1.45	26,200,000	19.6
		1.50	21,400,000	16.0

Note: 1 in. = 2.5 cm; 1 ksi = 6.9 MPa.

Figure 14. Deflected shape.

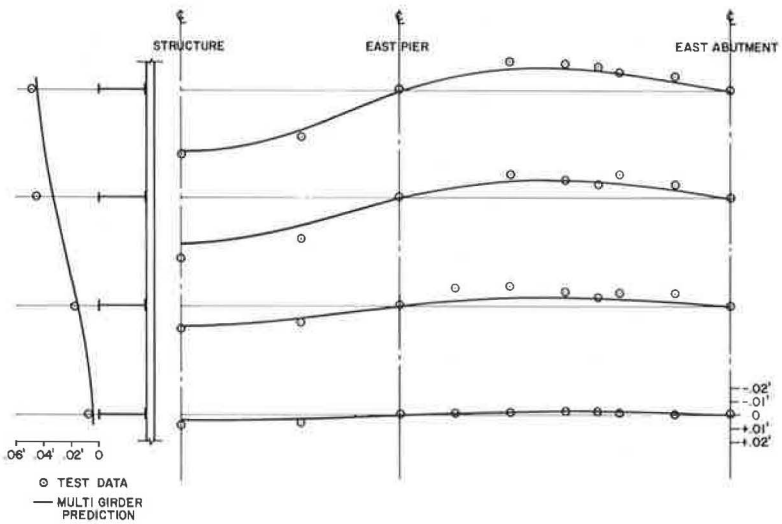

Figure 15. Cross-sectional moment distribution.

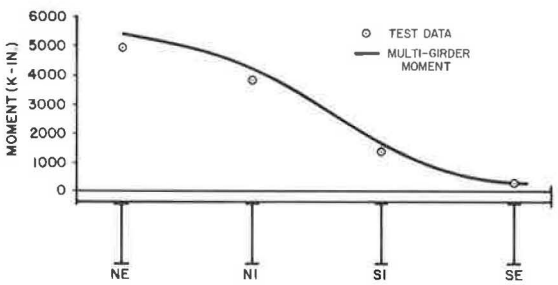

CONCLUSIONS

1. Throughout testing, commercial traffic using the structure consisted of a consisted of a considerable number of six-axle vehicles with an estimated gross weight of 112,000 lb (50 900 kg). With a 35 percent impact factor, these vehicles are imposing high cyclic stresses equal to or in excess of those in series 48 tests. Thus, the splice plates are damaged continually, which promotes crack growth and eventual failure.
2. From the evaluation of the experimental data, fatigue failures at the vertical groove welds in the beam web were inevitable with the large weld inclusions fabricated into the structure. With proper welding techniques the fatigue strength of the structure would be more than adequate.
3. A more detailed study of slab stresses could be carried out to better arrive at values of composite inertia. Slip between the steel and concrete could also be measured to provide a further check on the assumption of linear strain throughout the semicomposite section.
4. To satisfactorily model the structural behavior under load required that a value of 80 percent effective width of the deck slab be assumed. This value was used throughout the full length of the structure, even in the regions designed as noncomposite. This assumption could be substantiated by further tests of continuous structures with particular attention paid to slab and reinforcing steel stresses in the negative moment regions.

REFERENCES

1. P. F. Csagoly, C. Y. Chung, and B. Bakht. Computer Program for the Analysis of Multi-Girder Bridges. Ministry of Transportation and Communications, Downsview, Ontario.
2. Standard Specifications for Highway Bridges. American Association of State Highway Officials, 1973.
3. C. P. Siess, I. M. Viest, and N. M. Newmark. Studies of Slab and Beam Highway Bridges: Part III. Engineering Experiment Station, Univ. of Illinois, Bulletin Series 396, Vol. 49, No. 45, Feb. 1952, pp. 115-133.
4. J. W. Fisher, K. H. Frank, H. A. Hirt, and B. M. McNamee. Effect of Weldments on the Fatigue Strength of Steel Beams. NCHRP Rept. 102, 1970.
5. M. A. Miner. Cumulative Damage in Fatigue. Journal of Applied Mechanics, Vol. 12, No. 1, Sept. 1945.
6. L. Loch. Bridges Over Railways. Roads and Bridges, Nov. 1947.
7. L. Loch. Continuous Steel Girder Bridges. Roads and Bridges, Feb. 1947.
8. M. A. Hirt and J. W. Fisher. Fatigue Crack Growth in Welded Beams. Engineering Fracture Mechanics, Vol. 5, 1973, pp. 415-429.
9. J. W. Fisher, P. A. Albrecht, B. T. Yen, D. J. Klingerman, and B. M. McNamee. Fatigue Strength of Steel Beams With Welded Stiffeners and Attachments. NCHRP Rept. 147, 1974.
10. J. M. Barsom. Fatigue-Crack Growth Under Variable Amplitude Loading in ASTM A514 Grade B Steel. ASTM, STP 536, 1973.
11. C. G. Schilling, K. H. Klippstein, J. M. Barsom, and G. T. Blake. Fatigue of Welded Steel Bridge Members Under Variable-Amplitude Loadings. NCHRP, Research Results Digest 60, April 1974.

ANALYSIS OF A CONTINUOUS CURVED BOX GIRDER BRIDGE

C. Yoo,* Marquette University;
J. Buchanan, Ralph M. Parsons Company, Los Angeles;
C. P. Heins, University of Maryland; and
W. L. Armstrong, Federal Highway Administration

An analytical method for determining the response of horizontally curved bridges to loads is discussed. The predicted behavior of a curved box bridge under construction was compared to the actual behavior of such a bridge. The superstructure of the bridge tested consists of twin steel box girders in composite action with a 10-in. (25.4 cm) reinforced concrete slab. The portion of the bridge examined in this study was a three-span continuous structure designed for two-lane traffic. Two experimental testing programs were performed on the bridge. The first consisted of measuring the response of the steel box girders when a concrete deck was poured. When the construction of the bridge was completed, a second testing program involved measuring throughout the structure deformations and strains induced by the load of an FHWA test vehicle. Stresses, deformations, and load distributions are plotted, tabulated, and discussed. Comparisons of the analytical predictions, design values, and measured responses of the bridge are also presented.

•AS THE Interstate Highway System has grown, the demand for curved viaducts has increased. Curved viaducts are an efficient means of routing traffic at a multilevel interchange and thus optimize the use of limited rights-of-way. When curved alignments were introduced, they were generally composed of a series of straight girders used as chords, which dictated shorter spans, a large number of support units, large overhanging slabs, and less continuity.

Recently, however, sophisticated analytical methods for the design and analysis of curved girder bridges have been developed. One method of analysis (11, 12) was developed in 1973 at the University of Maryland. The analytical technique is based on differential equations that describe the behavior of single curved girders by using the finite difference and matrix displacement methods (10). The resulting equations are used to determine the response of nonprismatic single curved girders (CURSGL) and curved bridge systems (CURSYS) through use of computer programs (11, 12). Comparison of the results obtained from these analytical techniques (deflections, rotations, bending moments, vertical shears, St. Venant and warping torsion and bimoments) and those obtained from the experimental models (4, 9) shows excellent correlation.

This paper presents an analysis of a continuous curved box girder bridge and comparisons with the data based on the experiment conducted on the bridge. The correlation of analytical and experimental results establishes the effectiveness of and confidence in an analytical method for predicting the behavior of a curved box girder bridge. The bridge, instrumentation, test data, and formulation of an analytical model are described, and the results are discussed.

*When this paper was written, Mr. Yoo was visiting assistant professor, University of Maryland.

Figure 1. Plan of bridge.

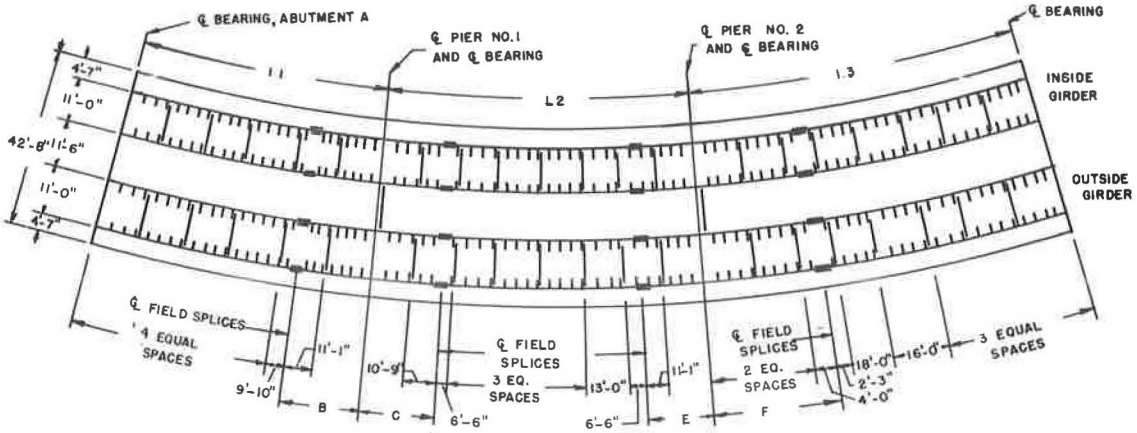

Figure 2. Typical cross section of bridge.

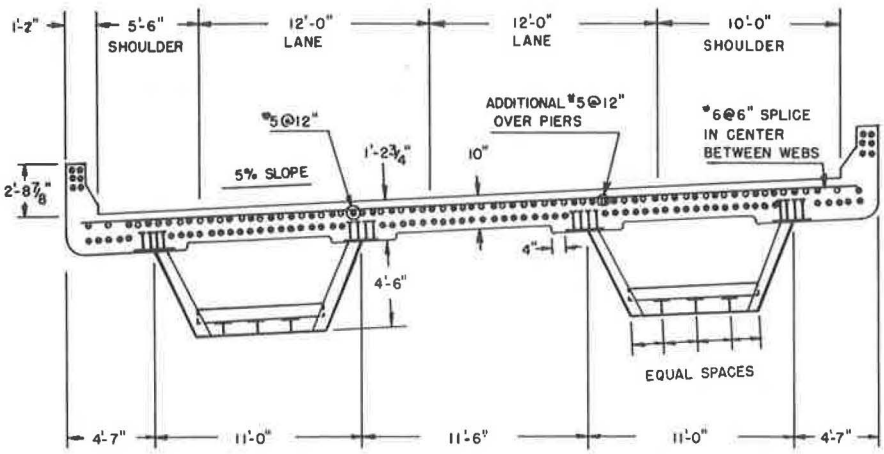

Figure 3. Detail of girder.

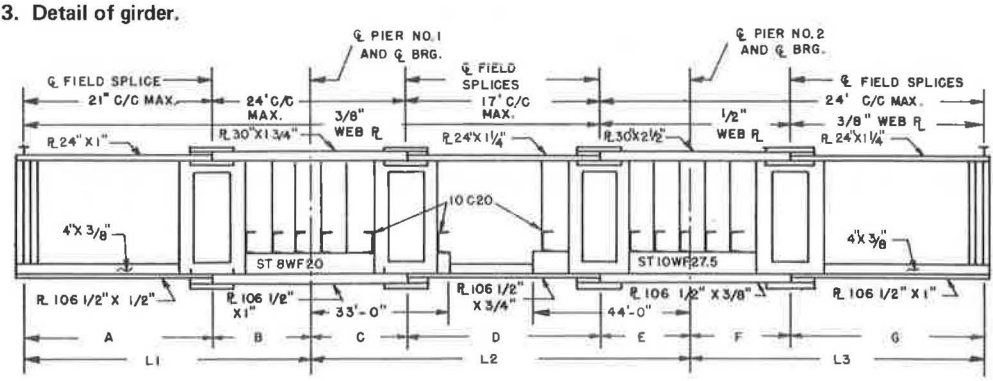

TABLE OF DIMENSIONS

GIRDER		A	B	L1	C	D	E	L2	F	G	L3	R
INSIDE	℄ LEFT TOP FLANGE	70'-6 3/4"	29'-2 15/16"	99'-9 11/16"	28'-0 5/16"	75'-2 3/8"	28'-0 5/16"	131'-3"	34'-7 5/16"	86'-1 7/8"	120'-9 3/16"	1300.981
	℄ RIGHT TOP FLANGE	71'-1 7/8"	29'-5 15/16"	100'-7 13/16"	28'-3 3/16"	75'-9 15/16"	28'-3 3/16"	132'-4 5/16"	34'-10 13/16"	86'-10 3/4"	121'-9 9/16"	1311.981
OUTSIDE	℄ LEFT TOP FLANGE	71'-9 3/8"	29'-9 1/16"	101'-6 7/16"	28'-6 3/16"	76'-5 13/16"	28'-6 3/16"	133'-6 3/16"	35'-2 1/2"	87'-7 15/16"	122'-10 7/16"	1323.481
	℄ RIGHT TOP FLANGE	72'-4 9/16"	30'-0"	102'-4 9/16"	28'-9"	77'-1 1/2"	28'-9"	134'-7 1/2"	35'-6"	88'-4 13/16"	123'-10 13/16"	1334.481

DESCRIPTION OF BRIDGE AND TESTING PROGRAMS

During fall 1973, the I-695 and I-83 interchange, C viaduct, located near Baltimore (Figure 1) was tested and analyzed for both dead and live loads. The superstructure consists of two large trapezoidal 4.5 by 11.0-ft (1.4 by 3.4-m) steel box girders with a 10-in. (25.4-cm) composite reinforced concrete deck (Figure 2). The bridge is a 12-span structure consisting of four units, each unit continuous over three spans. Unit 1 located at the north end of the bridge was selected for testing because it was most easily accessible in terms of elevation and existing traffic conditions. The bridge has a centerline radius of approximately 1,318 ft (402 m), and the span lengths are 100, 133, and 122 ft (30.5, 40.5, and 37.2 m) as shown in Figure 3.

The design of unit 1 is typical of that of the other three units. It was fabricated of five sections of steel, spliced at four locations of zero or small bending moment in the longitudinal direction as shown in Figures 1 and 3. The sections over the interior supports were designed under the assumption that the reinforced concrete deck does not yield composite action; however, the designer included shearing studs throughout the length. In the analytical model, it was assumed that the 10-in. (25.4-cm) concrete deck acted compositely. The dimensions for both boxes at any given point in the longitudinal direction are the same. The typical cross-sectional dimensions of unit 1 are shown in Figure 2. Details of construction can be found elsewhere (5).

Two testing programs were conducted on the bridge during two phases of construction. The first, the dead load test, measured the response of the bridge to the different phases of the placement of concrete deck. The second program, the live load test, measured the stresses and deformations induced by the load of an FHWA test vehicle on the completed structure.

Instrumentation

Eighteen rosette and 72 uniaxial strain gauges were mounted at four locations in the longitudinal directions (Figure 4). FHWA deflectometers were used. The response of the gauges was recorded on a 100-channel automatic digital strain indicator and two 10-channel portable units for dead load and on an FM analog tape recorder and oscillographs for live load.

Dead Load

The four locations of the strain gauges were selected on the basis of where the maximum positive and negative bending moments were expected to occur. The concrete was placed for each of the five steel sections separately by using the splice locations as boundaries. A summary of the dead load test results is given in Tables 1 and 2. The design values given in the tables were obtained directly from the designer. The design values shown for LL+I are not comparable with analytical and experimental values because the design loading condition was not consistent with the analytical and experimental loading condition.

Live Load

An FHWA test vehicle simulating an HS20-44 truck loading was used. The actual load distribution for the vehicle was 10,250 lb (4650 kg) on the front axle, 32,500 lb (14 750 kg) on the drive axle, and 31,750 lb (14 400 kg) on the trailer axle. The gross weight of the vehicle was 74,500 lb (33 800 kg).

The test was designed to measure the response of the bridge at various positions and speeds of the test vehicle. The vehicle traversed the bridge in four specified lanes (Figure 5) at speeds ranging from a crawl of 2 mph (3.2 km/h) to 50 mph (80 km/h).

Figure 4. Locations of (a) longitudinal and (b) transverse strain gauges.

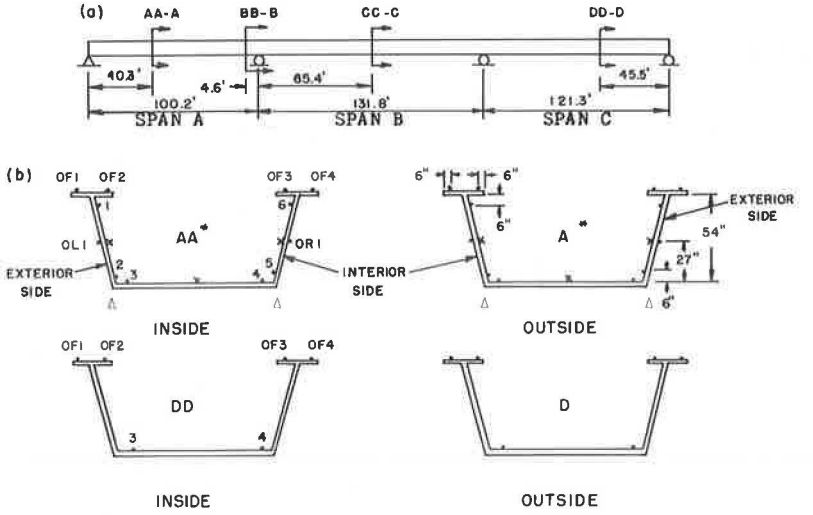

Δ Deflectometer Section AA-A (Section CC-Δ Exterior Sides only)

• UNIAXIAL GAGE

× ROSETTE GAGE

■ SAME GAGE LOCATION FOR SECTIONS BB-B AND CC-C, EXCEPT GAGES OL1 AND OR1 WHICH ARE PRESENT ONLY AT AA-A

Table 1. Comparison of experimental, analytical, and design deflections.

Location	Loading	Maximum Deflection (in.) Experimental	Analytical With Bracing[a]	Analytical Without Bracing[a]	Design	Allowable[b]
Δ 1-4	DL	1.19	0.88	0.93	1.00	
	LL+I	0.20	0.23	0.23	0.61	
	DL+LL+I	1.39	1.11	1.16	1.61	1.50
Δ 5, 6	DL	0.50	0.51	0.47	0.69	
	LL+I	0.26	0.27	0.27	0.94	
	DL+LL+I	0.76	0.78	0.74	1.63	1.98

Note: 1 in. = 2.5 cm.

[a]The impact factor applied to the analytical deflections for LL+I is based on the maximum average impact factor of 28.6 percent measured experimentally.

[b]According to AASHTO (span length/800).

Table 2. Comparison of experimental, analytical, and design stresses.

Section	Loading	Maximum Normal Stress at Bottom Flange (ksi) Experimental[a]	Analytical With Bracing	Analytical Without Bracing	Design	Allowable
A	DL	+7.70	+6.25	+9.02	+9.31	
	LL+I	+2.32	+2.65	+2.65	+6.86	
	DL+LL+I	+10.02	+8.90	+11.67	+16.17	+19.36
B	DL	-5.14	-4.96	-6.66	-11.51	
	LL+I	-0.76	-1.05	-1.05	-4.73	
	DL+LL+I	-5.90	-6.01	-7.71	-16.24	-19.63
C	DL	+6.12	+3.26	+4.27	+7.06	
	LL+I	+1.83	+2.07	+2.07	+6.97	
	DL+LL+I	+7.95	+5.33	+6.34	+14.03	+19.78

Note: 1 ksi = 6.9 MPa.

[a]Experimental dead load stresses were limited in quantity. Therefore, those shown may not be the maximum although they should be representative.

The crawl speed was assumed to eliminate virtually all dynamic effect of the moving vehicle.

Too few rosette gauges were mounted to justify a comparison of the measured shearing stresses with those obtained analytically. To reduce the test data, various computer programs were used (5). A summary of the results is shown in Figures 6 and 7 and in Table 2.

ANALYTICAL MODEL

Detailed descriptions of the two programs used in the analysis can be found elsewhere (12). Capabilities of these programs are given in Table 3. For the dead load test, the only structural member to connect the two boxes was the steel corrugated sheet, which was assumed to have negligible effects. Because there would be no interaction between the two boxes, each girder would act independently and the results from CURSGL would be identical to those from CURSYS. CURSGL was therefore selected for the dead load analysis, and CURSYS was used for live load analysis. Variations in the dimensions of the longitudinal cross section were incorporated by treating the governing differential equations with variable coefficients. To eliminate the numerical disturbance, it was assumed that the variation of the section properties spread to several nodal points in each side.

Dead Load Analysis

Top lateral bracing was added to the design to prevent excessive distortions of the cross section during the placement of concrete. This bracing in effect changed the configuration of the box girder from an open cell to a semiclosed cell. Therefore, both open cross section and closed cross section properties were used in the dead load analysis. To determine the section properties of the closed section, the top lateral bracing was replaced with an equivalent plate of constant thickness t_{eq}, determined from an equation developed by Dabrowski (6) and checked against equations developed by Kollbruner and Basler (8). The values from these two equations are approximately the same. The transverse K-bracing and the longitudinal lateral stiffeners were not included in the determination of section properties. The section properties were determined from a program developed by Blank (3). Properties used in the analytical procedure for sections with and without top bracing are given in Table 4.

The loading scheme in CURSGL requires vertical or torsional loads to be applied directly to the center of the girder. The total vertical load of concrete deck per unit length in the longitudinal direction, acting at the center of mass, was resolved into the centerline of the curved element with an equivalent vertical and torsional load. The bending stresses were computed by using

$$\sigma_f = M_x * c/I_x$$

The warping normal stresses were calculated by using

$$\sigma_w = BM * W_n/I_w$$

These stresses were then superimposed to obtain the final normal stresses, σ_t.

Figure 5. Location of lanes for test vehicle.

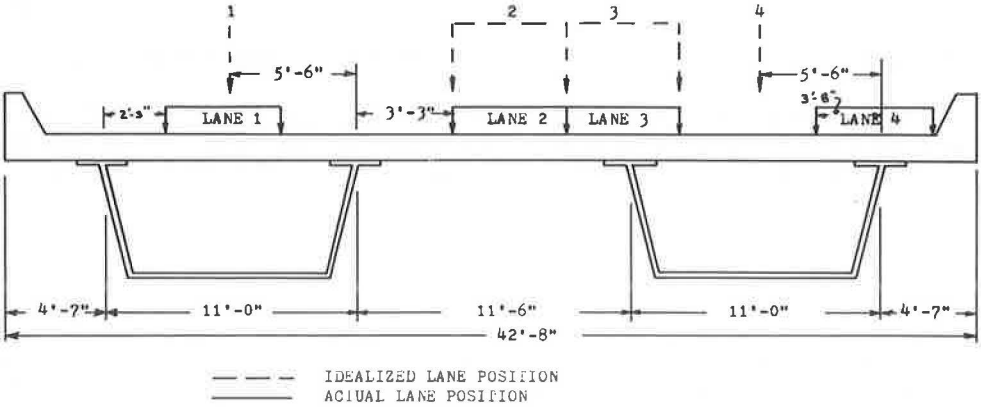

Figure 6. Normal stress, live load test (load point 3).

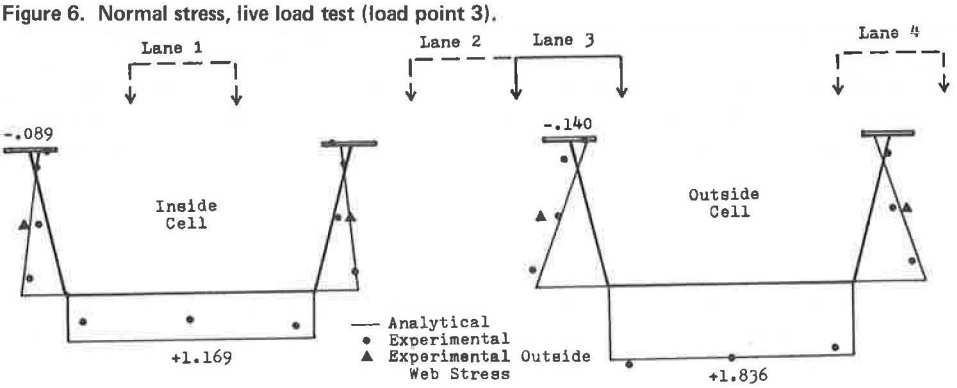

Figure 7. Normal deflection, live load test (load point 4).

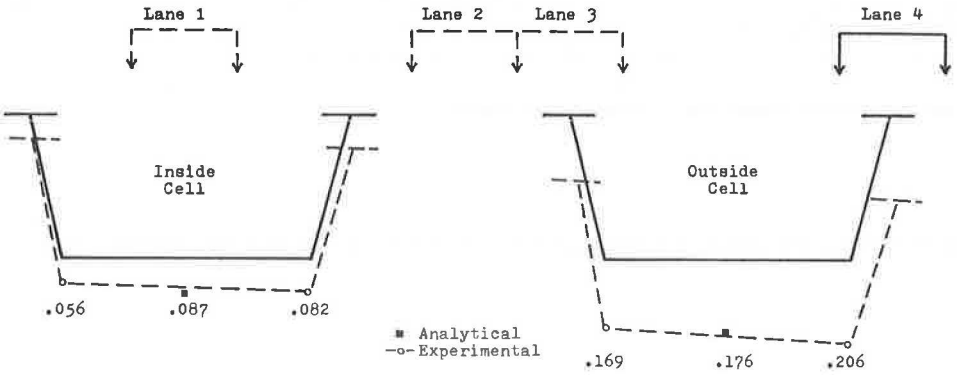

Table 3. Capabilities of CURSGL and CURSYS programs.

Capability	CURSGL	CURSYS
End support conditions may be either fixed or pinned or a combination in bending and torsion.	Yes	Yes
Simple span and multispan can be considered.	Yes	Yes
Dynamic storage allocation and segmentation are used.	No	Yes
Supports and diaphragms are assumed to lie along the radial direction, and diaphragms can be placed at any arbitrary locations and spacing.	—	Yes
Composite or noncomposite girder may be analyzed.	Yes	Yes
Girders are assumed to be equally spaced and concentric, and each girder is assumed to have a constant radius of curvature.	Yes	Yes
Cross-sectional properties may be varied from girder to girder and also along the span of each individual girder.	Yes	Yes
Any type of diaphragm (beam, truss, etc.) may be considered.	—	Yes
Any combination of dead and live loads may be considered for a given structure. Many loading cases may be considered for the given structure.	Yes	Yes
Deflections, rotations, bending moments, shear, bimoments, St. Venant torsion, warping torsion are evaluated at each nodal point.	Yes	Yes

Live Load Analysis

CURSYS was used in the live load analysis. The bridge model consisted of two curved elements with section properties equivalent to those of the box girders. The elements were connected with discrete diaphragms having equivalent transverse stiffness representing the concrete deck (12). These composite section properties were again computed by SECTP (3); the resulting values are given in Table 4.

The transverse stiffness of the concrete deck was idealized by specifying the discrete diaphragm between two girders at each nodal point. Average nodal spacing was 31.91 in. (81 cm). The concrete deck was transformed to an equivalent area of steel, as was done in the case of composite section. Reinforcing bars in the transverse direction were also added to the final stiffness properties.

Concentrated truck wheel loads were inputed into CURSYS in a manner that produced maximum stresses. The individual wheel loads were automatically resolved into concentrated vertical and torsional load with respect to each adjacent nodal point. The locations of the truck wheel loads are shown in Figure 8.

The stiffness coefficients for the discrete diaphragms are a function of flexural rigidity and effective length, L_t. Because CURSYS was written such that each girder is connected at the centerline, the effective length of the equivalent discrete diaphragm connecting each box varies considerably and is not readily determined. To determine the effective length of the equivalent diaphragm, we computed the normal stresses for one test vehicle position at five different effective lengths, which varied from 108 to 270 in. (274 to 685 cm). The 108-in. (274-cm) dimension represents the distance between two extreme inner flanges, and 270 in. (685 cm) is the distance between the centerlines of two girders. The analytical stress ratio was then determined for each of these lengths by forming a ratio of the analytical stress in the bottom flange of one box to the stress of the other box. The experimentally measured stresses for the bottom flange of each cell were averaged, and then the average stress was divided by the average stress of the other box to determine the experimental stress ratio. Comparison of each analytical stress ratio with the experimentally determined value indicated that the effective length can be taken as the average of the shortest distance of unsupported concrete length and the length between the centerlines of two adjacent box girders. For this bridge, the effective length of 189 in. (480 cm) had a ratio of stress distribution within 3 percent of that measured experimentally.

The normal warping stresses were computed and were on the order of 0.1 percent of the normal bending stresses, as expected. Therefore, the normal stresses for the live load analysis were entirely based on plane bending stresses. Thus, the neutral axis was assumed to lie parallel to the bottom flange, and the analytical stress distribution at any given height from the neutral axis on the cross section was constant.

DISCUSSION OF RESULTS

Dead Load

The normal stress distribution determined analytically is composed of the normal bending stress and normal warping stress. The normal bending stresses determined analytically account for approximately 95 percent of the total normal stresses in the section with lateral bracing. The experimental normal stresses are generally larger than those determined analytically. The low percentage of gauges in working order for the dead load test does not justify a conclusive statement on the normal stress distribution. However, those gauges that were functioning properly generally indicated a fair correlation with the analytically obtained normal stresses. A sample plot of normal stress distribution is shown in Figure 9. The experimentally measured deflections agreed well with those predicted by CURSGL for the first two pours of concrete, but the values for pour three did not agree so well. A similar trend was also noted by Greig (7). This may be attributed to the initial setting of the concrete. A sample deflection plot is shown in Figure 10.

Table 4. Section properties for dead load test.

Section	Analytical I_x (in.^{4})	Analytical I_w (in.^{6})	Analytical K_t (in.^{4})	Analytical A (in.^{2})	Analytical $\bar{y}$ (in.)	Design I_x (in.^{4})
No top bracing						
1	85872	124600000	22.39	143.00	26.00	85373.2
2	172310	249200000	144.6	253.25	26.84	171191.8
3	114260	160600000	48.18	181.62	24.05	90161.7
4	245520	347300000	409.5	352.10	27.27	244623.1
5	128730	182800000	68.71	208.25	20.97	120867.2
Noncomposite section, 0.042-in. bracing						
1	89664	84600000	57630	148.03	26.961	
2	175720	158200000	62900	258.01	27.341	
3	118650	105100000	59170	186.66	24.854	
4	248820	245800000	65560	356.86	27.630	
5	134120	117200000	59920	213.28	21.751	
Modified composite section[a], 2.64-in top flange						
1	212153	342500	344500	523.62	49.704	
2	374771	46780000	431700	648.89	46.047	
3	280686	15060000	395200	563.53	47.717	
4	496350	60540000	576300	765.71	44.230	
5	341320	4149000	424400	590.16	45.565	

Note: 1 in. = 2.5 cm; 1 in.^{2} = 6.45 cm^2; 1 in.^{4} = 41.6 cm^4; 1 in.^{6} = 26.8 cm^6.

[a]Live load test.

Figure 8. Analytical load point location for static live load test.

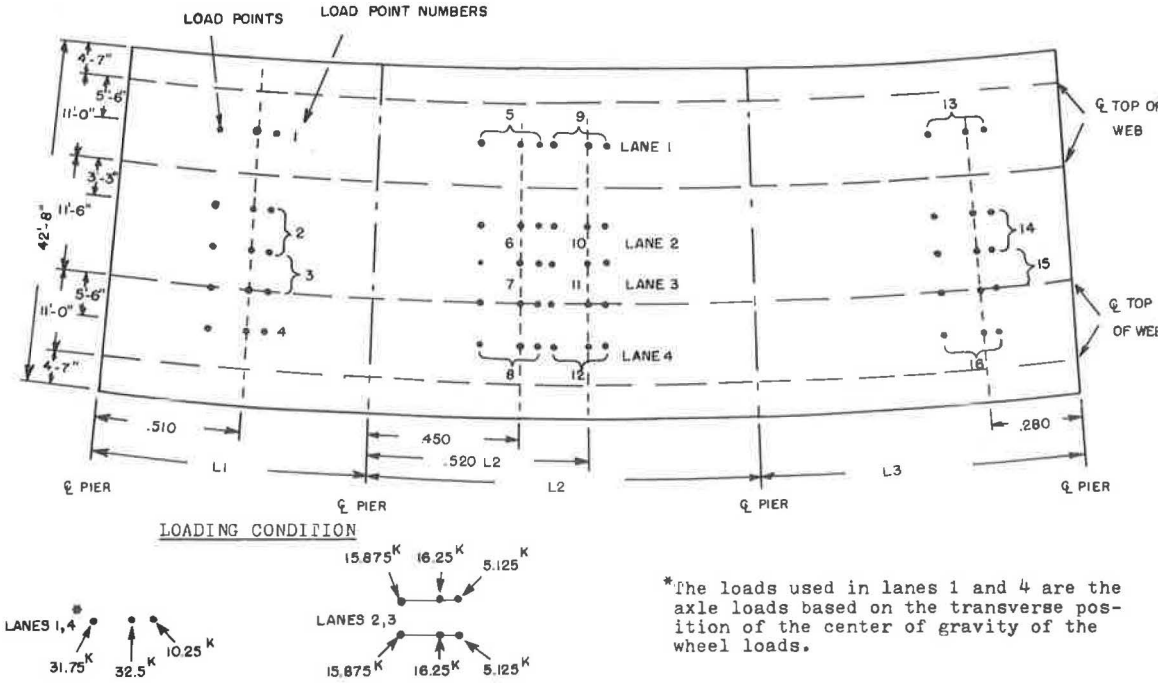

*The loads used in lanes 1 and 4 are the axle loads based on the transverse position of the center of gravity of the wheel loads.

Figure 9. Normal stress, dead load test (pour two).

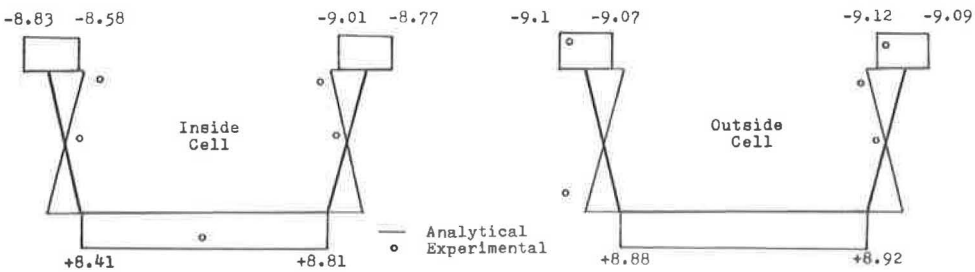

Figure 10. Normal stress, dead load test (pour three).

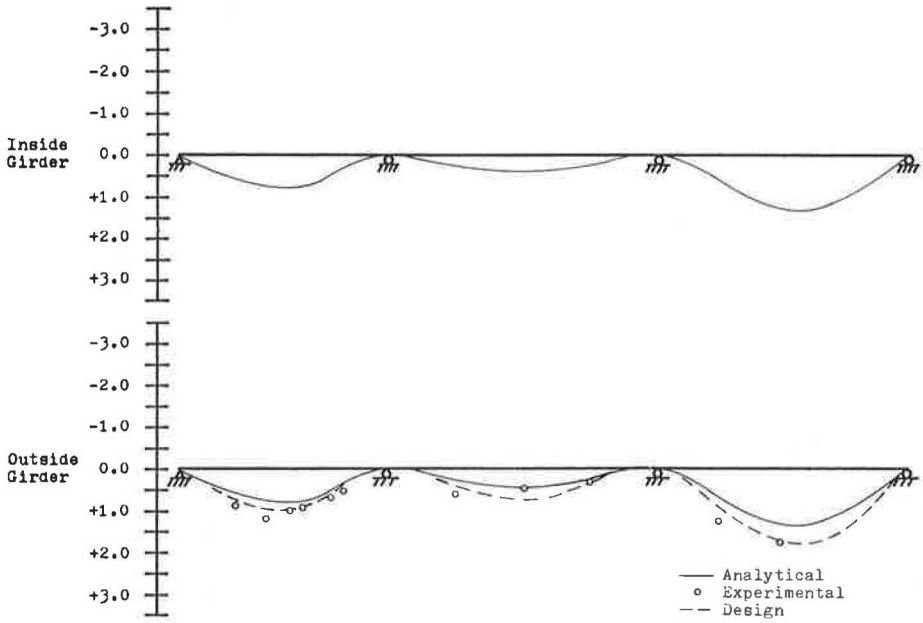

Live Load

The normal stresses obtained analytically generally agreed well with the measured stresses (Figure 6). However, the gauge at the top of the left web on the outside box deviated considerably from the analytical stress. This may be due to the local effect, i.e., the wheels of the test vehicle passing in the vicinity of the gauge. This local effect is most significant on the gauges at the top of the web. This phenomenon deserves further study.

Four strain gauges were mounted on the outside of the box at approximately upper midheight of the webs (section AA-A) so that possible web bending could be observed. Stresses measured on these gauges are shown in Figure 11. Note that the stresses on the outside of the web were consistently larger than the stresses on the inside, which indicates that the vertical webs of each cell bulged out. This trend is somewhat contradictory to that noted by Armstrong (2), which points to the need for further study in this area.

The analytical and experimental transverse load distribution factors were evaluated for each of the four sections where gauges were located. The distribution factor computed according to the AASHO specification (1) for two truck lane loadings on the bridge under study was 2.93. The truck positions are for those lanes that yield the most critical loading condition: lanes 3 and 4 in this study (Figure 5). The analytical and experimental distribution factors, therefore, were computed by adding the values from lanes 3 and 4 at each of four sections. The experimental distribution factors for the four sections ranged from 2.46 to 3.01 with an average value of 2.73. This accounts for 93 percent of the value given by AASHO. The analytical values ranged from 2.54 to 2.64 with an average of 2.58. The lower value for the analytical distribution factor would be expected because the designated lane position 4 was idealized closer to the center of the two girders than it was for the actual truck position in the field test.

The analytical and experimental deflections yield an excellent correlation as shown in Figure 7. The analytical and experimental rotations were also compared when the test vehicle was in lanes 1 through 4. The magnitude of the experimental rotations was generally within 15 percent of those predicted by analysis. The loading scheme for CURSYS was unable to place any loadings beyond the centerline of two outside

girders. CURSYS is being modified to eliminate this inconvenience. However, the idealization of the positioning to the test vehicle in lanes 1 and 4 had little effect on the normal stresses and deflections, but the effect on the rotations and corresponding torsional behavior was rather significant.

Impact

No dynamic analysis was made for comparative purposes. The experimentally measured values, however, were used to compute the impact factors. Averaging the 10 highest impact factors yielded a stress impact factor of 34.3 percent and a deflection impact factor of 31.4 percent. It should be noted that the live load stresses were small with a maximum of 2.15 ksi (14.8 MPa); thus, a conclusive statement may not be justified. The oscillograph trace exhibited somewhat steady-state frequency of vibration of 3 or 4 Hz.

FINDINGS AND CONCLUSIONS

The experimental normal stresses for the dead load test (Table 1) clearly show that the actual behavior of the box girders was somewhere in between the assumptions of open and closed cross sections as expected. The analyses were conducted by assuming the section properties with and without top transverse bracing. The torsional stiffness of the closed section was much higher (on the order of 200 or 1,000 times) than the open section stiffness, but the bending stiffness was essentially the same. This difference in torsional rigidity contributed to reduction in the warping normal stresses such that the total normal stresses account for approximately 30 percent for the open section to 5 percent for the closed section, even though the subtended angle of the bridge under study was relatively small. This suggests that the lateral bracing in the box section should be added inherently to prevent excessive distortions of the steel section when a concrete deck is poured.

The design of the box girders did not include any consideration of the lateral bracing or composite action over the supports, even though the design included standard shear studs throughout the length of the bridge. The design stresses are much higher than those determined analytically, with consideration of top bracing (Table 2).

Generally, the experimental results were predicted well by the analysis. Correlation of the analytical and experimental results for the live load tests yielded a maximum deviation of 10 percent, which indicates that the analytical method is accurate and effective. However, as can be seen in Figure 6, the normal stresses at the middle of the bottom flange were always smaller than the ones under the web because of shear lag. Currently, CURSYS only gives the average stresses.

It is interesting to note the close correlation between the distribution factors determined experimentally and the AASHO value, indicating that the equation given in the AASHO specifications is valid. AASHO recommends that a simple beam isolation be made for a large girder spacing for steel I-beam, concrete T-beam, timber stringer, and concrete box girders. The results obtained in this study clearly show that a simple beam idealization would be very conservative inasmuch as the distribution factor thus obtained would be 3.51.

ACKNOWLEDGMENTS

This research was conducted as a cooperative project of the Civil Engineering Department, University of Maryland; the Maryland Highway Administration; and the Federal Highway Administration. Their encouragement and guidance are gratefully acknowledged.

REFERENCES

1. Standard Specifications for Highway Bridges, 10th Ed. American Association of State Highway Officials, 1969.
2. W. L. Armstrong and J. A. Langdon. Dynamic Testing of a Curved Box Beam Bridge. Federal Highway Research and Development Report 73-1, Feb. 1973.
3. D. Blank. Stiffening of Box Beam Using Corrugated Shapes. Department of Civil Engineering, Univ. of Maryland, MS thesis, Aug. 1973.
4. B. Bonakdarpour, L. C. Bell, and C. P. Heins. Analytical and Experimental Study of a Curved Bridge Model. Univ. of Maryland, Civil Engineering Rept. 36, June 1970.
5. J. Buchanan. Experimental and Analytical Study of a Curved Box Girder Bridge. Department of Civil Engineering, Univ. of Maryland, MS thesis, June 1974.
6. R. Dabrowski. Curved Thin-Walled Girder Theory and Analysis. Cement and Concrete Association, England, Translation 144, 1968.
7. R. A. Greig. Field Testing of a Curved Steel Box Girder Bridge in Springfield, Massachusetts. Univ. of Rhode Island, Technical Rept. 1 (L), March 1973.
8. C. F. Kollbrunner and K. Basler. Torsion in Structures. Springer-Verlag, 1969.
9. K. R. Spates and C. P. Heins. The Analysis of Simple Curved Girders With Various Loadings and Boundary Conditions. Univ. of Maryland, Civil Engineering Rept. 20, June 1968.
10. V. Z. Vlasov. Thin-Walled Elastic Beams. National Science Foundation, 1961.
11. C. Yoo, D. Evick, and C. P. Heins. Non-Prismatic Curved Girder Analysis. Journal of Computers and Structures, London, Vol. 3, 1973.
12. C. Yoo and C. P. Heins. Users Mannual for the Static Analysis of Curved Bridge Girders. Univ. of Maryland, Civil Engineering Rept. 55.

PREDICTION OF BRIDGE GIRDER STRESS HISTOGRAMS FROM TRUCK TYPE DISTRIBUTION

David W. Goodpasture, Edwin G. Burdette, P. Cooper Patrick, Jr., and John N. Snider, University of Tennessee

Stress history studies are conducted so that bridge girder stresses due to various types of truck loadings can be predicted. Being able to predict these stresses obviates having to measure them for every bridge. This paper presents a seven-step procedure for using stress history data to predict stress in bridge girders. Stress data for 3,120 trucks identified by type and lane location and weight data from 3,865 trucks identified by type were obtained. A comparison between the stresses and weights showed that there were notable similarities in the shapes of the two distributions. The ability to simulate or predict stresses based on truck type, lane location, and weight distribution will eliminate the need for complicated and costly field measurement of stresses.

•DURING the last several years the Federal Highway Administration has actively encouraged and supported a program of data collection and analysis related to the determination of the stress history of highway bridges. Results of a number of investigations conducted as a part of this program have been reported (1 through 5).

The objective of the stress history program may be stated as follows: Given a distribution of major truck types (obtained by visual count or projection) and a distribution of truck weights for each major truck type (obtained from state weight data), predict, on the basis of calculated girder stresses under the action of each major truck type, the stress histogram for each girder in a bridge. From this stress histogram and a knowledge of the fatigue characteristics of the girder (which is currently incomplete), the fatigue life of a member or bridge may be predicted.

This paper presents a logical and practical approach to achieving the objectives of the stress history program, applies this approach to predict girder stress histograms for a particular bridge, and compares these results to field strain data.

Once the stress histograms obtained from strain data can be approximately duplicated by prediction based on truck weight distribution data, a significant step has been taken toward the accomplishment of the ultimate objective of the stress history program.

APPLICATION OF STRESS HISTORY DATA

Girder strain data and truck weight data are used to predict the stress histograms for the girders in a bridge. The bridge for which strain data are presented is the westbound roadway of Interstates 40 and 75 over Twenty-Second Street in Knoxville, Tennessee. Truck traffic over this bridge averages 250 to 300 trucks per hour. The bridge is a simple span, composite steel girder bridge with a 62-ft (19-m) span, and it has seven longitudinal girders.

The proposed method, as it is applied later to the bridge described above, is outlined in the following paragraphs in step-by-step fashion. It is assumed, as a starting point, that a multigirder bridge exists for which facilities are available to obtain strain data, truck traffic data, and truck weight data as needed.

1. Obtain a stress histogram for each girder in the bridge for each major truck type traveling in each traffic lane. To ensure that the histograms are statistically meaningful requires that strain measurements for a relatively large number of trucks of

each type in each lane be obtained.

2. Obtain weight histograms for each major truck type. Again, weights for a relatively large number of each truck type should be obtained.

3. Correlate the stress and weight histograms obtained in steps 1 and 2. This is obviously a key step that requires judgment not only in the choice of statistical methodology but also in the interpretation of the results for the particular bridge. For example, the stress histogram for the extreme left girder for a particular truck type in the extreme right lane may bear little resemblance to the weight histogram for that truck type because a lightly loaded truck may not cause stresses high enough to be included in the stress histogram. After the completion of step 3, the stress histogram for a particular girder can be predicted for a known distribution of major truck types in the different traffic lanes.

4. Determine the percentage of each major truck type traveling in each traffic lane.

5. For a known distribution of truck types on the bridge, predict the stress histogram for each girder. Compare results with field data.

6. Relate measured stress in a girder due to a truck of known type and weight in a particular traffic lane to computed stress in the girder under similar conditions. This step also is a key one. The analytical method chosen should be both easy to use and reasonably accurate. This paper offers no guidelines with regard to step 6.

7. Finally, for a known distribution of truck types, predict the stress histogram for each girder on the basis of the calculated stress in the girder.

The remainder of this paper describes the application of steps 1 through 5 to the bridge described earlier.

DATA COLLECTION

To achieve the objectives of this study requires much information about the stresses caused by different types of trucks in different lanes and the distribution of weights of different types of trucks. The collection of the data used in this report is described in the same sequence as the steps outlined above.

Stress Histogram According to Truck Type and Lane Location (Step 1)

For 2 weeks, a total of 11 tests were conducted on a single bridge. All strain gauges were located on the bottom surface of the bottom flange at the center of the span. Truck type and lane location were noted for each truck, and the strains in the seven girders of the bridge were recorded after they were digitized at a rate of 240 samples per second per gauge. Approximately 3½ sec of data were recorded for each truck passage. Particular care was taken to ensure that the truck type and lane location could be related to the corresponding strain record. A total of 3,120 trucks were observed during the tests. After the data were recorded on the digital magnetic tape, a computer program was used to scan the strain range caused by the passage of that vehicle. The strain range was converted to a stress range and printed on the teletype for each truck. The type of truck and lane location were then written on the computer output sheet, and any inconsistencies were resolved. No multiple crossings were included in these data. A description of the equipment and computer program used has been published by Goodpasture (1).

Weights of Trucks (Step 2)

A weight station for trucks on Interstates 40 and 75 is located approximately 10 miles (16 km) from the bridge site used for this study. The weight station is operated by the Tennessee Department of Revenue. Because there were numerous interchanges between

the bridge site and the weigh station, the trucks that had actually caused the recorded strains could not be weighed. Therefore, 3,865 trucks were weighed during three time periods: May 1972, December 1972, and June 1973. The weights were obtained by the use of three scales connected to a printer at the weigh station. The front steering axle of the truck was weighed on the first scale, the drive axle weight was obtained on the second scale, and the trailer axles were weighed on the third scale. The printer recorded each scale weight and summed the three scales for the gross vehicle weight. Only gross vehicle weights were used.

Truck Type, Lane Location, and Stress Data (Steps 4 and 5)

A second computer program was written to collect data and reduce them in terms of strain ranges in real time. This program is very similar to the program used by the FHWA during the early stress history studies. The main difference between the FHWA program and the University of Tennessee program is that no data are lost during the testing period with the UT program. Intermediate results are written on magnetic tape each 15 min during the test. The time required for recording the data is less than 1 sec, which, therefore, does not interfere with the test in progress. After the test is completed, the results are read from the tape and printed by the computer at any convenient time. These results form the field data mentioned in step 5.

The type and lane location of all trucks crossing the bridge are noted in 15-min intervals corresponding to the strain data. Multiple crossings are also noted on the data sheet. This information forms the basis of the information required in step 4.

ANALYSIS OF RESULTS

Traffic Characteristics

The traffic mix varies throughout the day, but distinctions can be made between day and night. The day data contain a high percentage of local delivery trucks; large tractor trailers are the dominant truck traffic at night.

Table 1 gives the distribution of truck type by lane. Note that during the day approximately 50 percent of the trucks are single-unit types 2D, 3, and 4. However, at night approximately 20 percent of the trucks are single-unit types. Total truck traffic volume is essentially the same for 1973 and 1974 during the day. The number of type 3S2 trucks each hour changes slightly during the 24-hour period. Earlier tests (1) indicated, however, that a significant number of 3S2 trucks pass over the bridge every hour of the day.

Table 2 gives the types and lane locations of the trucks used in step 1. The objective was to record data on approximately 300 trucks per lane. This was achieved for truck types 2D and 3S2, but only one-half that number was recorded for types 3 and 2S2. It appears highly unlikely that the required number of truck types 4 and 2S1 can be recorded within a reasonable test length. Several test periods were chosen during July 1974 in which strains from only truck types 3, 4, 2S1, and 2S2 were recorded. These tests lasted from 6 to 8 hours during the day, and fewer than 300 of all these types combined were noted.

Stress Distribution

The maximum stress ranges for types 2D and 3S2 trucks are given in Table 3. Table 3 was constructed by noting the maximum stress range in each of the seven girders and recording that range by the lane location of the truck. The maximum observable stresses occur in the girders centered underneath the lane in which the vehicle is operated. The distributions are skewed to the right and then are skewed to the left as the vehicle moves from the left lane to the right lane. The type of data shown in Table 3

Table 1. Truck type and lane distribution.

Date	Time	Truck Type	Lane			Total	
			Left	Middle	Right	Number	Percent
August 1973	9:15 a.m. to noon	2D	58	128	110	296	38.6
		3	15	62	37	114	14.9
		4	0	3	3	6	0.8
		2S1	8	3	3	14	1.8
		2S2	16	33	22	71	9.3
		3S2	113	65	83	261	34.1
		Others	1	3	0	4	0.5
		Total				766	
July 1974	9:00 a.m. to noon	2D	59	116	139	314	39.3
		3	18	21	33	72	9.0
		4	0	0	3	3	0.4
		2S1	8	4	4	16	2.0
		2S2	24	21	23	68	8.5
		3S2	147	77	97	321	40.2
		Others	2	1	2	5	0.6
		Total				799	
	8:00 p.m. to midnight	2D	26	34	27	87	16.7
		3	5	8	10	23	4.4
		4	0	0	0	0	0
		2S1	4	7	0	11	2.1
		2S2	20	25	12	57	10.9
		3S2	126	121	96	343	65.7
		Others	0	0	1	1	0.2
		Total				522	

Table 2. Trucks included in study.

Truck Type	Lane			Truck Type	Lane		
	Left	Middle	Right		Left	Middle	Right
2D	271	360	318	2S2	161	189	119
3	139	178	160	3S2	381	361	300
4	11	13	17	Others	8	9	8
2S1	30	41	46				

is required for all truck types for step 1.

Weight Distribution (Step 2)

The distribution of the gross weight for six truck types is given in Table 4. These weights were obtained during the three sampling periods. Again, the large number of truck types 2D and 3S2 is evident. The weight interval is the same for all types of trucks in order to simplify the presentation of the data. However, different weight intervals were used for each truck type in order to correlate these data with those from step 1. The weight distribution for type 3S2 trucks is definitely bimodal, and a large number of trucks were at the maximum legal loading. The weight distribution for type 3S2 trucks is shown as a histogram in Figure 1. Single-unit trucks such as type 2D do not exhibit the bimodal distribution so clearly.

Correlation Between Stresses and Truck Weights (Step 3)

Although extensive data were collected regarding vehicle weight distribution and stress range for all commercial vehicles on the road, only type 3S2 vehicles are discussed here. One method of exhibiting the stress range data is to pool all values for all seven girders and ignore lane position. The result of these pooled data is shown in Figure 2.

Table 3. Stress ranges for 2D and 3S2 trucks by lane.

Trucks			Stress Range (ksi)	Lane						
Type	No.	Lane			Left		Middle		Right	
2D	271	Left	0.50 to 0.75	53	85	91	17	1	3	0
			0.75 to 1.00	24	65	55	3	2	1	
			1.00 to 1.25	8	30	17				
			1.25 to 1.50		19	16				
			1.50 to 1.75		13	6				
			1.75 to 2.00		8					
			2.00 to 2.25		3					
			2.25 to 2.50		1					
	360	Middle	0.50 to 0.75	2	36	104	118	73	10	1
			0.75 to 1.00		1	49	48	55		
			1.00 to 1.25		1	34	34	37		
			1.25 to 1.50			10	28	27		
			1.50 to 1.75			2	26	8		
			1.75 to 2.00			0	27	3		
			2.00 to 2.25			1	16	1		
			2.25 to 2.50				5			
			2.50 to 3.00				1			
	318	Right	0.50 to 0.75	0	3	1	12	90	138	43
			0.75 to 1.00					29	48	10
			1.00 to 1.25					13	23	2
			1.25 to 1.50					3	10	
			1.50 to 1.75					1	4	
			1.75 to 2.00						1	
			2.00 to 2.25						1	
3S2	381	Left	0.50 to 0.75	103	0	23	137	27	16	7
			0.75 to 1.00	104	44	100	79	3	1	
			1.00 to 1.25	102	94	73	11			
			1.25 to 1.50	32	56	52	1			
			1.50 to 1.75	16	42	44				
			1.75 to 2.00	6	42	47				
			2.00 to 2.25	1	36	29				
			2.25 to 2.50	2	31	4				
			2.50 to 2.75		18	0				
			2.75 to 3.00		5	1				
			3.00 to 3.25		0					
			3.25 to 3.50		0					
			3.50 to 3.75		0					
			3.75 to 4.00		1					
	361	Middle	0.50 to 0.75	36	132	82	4	57	118	24
			0.75 to 1.00	2	25	90	44	69	23	
			1.00 to 1.25			94	48	54	0	
			1.25 to 1.50			50	38	36	0	
			1.50 to 1.75			16	32	72	1	
			1.75 to 2.00			4	40	34		
			2.00 to 2.25				65	14		
			2.25 to 2.50				38	5		
			2.50 to 2.75				17	2		
			2.75 to 3.00				3	0		
			3.00 to 3.25				3	0		
			3.25 to 3.50				2	1		
	300	Right	0.50 to 0.75	0	6	20	95	22	4	75
			0.75 to 1.00				20	61	30	60
			1.00 to 1.25				7	32	53	47
			1.25 to 1.50				2	35	30	31
			1.50 to 1.75					37	20	7
			1.75 to 2.00					23	29	4
			2.00 to 2.25					12	38	1
			2.25 to 2.50					4	21	
			2.50 to 2.75					0	6	
			2.75 to 3.00					2	2	
			3.00 to 3.25					0	1	
			3.25 to 3.50					1	0	
			3.50 to 3.75						2	

Note: 1 ksi = 6.9 MPa.

Table 4. Weight distribution of each truck type.

Weight (kips)	Truck Type						
	2D	3	4	2S1	2S2	3S2	Other
0 to 3	3	0	0	0	0	0	0
3 to 6	13	0	0	0	0	0	0
6 to 9	79	0	0	0	0	2	0
9 to 12	134	2	0	1	4	0	0
12 to 15	133	23	0	3	3	0	1
15 to 18	96	16	0	3	1	2	0
18 to 21	61	12	0	10	13	0	0
21 to 24	74	12	0	9	36	16	0
24 to 27	36	6	0	43	71	104	2
27 to 30	6	13	0	15	69	336	3
30 to 33	4	11	0	29	62	174	0
33 to 36	2	5	0	18	44	95	1
36 to 39	6	9	1	11	35	70	0
39 to 42	1	12	0	7	60	60	0
42 to 45	0	9	0	5	38	64	2
45 to 48	0	0	3	1	55	79	1
48 to 51	0	4	2	0	24	96	1
51 to 54	0	0	2	0	20	101	2
54 to 57	0	0	0	0	9	91	0
57 to 60	0	2	3	0	9	104	0
60 to 63	0	8	3	0	5	150	0
63 to 66	0	2	0	0	0	139	2
66 to 69	0	0	0	0	0	177	1
69 to 72	0	0	0	0	0	285	2
72 to 75	1	0	0	0	0	160	0
75 to 78	0	0	2	0	0	6	0
78 to 81	0	0	0	0	0	6	1
>81	0	0	0	0	0	4	1
Total	649	146	16	155	558	2,321	20

Note: 1 kip = 450 kg.

Figure 1. Weight distribution of 3S2 trucks.

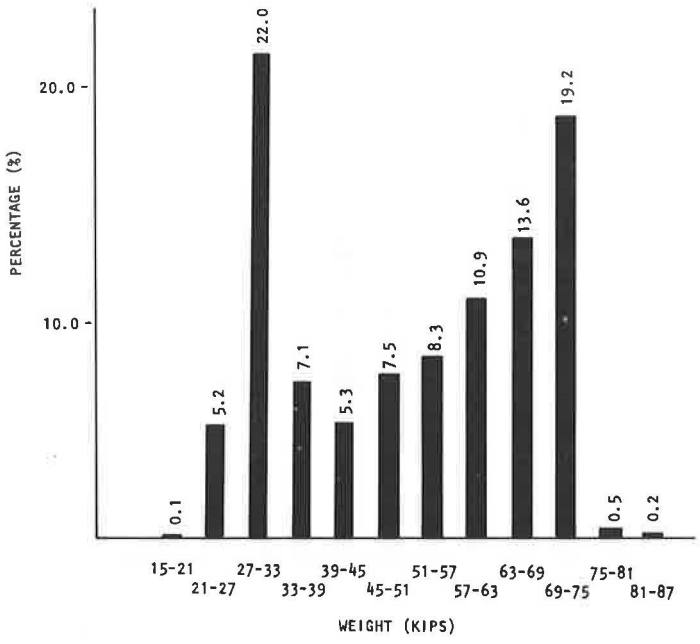

Figure 2. Pooled stress distribution from all girders for 3S2 trucks.

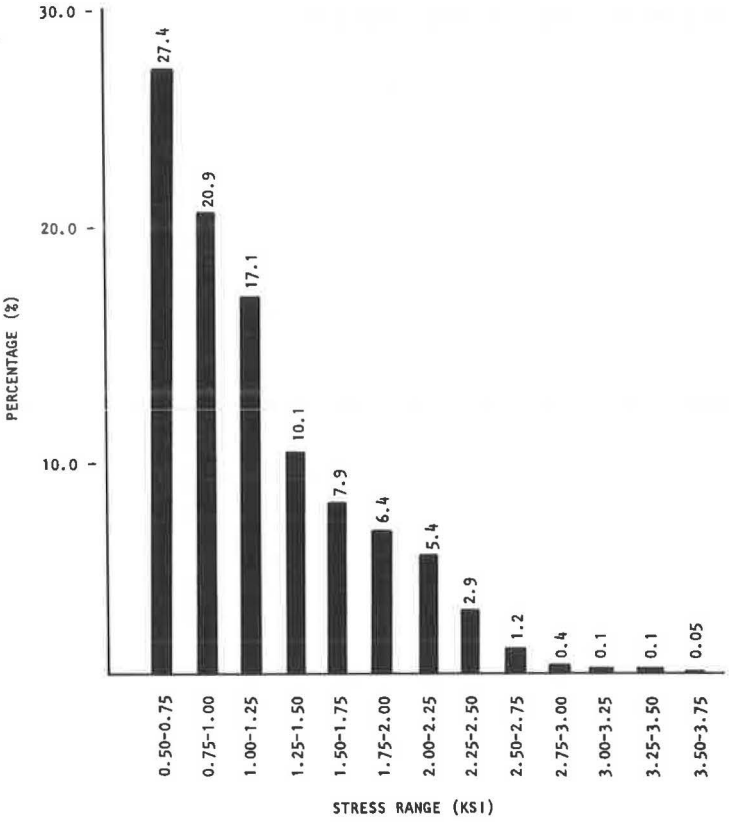

Figure 3. Pooled stress distribution for principal load-carrying girders in right, middle, and left lanes.

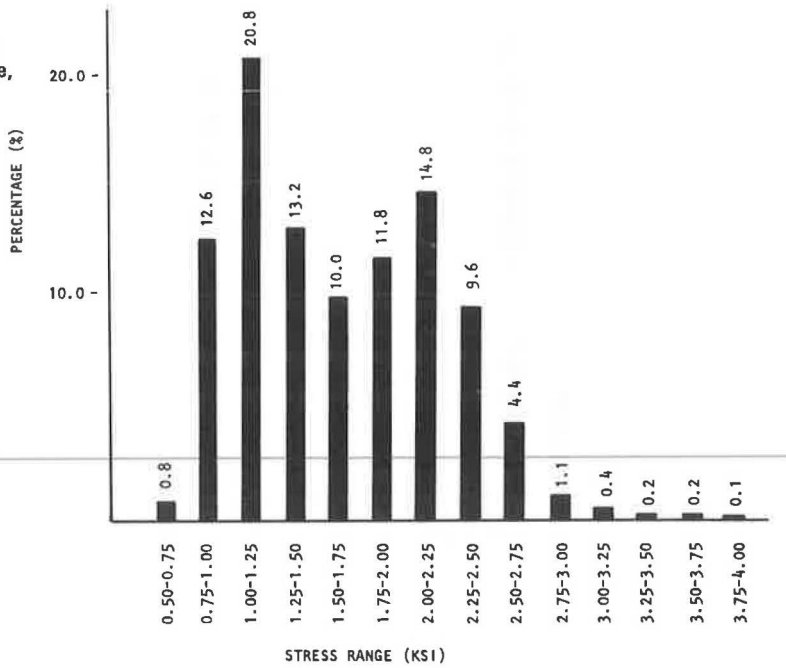

It is obvious that this distribution is of the general form of a decaying exponential, and there appears to be little specific relationship between this pool distribution and the distribution of vehicle weights shown in Figure 1.

To further define the stress ranges observed on the bridge as a function of 3S2 vehicles, we generated the histogram shown in Figure 3. This figure presents the distribution of maximum stress ranges observed in the girder centered under the lane used by the vehicle. Thus, for each vehicle there is one specific stress range value that contributed to the makeup of this figure.

Note that the distribution in Figure 3, although by no means identical to the weight distribution for 3S2 vehicles (Figure 1), has a somewhat similar shape. It would appear that this distribution is bimodal in nature, as was the weight distribution. However, the development of the stress range intervals for these data greatly influences the apparent shape of the distribution. Furthermore, it is possible that some of the unusually high stress ranges observed in this distribution are the consequence of either noise in the instrumentation or interaction between the natural frequency of the vehicle suspension and that of the bridge.

To understand the nature of these data, we summed the stress ranges in the two girders adjacent to the girder directly under the path of the vehicle. The resulting distribution is shown in Figure 4.

A comparison of the distributions shown in Figures 3 and 4 indicates that the stress ranges in the girders adjacent to the principal load-carrying girders are indeed less than the stress ranges in the principal load-carrying girders themselves. The shape of the distribution in Figure 4 is similar to the shape shown in Figure 2, i.e., the negative exponential form. To determine the precise nature of the distribution in Figure 4 would require larger sample sizes than were used.

So far, a direct correlation between the stress ranges and the weights has not been developed. The data obtained thus far do indicate that a positive correlation between truck weight and stress range is possible, but it is very sensitive to the stress range and weight intervals chosen.

Another possible method of correlation is a direct correlation between the sum of all girder stresses and the weight of the vehicle operating on the bridge at that time, independent of the position of the vehicle on the read. This, of course, assumes that the bridge cross section is essentially uniform relative to girder size and deck thickness. When this correlation is studied, the stress ranges for all seven girders will be added for each vehicle. These sums will then be compared to the gross weight data for the particular type of truck. Preliminary results indicate that this relationship is a straightforward one.

Field Data for Steps 4 and 5

During the July 1974 tests, stress histograms for the bridge under study were obtained as described earlier. One of these tests contains data taken during a 4-hour period. The types of trucks observed and their lane location are the night data given in Table 1.

Although, as indicated earlier, the correlation between weights and stress ranges has not been fully developed, a prediction of the stress histogram based on the measured stress ranges is possible. In fact, if the stress histogram cannot be approximated by superposition of measured stresses, then there is little hope that the truck weights can be used even after correlation with the stress ranges.

A comparison of measured stress ranges and predicted stress ranges was made for the principal load-carrying girder for each lane. Table 5 gives the values used for the comparison. Stress ranges of less than 1,000 psi (6900 kPa) were neglected because only one stress range per truck is considered in predicting the histogram, whereas all stress ranges are considered in the continuous sampling program described earlier. In addition, it is doubtful that stress ranges of less than 1,000 psi (6900 kPa) have any effect on the fatigue lives of the girders. An additional source of difference is the fact that 41 multiple crossings were recorded during the 4-hour period. In other words, there were two trucks on the bridge at one time a total of 41 times during the test.

Figure 4. Pooled stress distribution for girder adjacent to principal load-carrying girders.

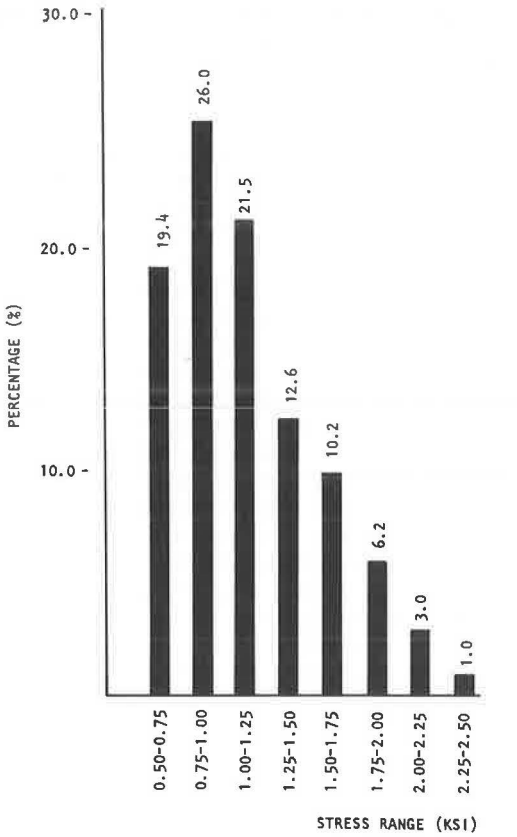

Table 5. Comparison of measured and predicted stress ranges.

	Lane							
	Left		Middle		Right		Total	
Item	Measured	Predicted[a]	Measured	Predicted[a]	Measured	Predicted[a]	Measured	Predicted[a]
Stress range, ksi								
1.00 to 1.25	42	39.7	40	24.8	27	20.9	109	85.4
1.26 to 1.50	26	25.2	16	20.8	13	11.2	55	57.1
1.51 to 1.75	17	17.4	20	16.6	13	7.1	50	41.2
1.76 to 2.00	13	15.3	12	17.5	21	9.7	46	42.4
2.01 to 2.25	15	12.3	19	24.3	15	12.4	49	48.9
2.26 to 2.50	16	10.6	27	13.8	11	6.7	54	31.1
2.51 to 2.75	9	6.0	14	6.1	2	1.9	25	14.0
2.76 to 3.00	8	1.7	3	1.2	1	0.6	12	3.5
3.01 to 3.25	4	0	2	1.0	0	0.3	6	1.4
3.26 to 3.50	1	0	1	0.7	0	0.0	2	0.7
>3.51	0	0.3	1	0	0	0.6	1	0.9
Truck type								
2D		26		34		27		87
2S2		20		25		12		57
3S2		126		121		96		343
Others		9		15		11		35
Total								522

Note: 1 ksi = 6.9 MPa.

[a]Neglecting trucks classified as others, i.e., 7 percent of the total.

The agreement between the measured and predicted stress ranges is remarkably good in view of the approximations used. First, only 2D, 2S2, and 3S2 trucks were considered for the predicted values; other types (7 percent) were neglected. For the left, middle, and right lanes, 161, 189, and 119 2S2 trucks were used. As mentioned earlier, 300 trucks per lane was considered the minimum number for meaningful results. This example indicates clearly that the methods described herein have been justified and that work in this direction should continue.

CONCLUSIONS

The seven steps outlined for using truck type and weight data to predict the stress histogram for a given bridge and subsequently the fatigue life of the bridge girders are merely a first step. After these steps have been completed for a number of bridges in the nationwide stress history study, it is expected that a somewhat more direct approach will evolve that will be useful to the bridge designer. There is much potential in the method outline, but more data are required before a satisfactory solution can be achieved. Therefore, one of the main objectives of this paper was to present a methodology and invite comments, suggestions, and criticism as applicable.

Many data related to truck type, lane position, and resulting stress range were presented. Analyses of the shapes of the stress range and weight distributions were made for type 3S2 trucks. There is a relationship between stress range and weight as expected, but the exact form of the correlation has not yet been identified.

ACKNOWLEDGMENTS

Appreciation is expressed to the Bureau of Highways, Tennessee Department of Transportation, for assistance in the performance of the research studies described.

This report was prepared in cooperation with the Federal Highway Administration, U.S. Department of Transportation. The contents of this report reflect the views of the authors, who are responsible for the facts and the accuracy of the data. The contents do not necessarily reflect the official views or policies of the state of Tennessee or the Federal Highway Administration. This report does not constitute a standard, specification, or regulation.

REFERENCES

1. D. W. Goodpasture. Final Report on Stress History of Highway Bridges. Univ. of Tennessee, Dec. 31, 1972.
2. D. W. Goodpasture and E. G. Burdette. Comparison of Bridge Stress History Results With Design Related Analyses. Highway Research Record 428, 1973.
3. C. P. Heins, Jr., and R. L. Khosa. Comparison Between Induced Girder Stresses and Corresponding Vehicle Weights. Highway Research Record 382, 1972.
4. W. T. McKeel, Jr., C. E. Maddox, H. L. Kinnier, and C. F. Galambos. Loading History Study of Two Highway Bridges in Virginia. Highway Research Record 382, 1972.
5. G. G. Goble, F. Moses, and A. Pavia. Field Measurements and Laboratory Testing of Bridge Components. Case Western Reserve Univ., Final Rept. OHIO-DOT-08-74, Jan. 1974.

FATIGUE ANALYSIS FROM STRAIN GAUGE DATA AND PROBABILITY ANALYSIS

Robert C. Deen and James H. Havens, Bureau of Highways,
Kentucky Department of Transportation

This report presents a rational approach for determining remaining fatigue life of a bridge. A methodology was developed to determine fatigue damage from a probability analysis of traffic data by reconstituting or synthesizing the load (traffic) history of bridges. A mechanical scratch gauge was used to obtain a short period of stress history of bridge members on the Central Bridge over the Ohio River at Cincinnati. Stress histories deduced from the strain gauge records were used to evaluate fatigue damage to the bridge. The remaining life of the bridge obtained by these two methods was then compared.

•THE Central Bridge over the Ohio River between Newport, Kentucky, and Cincinnati, Ohio, was completed in 1891 and in 1972-73 was considered to be in danger of fatigue failure. A series of investigations was undertaken to determine the likelihood of failure and to estimate the time of probable failure. During the investigation, a methodology was developed to determine fatigue damage from a probability analysis of traffic data by reconstituting or synthesizing the load (traffic) history of bridges. Strain gauge data obtained with Prewitt scratch gauges and SR-4 resistivity gauges were used to evaluate fatigue damage incurred by the Central Bridge.

Repeated stressing of metals above certain limits induces intercrystalline and intracrystalline dislocations and cleavages and eventually cracks that propagate to failure. This internal damage is insidiously cumulative and irreversible. This phenomenon was recognized as early as 1829 and was termed fatigue as early as 1839 (1). From the beginning of fatigue testing (Wholer, 1858-1870), results have been reported as S-N, S-log N, or log S-log N curves, where N is the number of repetitions of stress S. One purpose of fatigue testing was to find the endurance or fatigue limit (i.e., f_e) and thereby to establish the design or working stress.

To plot S-N graphs required that many specimens be tested at several stress levels, each in simple, repetitive cycling. About 1910, compound loading tests evolved. The linear summation of cycle ratios is believed to have originated with A. Palmgren in 1924. In this country, it was proposed by B. F. Langer in 1937, although credit is often given to M. A. Miner in 1945. This hypothesis suggested that the fractional fatigue damage in a specimen caused by N repetitions of a stress S is the ratio of the number of those repetitions to the number of repetitions at the same stress level that would cause failure (determined from other specimens). Inherent in this notion is the fact that fractional damages are additive and that the totality of fractions cannot exceed one. It is therefore possible, on this premise, to predict remaining fatigue life from S-N envelopes and to do so in terms of compound stressings. Unfortunately, the simplicity implied here is perhaps unreal. Indeed, the variability attending fatigue tests may introduce incertitudes that may otherwise limit the summation of damage increments (fractions) to a value less than 1, perhaps 0.80. Some commentaries have suggested fail-safe values of 0.30. More complete reviews of fatigue technology are available elsewhere (2, 3, 4).

Many bridges built more than 50 years ago were designed to resist fatigue due to the then-standard loads. Legal allowable gross weights of trucks have increased more than fourfold in 20 years. The possibility of fatigue failure becoming imminent demanded investigation and analysis. The catastrophic failure of the bridge at Point

Pleasant, West Virginia (5), and the necessary subsequent retirement of the C&O Bridge (US-25) at Covington, Kentucky, are conspicuous events in engineering history and both examples of delimited service life.

PROBABILITY ANALYSIS OF TRAFFIC DATA

Basic Fatigue Equation

In addition to stresses due to the dead load DL and live load LL, stresses due to wind loading WL and temperature changes TC must be considered if they significantly affect the stress level. The fatigue F of a bridge member due to one repetition of a particular loading combination LC can be computed from

$$F = f(LC) \times f(S_{LC}) \times f(F_{LC}) \quad (1)$$

where $f(LC) = I \times f(LL + WL + TC) + f(DL)$. $f(S_{LC})$ is a function for transforming the total equivalent load of the loading combination to the corresponding stress level in the structural member and the fatigue damage in the member due to the stress induced by one repetition of LC.

Equation 1 is a generalized relationship for computing the fatigue damage of a bridge member due to a single repetition of a particular loading combination. The total fatigue damage F_t in a design period includes the cumulative fatigue contributions of all loading combinations placed on the structure, or

$$F_t = 365 \sum_{\text{all years}} \sum_{\text{all LC}} AADT \times P_{LC} \times F \quad (2)$$

where P_{LC} is the probability of any loading combination LC occurring on the bridge section.

Vehicle Loading Distributions

Because many bridge spans are very long, the load cannot be designated simply as that for a single vehicle or series of axle trains. A long span, for example, could hold several large combination trucks at one time if both lanes were completely loaded. All of these vehicles must be considered as contributing to fatigue. The occurrence of such a fully loaded bridge span is rare. The probability of a lesser number of vehicles occurring on the span at the same time is of course much greater. Therefore, probabilities of each of the loading possibilities must be determined. Because of the extreme length of many bridge spans and because stresses in members vary as the load moves along the span, gross vehicle weight was chosen in this study as the smallest unit weight to be considered.

Loading Probabilities

One-Directional Probabilities

When a single vehicle passes a designated point on a highway, the probability that this vehicle is of vehicle classification i is given by P_i, the frequency of vehicle type i in the total traffic stream. The probability that n consecutive vehicles traveling in the same direction past a point are type i is given by

$$P_{n_i} = P_i^n \tag{3}$$

Equation 3 can be modified to give the probability that these vehicles will pass the point of interest within a specified time interval t:

$$P_{n_iG} = P_i^n \, P_{G(t)}^{(n-1)} \tag{4}$$

where $P_{G(t)}$ is the probability of a gap being of average length G(t). Gap length probabilities required in equation 4 were developed previously for specific bridges spanning the Ohio River in Kentucky (6). Final probability curves were developed by recording actual vehicle gap lengths (in seconds) and then converting the gap distributions from units of time to units of length by considering the average vehicle spot speeds at these locations.

If we assume that gap distances are equal, the average gap length for vehicles within the critical length of roadway L is found to be

$$G(t) = (L - n_i VL_i)/(n_i - \tfrac{1}{2}) \tag{5}$$

where VL_i is the average length of vehicle type i (Table 1). The average gap for mixed traffic (Figure 1) in one direction is found from

$$G_{mix} = \left(L - \sum_{\text{all } i} n_i VL_i\right) \Big/ \sum_{\text{all } i} (n_i - \tfrac{1}{2}) \tag{6}$$

where

$$\sum_{\text{all } i} n_i \, VL_i < L$$

Because of the large number of variable combinations, we restricted the vehicle classification to the following three vehicle types:

Vehicle Type	Code
Automobiles	i = 1
Single-unit trucks	i = 2
Combination trucks	i = 3

In this classification, automobiles include four-tired, single-unit trucks, and single-unit trucks include buses. For this vehicle classification system, the probability of any one-directional, mixed vehicle grouping occurring in the critical length L is given by

$$P_{n_1,n_2,n_3} = \frac{(n_1 + n_2 + n_3)\,!}{n_1! \times n_2! \times n_3!} \times \frac{\prod (P_i P_G)^{n_i}}{\sum_{\text{all } i} n_i P_G \Big/ \sum_{\text{all } i} n_i} \tag{7}$$

where P_G is the probability of an average gap of G_{mix} occurring.

Two-Directional Probabilities

Equations 3 through 7 concern the probabilities of the occurrence of various vehicle groupings on a specified length of highway for only one direction of travel. However, vehicle loadings in both traffic streams contribute to the fatigue of a bridge member. A previous study (6) of Ohio River bridges indicated that the effects of direction of travel on parameters such as vehicle spot speed, traffic volume, percentage of each vehicle type, gross vehicle weight, axle weight, vehicle length, and axle spacings were not statistically influenced at the 10 percent level of significance; i.e., the directional flows are essentially the same in composition and operational characteristics.

Because previously derived probabilities (7) relative to a particular point did not consider the parameter time, they were not instantaneous probabilities. To obtain instantaneous probabilities, necessary when more than one lane is to be considered concurrently, requires that an assumption be made concerning the acceptable distance D within which the effects of vehicle placements are considered as equal. D = ±50 ft (15 m) was thought reasonable because this would be less than 2 sec in most cases. These values are maximum; i.e., at least 50 percent of the time the error would be less than a second. This assumption was adapted to the procedure by developing the instantaneous probability that a vehicle is present within this time limit. Based on the ratio of the total time (in seconds) that this length D contains a vehicle to the total number of seconds in the day, this probability is found to be

$$P_D = AADT \times D/255{,}640\ SP \tag{8}$$

where SP is the average spot speed.

The traffic composition probabilities for r lanes of a one-directional highway can be found from

$$PR = \left[\prod_{\text{all } r} (P_D P_{n_i,n_2,n_3,r})\right] \Big/ P_D \tag{9}$$

Corresponding probabilities for two-lane, two-directional traffic can then be computed from

$$\bar{P} = P_D \prod_{r=1}^{r=2} P_{n_1,n_2,n_3,r} \tag{10}$$

Although these probabilities are based on numerous assumptions, the fact that traffic operation is continuous requires such assumptions. Any such probability derivation must be made with similar qualitative assumptions, although the quantitized criteria are subject to reevaluation based on actual traffic and loading studies at the particular point under consideration. Here, the number of vehicle loading combinations to be considered by these probability equations increases rapidly as the length of roadway under study increases.

Use of Probability Equations

Before final loading distributions can be developed, traffic data must be analyzed to find the frequency of occurrence of each vehicle grouping. Based on these frequencies (probabilities), the total number of repetitions for a particular vehicle grouping (N_{n_1,n_2,n_3}) during an analysis period of Y years can be computed from

$$N_{n_1,n_2,n_3} = 365 \sum_{\text{all years}} AADT \times \bar{P} \tag{11}$$

The total number of vehicle groups TOT to be analyzed by equation 11 during the minimum time period for an r-lane highway is obtained from

$$TOT = \left[\prod_{\text{all i}} (MN_i + 1) \right]^r \tag{12}$$

where $MN_i = L/VL_i$ = maximum number of vehicles of type i that can occur in length L at one time. When the stress level falls below the endurance limit of the member being analyzed, the computational routine presented in equation 12 is terminated.

Gross Load Distribution

Associated with each loading configuration is the probability distribution of the gross weight of that particular loading condition. To derive such a probability requires a knowledge of the parameters mentioned previously:

1. Total number of repetitions of each possible loading configuration N_{n_1,n_2,n_3} during each year,
2. Probability P_{n_1,n_2,n_3} of the occurrence of each loading condition in the length under consideration for each year, and
3. Individual gross vehicle load probability distribution PL_i for each vehicle type considered in the fatigue analysis.

The basic procedure considers all possible loading combinations for each gross vehicle load interval of GL_i for each vehicle of each type found in the loading configuration. The total gross loading probability distribution having q intervals can be found by combining the individual gross bridge loading distributions corresponding to the individual loading configurations ($P_{GL_{ijq}}$) by the following:

$$P_{TL_q} = \sum_{\text{all LC}} P_{GL_{ijq}} P_{n_1,n_2,n_3} \tag{13}$$

The P_{GL} terms can be developed for a particular loading distribution from

$$P_{GL_{ijq}} = P_{GL_{1,1,q}} \times P_{GL_{1,2,q}} \times \ldots \times P_{GL_{1,N_1,q}} \times P_{GL_{2,1,q}} \times P_{GL_{2,2,q}} \times \ldots \times P_{GL_{2,N_2,q}} \times P_{GL_{3,1,q}} \times P_{GL_{3,2,q}} \times \ldots \times P_{GL_{3,N_3,q}} \tag{14}$$

where $P_{GL_{ijq}}$ is the probability that the j th vehicle of type i is in the q th weight group.

The gross load level Q is computed from

$$Q = \sum_{\text{all i}} \sum_{\text{all q}} W_{iq} / K_1 + K_2 \qquad (15)$$

where

K_1 and K_2 = constants used to obtain a reasonable set of gross load intervals and
W_{iq} = mean of the q th weight interval for the i th vehicle type.

Equivalent Load Distributions

The influence (stress) in the member due to a particular load depends not only on the magnitude of the load combination but also on the relative positioning of the load and member. After due consideration, we modified the loading trains positioned in the span to an equivalent single load placed at the same position and in the same configuration as the design vehicle.

Consider loading configuration A shown in Figure 2. Alternative loadings containing the same vehicle types but distributed differently are shown as conditions B and C. The probability of the occurrence of each of these conditions in the span is identical. Because of the assumed random distribution of the vehicles over the length for any particular loading distribution, the loading conditions shown in Figure 2 can be modified to obtain the equivalent continuous loading distributions shown in Figure 3. Superpositioning of all three of these conditions results in the uniform continuous loading distribution shown in Figure 4.

The loading conditions shown in Figures 2, 3, and 4 illustrate equivalent loading distributions. Modification of these loading systems or combinations to an equivalent uniform loading for the design vehicle positioning and configuration is done by

$$LC_\epsilon = f(LC) \qquad (16)$$

where f(LC) is the load equivalency function relating these loads. Modifying the individual load distributions $P_{GL_{ijq}}$ allows the final equivalent loading distribution to be determined for input into the fatigue analysis presented later.

Specified loads can be simulated at different points on the span of a particular bridge. The stress induced in the critical member by the load placed at each of these positions can be computed. The magnitude of the loads at the critical point of the span corresponding to these stresses can then be computed. Based on this knowledge, ratios of the equivalent loads at the critical point to the load at different positions can be determined. A plot of such points—load ratio versus position of load in the critical length—is then made (Figure 5). A line of best fit is obtained either statistically or visually. This curve is the desired function f(LC). The determination of this curve for numerous members of the same bridge and for a number of bridges should provide the data required for developing a generalized relationship for f(LC).

FATIGUE ANALYSIS

Transformation of Load Distributions Into Stress Distributions

The development of a practicable methodology for transforming distributions of loads to corresponding stress distributions required certain basic assumptions.

Table 1. Average vehicle lengths used in fatigue analysis (7).

Vehicle Type	Average Vehicle Length (ft)	Vehicle Type	Average Vehicle Length (ft)
Automobile	19	C-5A	48
SU-2A-4T	21	C-6A	52
SU-2A-6T	24	Automobile	20
SU-3A	28	Single unit	25
C-3A	45	Combination	47
C-4A	48		

Note: 1 ft = 0.3 m.

Figure 1. Vehicle distribution on a two-lane, two-directional highway.

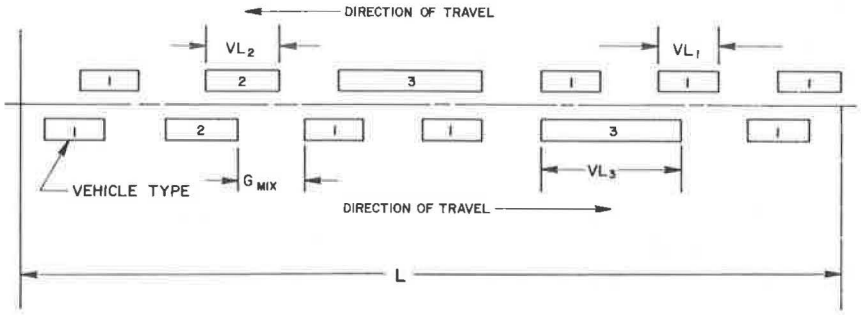

Figure 2. Vehicular loading conditions.

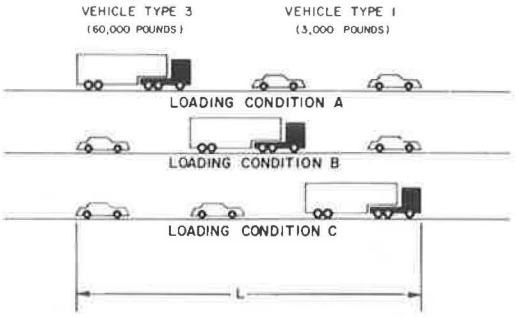

Figure 3. Equivalent vehicular loading conditions.

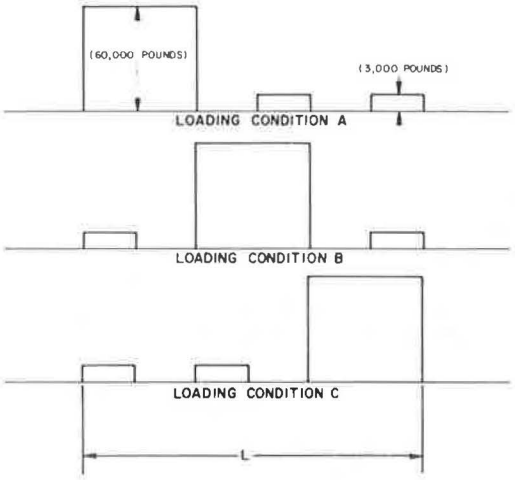

1. The influence of differential stresses resulting from the same gross load but different vehicular axle spacings (i.e., the same gross load but different equivalent rectangular load) is negligible (Figures 6 and 7). If significant stress differentials are observed, some simple parameter (such as number of axles or total vehicle length) should be used to resolve these differences. The methodology used here compromises these extremes. Instead of combining all vehicles into a single classification, we chose three vehicle classes (automobiles, single-unit trucks, and combination trucks).
2. Critical bridge members were designed such that the stress due to the dead load plus live load was at a specified level (e.g., 55 percent of the yield stress).

Figure 4. Equivalent uniform loading condition.

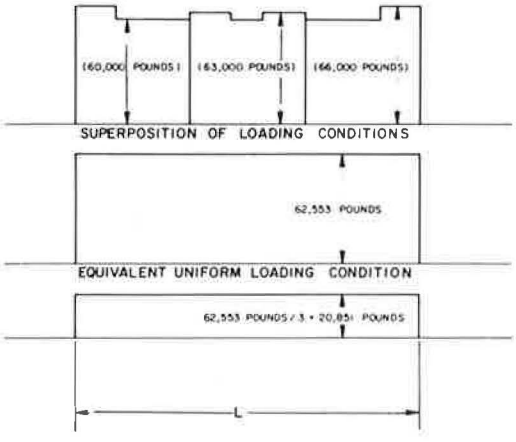

Figure 5. Effect of placement of load on force transmitted to structural member.

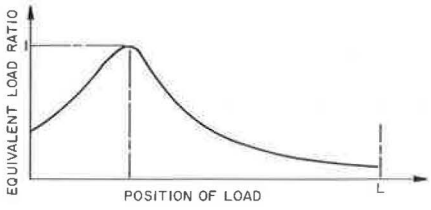

Figure 6. Bending movement due to combination four-axle vehicles.

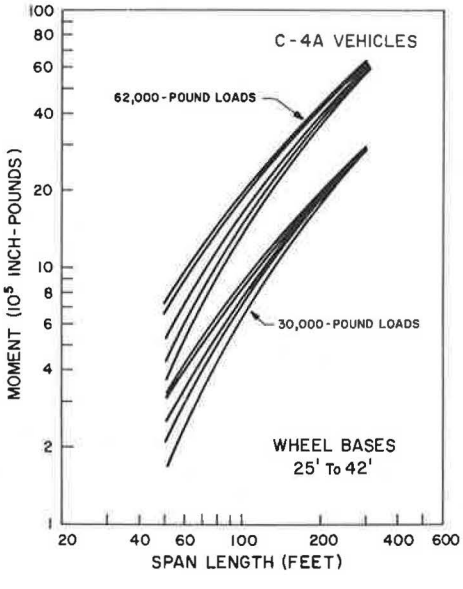

Figure 7. Errors in computations for combination four-axle vehicles.

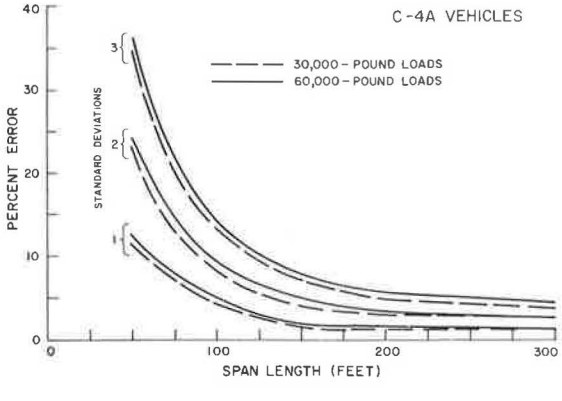

3. Stress in a structural member is approximately proportional to the load transferred to the member for all stress levels below the proportional limit.

Input Parameters

The following input parameters are believed to be minimal:

1. Actual design stress,
2. Dead load,
3. Vehicular live load (this requires a knowledge of the axle loads and configuration of the design vehicle),
4. Critical member section, and
5. A relationship between a measure of rusting and the time elapsed since the bridge was constructed.

These parameters, except the rusting relationship, are readily obtainable from design calculations. The degree of rusting of a member at a specific time might be available from periodical maintenance studies and observations. It should be emphasized that all input values must represent those of the particular bridge member under study.

The dead load of a bridge structure may change from time to time. Loss of section due to rusting will result in decreased weight; any overlays on the bridge deck will increase the dead load. If the fatigue analysis includes the time variable, no problems will arise because these weight changes can be considered.

Load-Stress Relationship

Based on these assumptions, generalized equations can be developed relating stress to loading conditions. Immediately after erection of the bridge, the actual designed stress of a particular bridge member can be found from

$$S_d = (LL \times I + DL)/Z \tag{17}$$

where Z is the cross-sectional area of the structural member in question.

If we assume that the percentage of section lost due to corrosion of a member is some function of time $f_r(y)$, equation 17 can be modified such that the design stress for a particular year can be computed from

$$S_d(y) = [LL(y) + I(y) + DL(y)] \Big/ Z\left[1 - \sum_{1}^{y} f_r(y)\right] \tag{18}$$

Load-Stress Curve

Under the assumption of a linear relationship, points on the load-stress curve can be obtained as follows:

1. The origin of the load-stress axis (zero stress, zero load);
2. Stress due to dead load,

$$S_{DL}(y) = DL \Big/ Z\left[1 - \sum_{\text{all } y} f_r(y)\right] \tag{19}$$

3. When maximum single load that can be carried by the member before yielding will occur,

$$LC(y) = Z\left[1 - \sum_{\text{all } y} f_r(y)\right] \times S(y) \times I(y) \tag{20}$$

4. Minimum fatigue-producing load,

$$LC_{EL} = Z\left[1 - \sum_{\text{all } y} f_r(y)\right] \times f_e(y) \times I(y) \tag{21}$$

where f_e is the endurance limit of the material.

Cumulative Stress Distributions

Development of stress distributions S_{TL_q} from load distributions P_{TL_q} is done by multiplying the frequencies of each loading interval in the load distribution by the unit stress for the mean load of the loading interval. This unit stress is obtained by substituting the midvalue of the loading interval into either equation 17 or 18. The results are in terms of a double array, i.e., the intermediate stress values are in the form of a discrete set of stress repetitions (R_{TL_q}) corresponding to a specified discrete stress distribution, or

$$S_{TLQ} = \sum_{\text{all } q} R_{TL_q} P_{TL_q} \tag{22}$$

The choice of stress intervals in this distribution depends on the accuracy of the input data, the total stress range, and the desired output accuracy.

Transformation of Stress Distributions Into Fatigue History

Load-fatigue relationships include the intermediary computations of stress. This was necessary because similar vehicle loadings result in different stress levels for different members of the same bridge. These situations occur because of (a) different levels and ratios of dead load to live load, (b) different impact values, and (c) the wide variety of structural frames.

Fatigue (S-N) Curves

The basic inputs required are

1. Ultimate strength f_u,
2. Yield strength f_y,
3. Endurance limit f_e, and
4. Number of repetitions N_e associated with the endurance limit.

Also, the following basic assumptions were made:

1. The S-log N curve passes through the point for one repetition of the maximum

stress (stress in the member when subjected to a maximum load),

2. The endurance limit is equal to one-half of the yield strength,
3. The member does not suffer damage by an unlimited number of stress repetitions below the endurance limit,
4. A finite number of stress repetitions N_e are required at the endurance limit before the member will fail, and
5. The slope of the S-log N curve between N_1 (at f_u) and N_e (at f_e) is constant, and the slope of the S-log N curve between N_e and $N > N_e$ is zero.

The applicability of the assumption concerning the linearity of the S-log N curve depends on the type of material used. Most steels now used in bridge construction have relationships approaching linearity. If this assumption cannot be considered applicable, the fatigue-stress relationships presented in the equations derived below should be modified.

Fatigue Factors

Consider a typical, idealized S-log N curve. The slope m of this curve in the fatigue range N_1 to N_e is

$$m = -(f_u - f_e)/\log N_e \tag{23}$$

The generalized S-log N curve equation can then be obtained by substituting the above parameters into the generalized form of a linear equation so that

$$S_1 = [(f_u - f_e) \log N_1/\log N_e] + f_u \tag{24}$$

where N_1 is the number of repetitions at the S_1 stress level causing fatigue. Rearranging equation 24 so that the dependent variable is in terms of the number of stress repetitions gives the S-log N relationship as

$$\text{Log } N_1 = (f_u - S_1) \log N_e/(f_u - f_e) \tag{25}$$

Comparing the N_1 values to a base value of N_e allows equivalent fatigue factors corresponding to differential stress levels to be computed. If we designate this equivalency factor as the equivalent bridge loading EBL, the equivalent number of endurance limit stressings required to fatigue a member to the same extent as one repetition of a S_1 stress is found from

$$EBL_1 = N_e \times 10^{\log N_e(S_1 - f_u)/(f_u - f_e)} \tag{26}$$

To computerize EBL calculations requires that another parameter be quantitized since discrete rather than continuous distributions are used as input. In addition to the input parameters previously designated, some measure of the discontinuity of these distributions must be developed. The relationship between the number of repetitions required for fatigue at a particular stress level has been found to be a geometric relationship (7). The normal form of this equation is

$$EBL_1 = N_e B^{(S_1 - f_u)/SI} \tag{27}$$

where B is a constant and SI is the stress interval. The value of B for a particular material is dependent on the ultimate strength, the yield strength, and either the stress interval of the input data or the total number of stress intervals (8). If the stress interval is specified, then B can be found from

$$B = \log^{-1} [SI \log N_e/(f_u - f_e)] \tag{28}$$

If the total number of stress intervals is known, the constant can be computed from

$$B = \log^{-1} (\log N_e/q) \tag{29}$$

Substituting into equation 27 yields

$$EBL_1 = N_e \log^{-1} [SI \log N_e/(f_u - f_e)]^{(S_1 - f_u)/SI} \tag{30}$$

and

$$EBL_1 = N_e \log^{-1} [(\log N_e/q)^{q(S_1 - f_u)/(f_u - f_e)}] \tag{31}$$

METHODOLOGY FOR PROBABILITY ANALYSIS OF FATIGUE

The total fatigue of a member for a specified time period is found by summing the fatigue contributions from all individual loading systems on the bridge during the time interval. The generalized procedure for obtaining this total fatigue contribution is as follows:

1. Determine the probability of the number of repetitions of each vehicle loading configuration occurring during the study period;
2. Transform the vehicle loading distribution generated in step 1 into a corresponding distribution of stresses in structural members;
3. Determine the appropriate fatigue (S-N) curve for the member based on available design criteria;
4. Determine the equivalent bridge loading contribution due to the application of one stress in each stress interval;
5. Multiply the number of stress applications in each stress interval by the corresponding EBL factor; and
6. Sum the EBLs over all stress groups, and compare the total to the maximum safe value N_e.

Formulating steps 5 and 6 as an equation gives the percentage of fatigue life PFL used during a design period of Y years as

$$PFL = 100 \sum_{\text{all } 1} \sum_{\text{all } y} N_{1y} EBL_{1y}/N_e \tag{32}$$

where N_{1y} is the number of stress repetitions of the 1th stress level using the bridge during the y th year and EBL_{1y} is the corresponding fatigue equivalency factor.

Most simply, past traffic trends may be assumed to be indicative of future traffic characteristics. Because various loading distributions from past traffic studies for a bridge are necessarily discrete, extending these parameters into the future is unreasonably tedious. Instead, it is recommended that a new traffic parameter be developed, average EBL per vehicle AEBL. This value is obtained for each time interval by dividing the total number of EBLs by the total number of vehicles. This ratio can then be plotted as a function of year to obtain AEBL over the design period.

The remaining parameter necessary for the development of the fatigue analysis is the AADT curve as a function of time. The portion of the curve representing the time from the bridge erection date to the time of the analysis is available from past traffic data.

When curves representing these parameters have been plotted, they are extrapolated into future years. Expected EBL's accumulated in any particular year are then found from

$$EBL(y) = 365 \times AADT(y) \times AEBL(y) \tag{33}$$

The total number of EBLs accumulated from the present time to the end of year Y can be computed from

$$TEBL = \sum_{\text{all } y} EBL(y) \tag{34}$$

STRAIN GAUGE ANALYSIS

Scratch Gauges

On April 18, 1972, scratch gauges were placed on four members of Central Bridge. Two additional gauges were attached on April 26. Gauges were placed on the following paired I-bars:

1. April 18, D14L3L2-3, D14L3L2-4, U14L6L'5-3, and U14L6L'5-4; and
2. April 26, U15L'5L'4-3 and U15L'5L'4-4.

The bars selected for instrumentation had the maximum loss of section according to a previous study (9, 10). Gauges were 48-in. (1.22-m), temperature-compensating Prewitt scratch gauges. The operation and use of those gauges were reported previously (9, 10).

Gauges were attached to the I-bars with C-clamps. Threads of the clamps were soldered to provide a more permanent attachment. Restraining straps made of aluminum foil were placed at 1-ft (0.3-m) intervals along the gauge to prevent possible buckling, which might induce errors in the records. The gauges were then covered with plastic to provide protection. Two gauge targets showed no record; one indicated two complete rotations and could not be read. This accounted for the differences in total number of days of record noted in the results.

Scratch gauges were monitored for approximately $4\frac{1}{2}$ months. Data collected from the discs are given in Table 2. These data were analyzed by the equivalent-bridge-load criterion and a Goodman diagram to determine fatigue damage. In EBL calculations, it was assumed that loading was constant (at the current rate) and that corrosion occurred linearly throughout the life of the bridge. Differences in stresses on parallel bars were also determined.

To calculate stresses given in Table 3, the following equation was used:

Table 2. Number of events per stress level.

Live Load Stress (psi)	Bar D14L3L2-3	D14L3L2-4	U14L6L'5-3	U14L6L'5-4	U15L'5L'4-3	U15L'5L'4-4
<200	324	338	278	513	323	44
200	597	502	462	830	543	91
400	1,009	530	367	779	338	129
600	742	313	267	448	157	132
800	99	60	103	97	69	32
1,000	33	25	45	29	35	31
1,200	13	9	44	21	26	11
1,400		4	9	3	9	4
1,600	3	1	6	2	5	1
1,800			3		2	2
2,000	1		4		1	
2,200		1			1	
2,400			1		2	
2,600						
2,800					1	
Total events	2,821	1,783	1,589	2,722	1,507	467
Total time, days	129	91	69	129	121	83
Average stress, psi	491	433	489	425	423	570
Dead load stress, psi	14,180	14,180	14,260	14,260	14,260	14,260
Percentage of original section remaining	78	85	78	NA	77	85

Note: 1 psi = 6.9 kPa.

Table 3. EBL (DL + LL) with loss of section considered.

Total Stress (psi)	Bar D14L3L2-3	D14L3L2-4	U14L6L'5-3	U15L'5L'4-3	U15L'5L'4-4
16,750		372			48
17,000		602			109
17,250		689			168
17,500		438			185
17,750		92			49
18,000		42			35
18,250	586	16	503		20
18,500	1,164	8	901	630	8
18,750	2,159	2	785	1,162	2
19,000	1,729		622	787	4
19,250	249	2	259	395	
19,500	90		122	187	
19,750	26		87	70	
20,000			29	85	
20,250	10		21	32	
20,500			11	19	
20,750	4		17	8	
21,000				5	
21,250			5	5	
21,500				10	
21,750					
22,000				6	
Total	6,017	2,263	3,362	3,401	628
Damage, percent per year	0.85	0.45	0.89	0.48	0.14

Note: 1 psi = 6.9 kPa.

$$S_T = 100\ (S_{DL} + S_{LL})/C \qquad (35)$$

where

S_T = total stress,
S_{DL} = dead load stress from Table 2,

S_{LL} = live load stress from Table 2, and
C = percentage of section remaining from Table 2.

The equivalent bridge load factor was calculated from equation 34. The number of cycles of each load was found from

$$N' = N \times EBL \tag{36}$$

where

N' = number of equivalent loads corresponding to total stress level S_T and
N = number of events from Table 2 for live load stress level S_{LL} corresponding to total stress level S_T.

The yearly damage caused by the recorded loads was found from

$$d = 365 \Sigma N'/N_e t \tag{37}$$

where

d = percentage of damage per year caused by recorded loads and
t = elapsed time of record, in days.

Values used in making EBL calculations were

1. Ultimate strength of steel (f_u) = 60 ksi (414 MPa),
2. Endurance limit of steel (f_e) = 16.5 ksi (114 MPa), and
3. Events to failure at endurance limit (N_e) = 2,000,000.

From data given in Table 3, it was apparent that damage caused by the recorded loads was significant when the EBL criterion was used. The most critical member noted in the analysis was U14L6L'5-3, which showed a yearly loss of service life of 0.89 percent. This would yield a service life of 112 years if damage remained constant over the life of the bridge. If we assume that corrosion occurs uniformly over the life of the bridge, the loss of fatigue life that has occurred can be computed. When damage was computed in this way, it was found that 30 percent of the service life had been used. Another computation was made that extended present conditions into the future; this showed that the bridge had 40 years of remaining service life if corrosion continued to increase at the same uniform rate previously considered. In these calculations, wind and temperature loadings were not considered. These loads could have considerable effect on the service life of the bridge.

The maximum damage stress (S_{DL} = 18.5 ksi or 127 MPa and S_{LL} = 3.6 ksi or 25 MPa of U15L'5L'4-3) was plotted on a Goodman diagram to show its relationship to the endurance limit. It was noted that the stress is well within the safe limits according to that criterion. Because of wind and temperature loadings and age and condition of the steel, the more conservative EBL criterion is probably more appropriate for this situation.

Comparisons (Figure 8) were also made of scratch gauge data to determine what percentage of the load was being carried by each of the paired parallel bars. Differences in stresses are apparent for all pairs. These differences are prominent at low stresses but also occur at higher stress levels. These differences do not appear on the figures at the higher stress levels because of the low percentage of events at those stresses. The cause of the differences in stress in the members cannot readily be identified but several possibilities are apparent:

1. There may be loose pin connections in the I-bars,
2. The strain gauges may not have been placed on sections of equal areas, or
3. The strain gauges might not have been exactly parallel.

SR-4 Resistivity Strain Gauges

On August 23, 1972, SR-4 resistivity strain gauges were placed on bars D14L3L2-3 and D14L3L2-4. The gauges were placed parallel to each other on a normal section of the I-bar so that any differences in recorded strain could be attributed to differences in stresses on those members.

A simultaneous record was made of strain in each bar. These data were then used in a least squares analysis to obtain equations relating stress in one bar to that in the companion bar. Channels of the recorder were then reversed, and the least squares analysis was rerun. An average equation was then computed so that any differences in recorder channels would be eliminated. The equations and their plots are shown in Figure 9.

Differences in stresses in the instrumented, paired members were relatively small. These differences could be attributed to any of the causes mentioned earlier regarding differences in scratch gauge data.

General

According to the equivalent-bridge-load criterion and data obtained from the scratch gauges, there is noticeable fatigue damage occurring in corroded I-bars of the Central Bridge. Although the calculations of remaining service life in the bars are vague, they do show that possible danger exists.

It was also found that strains in parallel members were nearly equal. Some differences were recorded, but this was more than likely due to gauge locations and recording differences rather than actual differences in strains in the bars themselves. The only large differences in recorded strains were for bars U15L'5L'4-3 and U15L'5L'4-4. In those cases, there were also large differences in numbers of events per day and in percentage of events per load increment, so it is possible that errors in the records for these bars may be present.

PROBABILITY ANALYSIS

Input Data

A computer program was developed to calculate loss of fatigue life by using probability analysis. All traffic data used in this analysis came from papers by Lynch (6, 7). Input data are given in Table 4.

All computations covered a period of 81 years (from 1891 to 1992). When corrosion was taken into account, the section was considered normal in 1891 but advanced to a 23 percent loss of section by 1972. Both uniform and parabolic aging (due to corrosion) were considered (Figure 10). Wind and temperature stresses were not considered because of the difficulty in measuring such stresses accurately.

Results and Discussion

Eight computer runs using different loads, considerations of corrosion, and endurance limits were made. Results of these runs are given in Table 5. In runs 1, 2, and 3, loss of section due to corrosion was not considered; it was found that very little damage resulted even when all vehicle classes were considered at their maximum recorded weight (Figure 11) and all recorded AADTs were doubled. All other runs took corrosion

Figure 8. Cumulative percentage of vehicles versus live load stress.

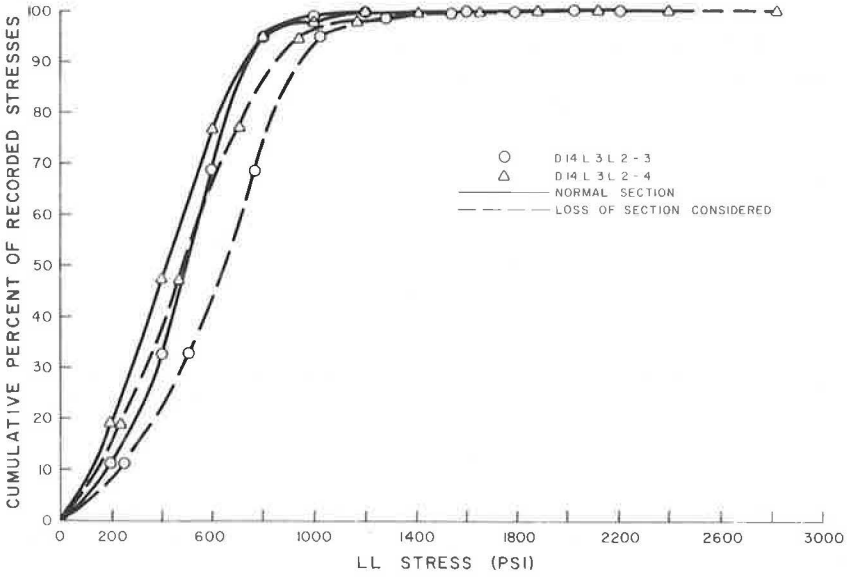

Figure 9. Stress in D14L3L2-3 versus stress in D14L3L2-4.

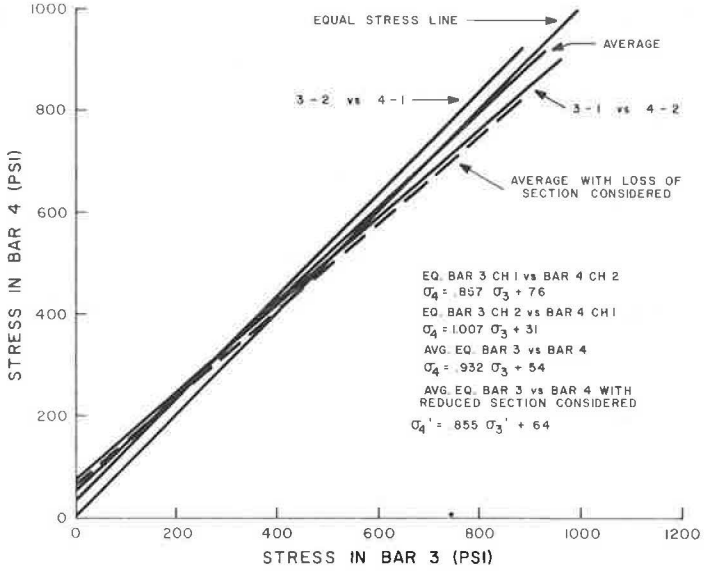

Table 4. Input data for probability analysis.

Data	Item	Value	Data	Item	Value
Vehicle	Percentage of total traffic		Material	Yield strength, psi	33,000
	Cars	91.4		Ultimate strength,	
	Trucks	7.3		psi	60,000
	Combination trucks	1.3		Endurance limit	As indicated
	Average length, ft			Events to failure at	
	Cars	20		endurance limit	2,000,000
	Trucks	25	Bridge	Length of span, ft	254
	Combination trucks	47		Width of span, ft	23
	Average spot speed, mph	28.2		Design load, lbf/ft^2	75
	Average weights	[a]	Critical	Dead load stress,	
	AADT	[b]	member	psi	14,260
	Gap probabilities	[c]		Design live load	
				stress, psi	5,950

Note: 1 ft = 0.3 m; 1 mph = 1.6 km/h; 1 psi = 6.9 kPa; 1 lbf/ft^2 = 48 Pa.

[a]See Figure 11. [b]See Figure 12. [c]See Figure 13.

Figure 10. Percentage of section remaining versus year for the critical member on Central Bridge.

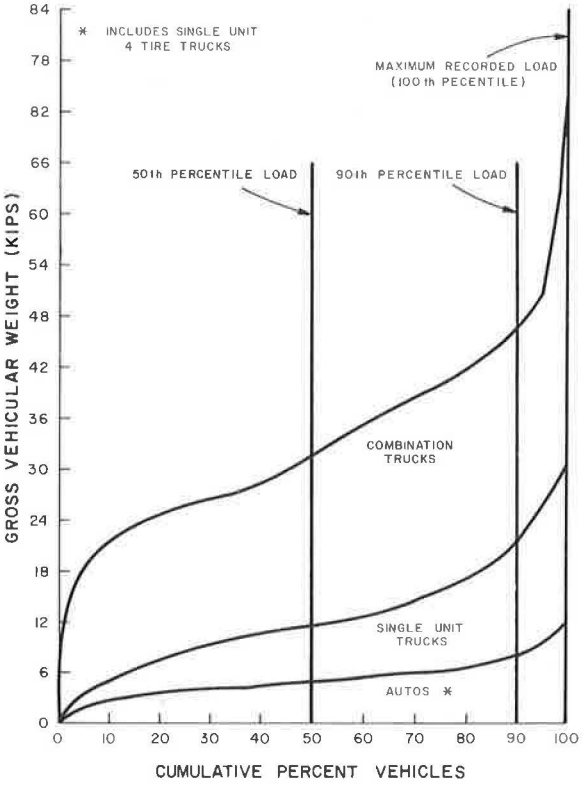

Figure 11. Cumulative percentage of vehicles versus gross weight for all vehicle types on Central Bridge.

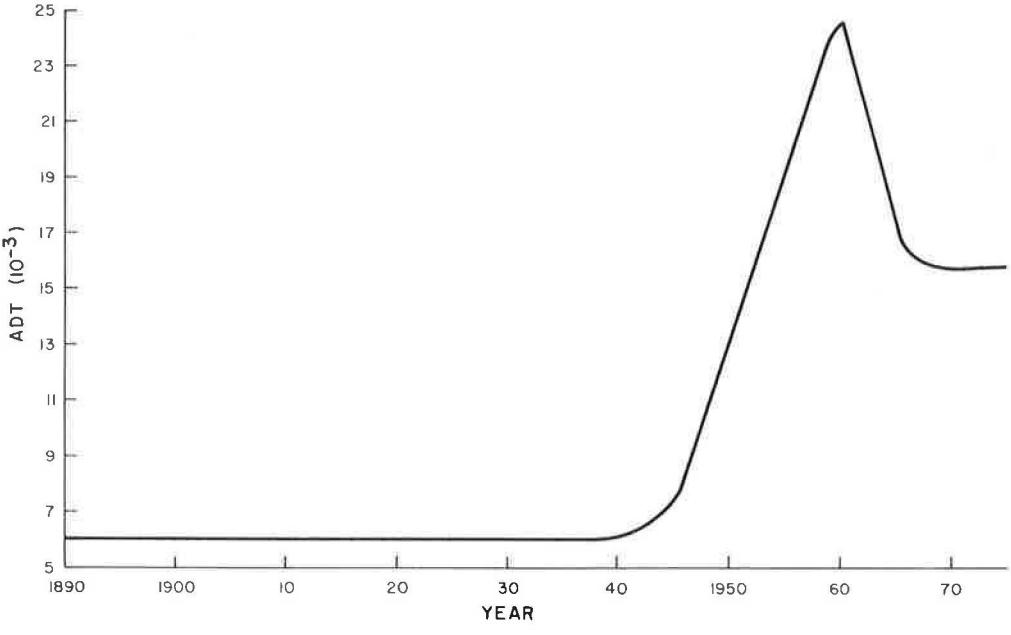

Table 5. Life estimates from probability analysis.

Run	Percentage of Life Used	Age (years)	Calender Year	Gross Vehicle Weight (percentile)[a]	Percentage of Section Loss Due to Corrosion	Endurance Limit (psi)	DL Stress at Calendar Year Shown (psi)
1	0	81	1972	50th	0	16,500	
2	0	81	1972	90th	0	16,500	
3	5	81	1972	100th[b]	0	16,500	
4	100+	25	1916	50th	23, linear	15,000	14,780
5	100+	45	1936	50th	23, linear	16,000	16,060
6	100+	55	1946	50th	23, linear	17,000	16,820
7	100+	66	1957	50th	23, parabolic	17,000	16,800
8	100+	68	1959	50th	23, linear	18,000	17,580

Note: For ADT, see Figure 13 (7). 1 psi = 6.9 kPa.

[a]See Figure 12. [b]Maximum recorded loading from 1968 weighings (7).

Figure 12. Gap versus probability of occurrence for all vehicle types on Central Bridge.

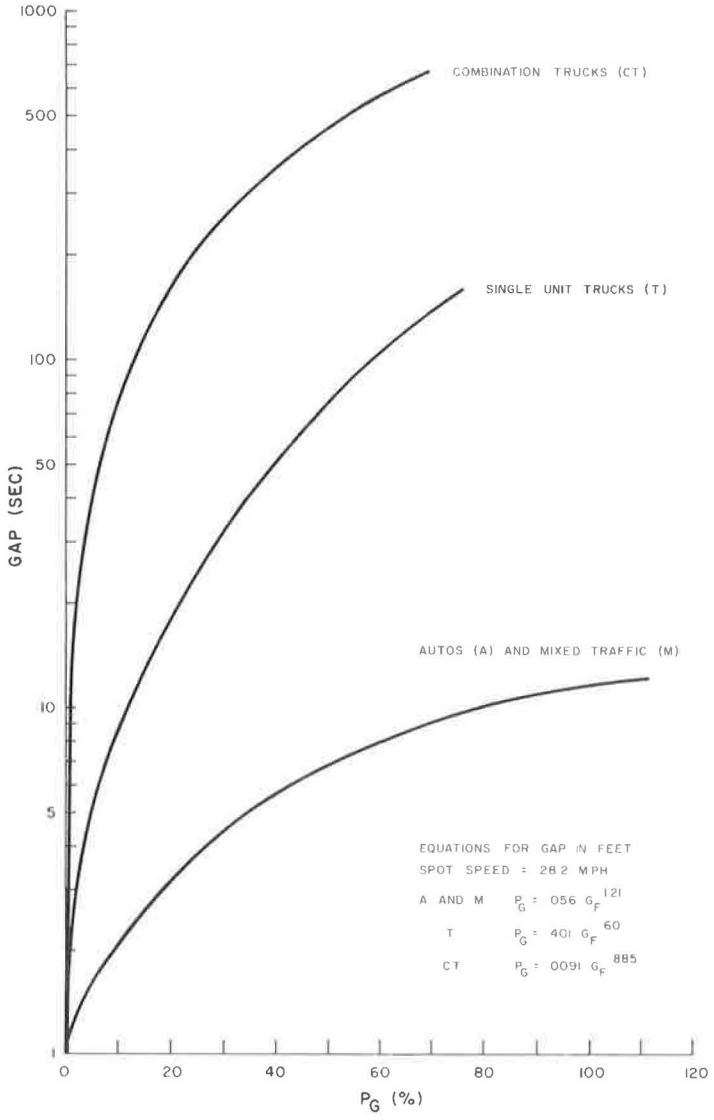

Figure 13. AADT versus year for all vehicle types on Central Bridge.

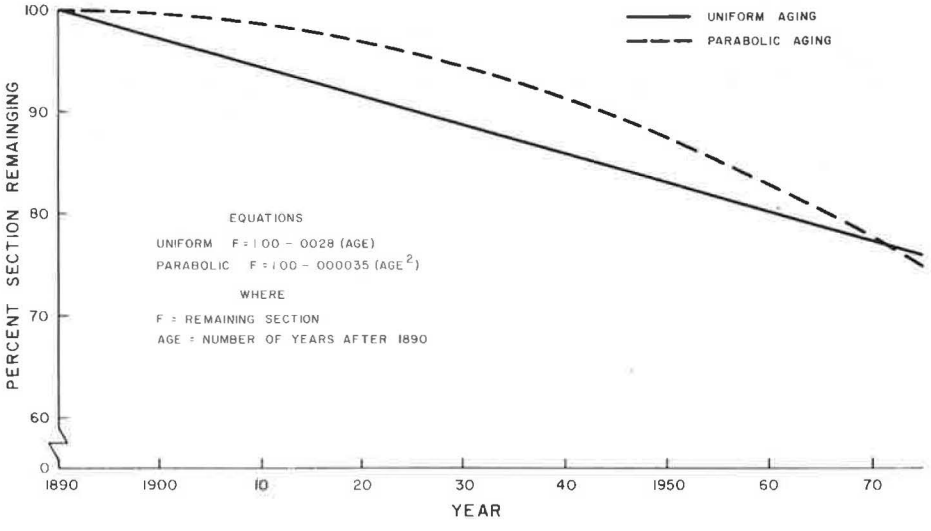

into account. These runs considered loading at the 50th percentile level and AADTs as recorded (Figure 12); variables were endurance limit and type of corrosion aging. From these results, it became obvious that the most important factor is the range between the dead load stress and the endurance limit of the steel. Also, the relationship assumed between loss of section and time, as seen from runs 6 and 7, greatly affects the duration of the range. Small changes in the assumed endurance limit caused great changes in the calculated service life of the bridge member. Inasmuch as failure was predicted in all runs where corrosion was considered, it appears that some assumptions regarding the severely corroded members in the Central Bridge are too extreme.

Failure was predicted when the dead load stress in the member reached a value near that of the endurance limit; thereafter, all vehicles crossing the bridge became damaging loads. However, fatigue damage is a function of dynamic (live load) and static stresses, and the Goodman diagram tends to moderate the damage attributable to the live loads in similar situations. Inasmuch as wind and temperature stresses have not been considered in these analyses, the original condition of the steel is not known, and because the effects of aging on the steel are not known (at this time), the calculations are somewhat overly conservative in assessing fatigue damage.

REFERENCES

1. G. R. Gohn. Fatigue of Metals: Part 1—The Mechanism of Fatigue. American Society for Testing and Materials, Materials and Research Standards, Feb. 1963.
2. American Institutes of Mining and Metallurgical Engineers. Metals Handbook. American Society of Metals, Cleveland, 1939, pp. 6, 10, 143, 149.
3. H. F. Moore and J. B. Kommers. The Fatigue of Metals. McGraw-Hill, 1927, pp. 1, 27, 119-148.
4. J. A. Deacon. Fatigue of Asphalt Concrete. Univ. of California, Berkeley, graduate thesis, 1965, pp. 86-129.
5. Collapse of US-35 Highway Bridge, Point Pleasant, West Virginia, December 15, 1967. National Transportation Safety Board, Highway Accident Report NTSB-HAR-71-1, 1970.
6. R. L. Lynch. Analysis of Traffic Loads on Bridges, Characteristics of Loadometer and Classification Data—1968. Kentucky Department of Highways, March 1969.

7. R. L. Lynch. Analysis of Traffic Loads on Bridges. Kentucky Department of Highways, Feb. 1968.
8. G. R. Cudney. The Effects of Loadings on Bridge Life. Michigan Department of Highways, Jan. 1968.
9. Kentucky Obtains Bridge Load Histories With Newly Developed Scratch Gage Device. Highway Research News, Highway Research Board, No. 36, Summer 1969.
10. R. D. Hughes. Stress Histories of Bridge Members From Scratch Gage Records. Kentucky Department of Highways, Feb. 1972.

SPONSORSHIP OF THIS RECORD

GROUP 2--DESIGN AND CONSTRUCTION OF TRANSPORTATION FACILITIES
W. B. Drake, Kentucky Department of Transportation, chairman

STRUCTURES SECTION
Arthur L. Elliott, California Department of Transportation, chairman

Committee on Dynamics and Field Testing of Bridges
Robert F. Varney, Federal Highway Administration, chairman
Charles F. Galambos, Federal Highway Administration, secretary
James W. Baldwin, Jr., Edwin G. Burdette, Paul F. Csagoly, Conrad P. Heins, Jr., Cornie L. Hulsbos, Henry L. Kinnier, Robert H. Lee, Kenneth H. Lenzen, Norman G. Marks, Fred Moses, Leroy T. Oehler, Frederick H. Ray, Ronald R. Salmons, W. W. Sanders, Jr., William H. Walker, George W. Zuurbier

Lawrence F. Spaine, Transportation Research Board staff

The organizational units and the chairmen and members are as of December 31, 1974.